Cellular Seismology Predictability as a Measure of Association Between Wastewater Injection Wells and Earthquakes in Oklahoma

Author: Hannah Elise Chambless

Boston College Electronic Thesis or Dissertation, 2018

CELLULAR SEISMOLOGY PREDICTABILITY AS A MEASURE OF ASSOCIATION BETWEEN WASTEWATER INJECTION WELLS AND EARTHQUAKES IN OKLAHOMA

Hannah E. Chambless

A thesis

submitted to the Faculty of

the Department of Earth & Environmental Sciences

in partial fulfillment

of the requirements for the degree of

Master of Science

Boston College
Morrissey College of Arts and Sciences
Graduate School

August 2018

CELLULAR SEISMOLOGY PREDICTABILITY AS A MEASURE OF ASSOCIATION BETWEEN WASTEWATER INJECTION WELLS AND EARTHQUAKES IN OKLAHOMA

Hannah E. Chambless

Advisor: Alan L. Kafka, Ph.D.

Discerning the interrelated effects of space and time on the potential for wastewater well injection to induce earthquakes in Oklahoma is important for accurately mapping seismic hazards. This study explores how distance from wells and time after initiation of injection affect the possibility that injection activity might induce earthquakes under different conditions of operational lifetime, injection volume, and well depth. A unique feature of this study is filtering of the injection well database to isolate, as much as possible, the effect of specific well injection on the potential to induce earthquakes. The method used here is a modified version of "Cellular Seismology", termed "Modified Cellular Seismology" (CS, MCS), where "CS Predictability" (CSP) is used as an operational definition of the extent to which injection wells are associated with earthquakes. I hypothesize that earthquakes associated with injection are most likely to occur within about 15 km of wells and within approximately the same year as active injection. Evidence shows that induced earthquake activity peaks primarily between about 2.5 and 3.5 km away from any given well, and this distance increases while CSP decreases over time. Temporal analyses suggest that CSP decreases by an average of about 5% over a period of five to seven years for any given well (or about 1% decrease per year), though there exists considerable scatter in this relationship. This change is variable across wells of different conditions, ranging from a decrease of 26% to an increase of 8% over the five to seven years covered by this study. Additionally, CSP

tended to peak at least a year after injection for the most spatiotemporally isolated wells, suggesting that there may be, on average, at least a year of lag before any given well is likely to induce earthquakes.

TABLE OF CONTENTS

LIST OF TABLES

LIST OF FIGURES

ACKNOWLEDGEMENTS

For providing insight into and context for the publically available oil and gas data files on the OCC website as well as for their interest in this work, I would like to thank Phillip Bailey, his team, and Jim Rosado. I would also like to thank the Eastern Section of the Seismological Society of America for providing me with funding to present my research as it progressed on a supportive and constructively critical platform. Thank you to my thesis committee members, Seth Kruckenberg and Gail Kineke, who provided support and review of my work during my time at Boston College. I would also like to thank my family, friends, and my boyfriend, Kevin Simans, for their support and advice throughout this experience. Lastly, to my advisor of seven years, Alan Kafka, I express my utmost gratitude for being not only a supportive, knowledgeable, and motivating adviser, but also a good friend and colleague.

INTRODUCTION

Human-induced seismicity has become a major concern for society and represents a new challenge for accurately mapping seismic hazards. Induced seismicity is a phenomenon associated with fluids and forces introduced into the subsurface by human activities, such as impounding reservoirs and injecting fluids into deep wells. These activities can sometimes "nudge" potential earthquake zones along to induce earthquakes that might not have been ready to occur or might not have occurred at all naturally. For the Central and Eastern United States (CEUS) beginning in 2016, the U.S. Geological Survey, which regularly publishes National Seismic Hazard Maps (NSHMs) (http://earthquake.usgs.gov/hazards/hazmaps, last accessed March 29, 2018), published its first short-term NSHM that includes the effects of both *natural* and *human-induced* earthquakes (Figure 1). Very prominent on this map is the high level of forecasted earthquake hazards in Oklahoma and southern Kansas in conjunction with a sharp increase in seismic activity in the CEUS since around 2009 (Figure 2). The increase in seismicity in the CEUS, and in Oklahoma and Kansas specifically, is thought to be associated with oil and gas extraction and injection activities.

Previous research implicates that petroleum extraction methods, including conventional methods, hydraulic fracturing (or "fracking"), and enhanced oil recovery (EOR) operations, induced earthquakes in the CEUS in the past (McGarr *et al.*, 2002). However, the primary contributor to inducing earthquakes in the CEUS is thought to be the disposal of brines (highly saturated salt water often mixed with other contaminants) that are brought to the surface during the extraction process (Ellsworth, 2013; Weingarten *et al.*, 2015; U.S. EPA, 2016). As saltwater disposal (SWD) wells inject large volumes of brine into subsurface pore space, pore pressure has the potential to increase above hydrostatic, reducing fault strength (Hubbert and Rubey, 1959; Healy *et al.,* 1968; McGarr *et al.*, 2002). This process, among other mechanisms that may be responsible for fault strength reduction, such as poroelastic or thermoelastic deformation, can induce earthquakes (Rubinstein and Mahani, 2015).

Of particular interest regarding the challenge of accurately mapping seismic hazards from induced earthquakes is the variation in spatial distribution and frequency of those earthquakes over time as a result of the onset and termination of injection at different well sites. Also of interest is the variation in those patterns due to changes in the volumes and rates of injection of wells over time, as high volumes and rates may enhance the probability of inducing an earthquake (Ellsworth, 2013; Weingarten *et al.*, 2015). Other characteristics of the injection process, such as depth to the bottom of the well and wellhead pressure, may also affect the potential for inducing earthquakes, though the reliability of the available data for those parameters is questionable (Weingarten *et al.*, 2015). Additionally, certain aspects of the subsurface geology can play a role in the potential for certain wells to induce earthquakes, such as the location and density of fluid pathways from the injection point to a basement fault (i.e. permeability), the required amount of fluid pressure to trigger fault failure, the pore pressure and ambient stress condition prior to injection, the overlying stratigraphy and the number, location, size, and orientation of basement faults (Ellsworth, 2013; Holland, 2013; Rubenstein and Mahani, 2015). However, a lack of comprehensive data on injection well pumping over a sufficiently large area and long time period, very few direct measurements of pore pressure, stress state, and permeability at well sites (Weingarten *et al.*, 2015), and inconclusive results regarding the relationship between basement fault locations and occurrence of induced seismicity (Chambless and Kafka, 2016) make these spatial and temporal assessments of future induced seismicity in the CEUS difficult.

Discerning how spatial and temporal patterns vary with differences in certain injection well parameters may help in forecasting the potential locations, and perhaps even the range of timing, of future injection-induced earthquakes. There are therefore two primary objectives of this research. The first is to explore the distance range from any given SWD well within which earthquakes are most likely to be induced. The second is to investigate how time after any given well's initiation of injection affects the possibility that a well's injection activity might induce earthquakes (within a specified distance of the well) under different operational conditions of the well. Specifically, this study investigates the following conditions: operational lifetime, injection volume and depth. Though the injection-induced earthquakes of interest are concentrated in both Oklahoma and southern Kansas, the lack of comprehensive well data in Kansas prior to 2015 limits the spatial scope of this study to Oklahoma alone, for which there is a very comprehensive and well-organized database.

The tool used in this study to meet these research objectives is a modified version of "Cellular Seismology" (CS), which was originally developed as a purely statistical way to investigate the extent to which the locations of past earthquakes delineate zones within which future earthquakes are likely to occur (e.g., Kafka, 2002, 2007). This tool tests the assumption that future earthquakes tend to occur near zones delineated by past seismicity, and the essential idea behind this thesis study is that a repurposed version of CS serves as a window into discerning spatial and temporal patterns of injection well-induced seismicity. This repurposed version of CS is referred to here as "Modified

Cellular Seismology" (MCS), and it involves replacing the past earthquake catalog of CS with a catalog of SWD well locations (e.g., Chambless, 2015; Chambless and Kafka, 2017).

The objective of MCS is to determine the extent to which injection well locations delineate zones within which earthquakes are likely to be induced. By varying the radius around wells within which an earthquake is considered to be potentially induced, MCS can be used to test assumptions regarding how far from those wells the injection activity influences the potential for inducing earthquakes and how that influence varies with distance (Figure 3). By analyzing variation in the amount of time from the initiation of injection to the occurrence of earthquakes, MCS can also test hypotheses regarding how long after injection these potentially induced earthquakes are most likely to occur. Each of these tests measures the extent to which injection wells are associated with induced earthquakes, so this study applies MCS analyses to wells of various operational conditions in order to compare the resulting spatial and temporal patterns of seismicity among these different catalogs of wells.

One hypothesis tested here is that earthquakes associated with injection are most likely to occur close to (i.e. within 15 km of) the active wells with which they are associated and within approximately the same year of active injection. Another is that our MCS measure of association will decrease over time, as the effects of injection might abate over time (Herrmann *et al.*, 1981; Keranen *et al.*, 2013). The last hypothesis tested is that these spatial and temporal patterns will hold true under various operational conditions, with higher volume and deeper wells having an overall higher measure of association with earthquakes over time than lower volume and shallower wells.

1.0 BACKGROUND

1.1 Petroleum Extraction and Disposal

Petroleum extraction has been occurring in the United States since the mid-19th century, and induced earthquakes have been recognized and studied since the late 1800s (McGarr *et al.*, 2002). Though these operations have been around for over a century, geologic sources and methods of extraction have more recently expanded from conventional to now include unconventional, which has greatly increased U.S. petroleum production (U.S. Energy Information Administration (EIA), 2011; Scanlon *et al.*, 2014). Unconventional reservoirs have low permeability and tightly hold hydrocarbon reserves, usually requiring artificially pressurized, directional hydraulic fracturing, or "fracking" to release them (U.S. EIA, 2011; Scanlon *et al.*, 2014). These unconventional reservoirs include tight formations, like sandstone and limestone, but the most highly exploited ones in the U.S. are shale plays (U.S. EIA, 2011, 2016; Figure 4). Extraction by fracking now accounts for about half of the total oil output and about two thirds of the total natural gas production in the United States (U.S. EIA, 2011, 2016). According to a 2013 shale oil and gas resource assessment by the EIA (U.S. EIA, 2013), the United States produces the 2nd highest volume of recoverable shale oil in the world (behind China) and the 4th highest volume of recoverable natural gas in the world (behind China, Argentina, and Algeria). The states that contain some of the most prolific shale plays are mainly concentrated in the CEUS (Figure 4). Oklahoma, which has neither the most subsurface coverage of shale plays, nor the most productive plays in the country, has a particularly high economic and public dependence on the oil and gas industry (Snead, 2002; U.S. EIA, 2011). This is in part due to its historical dependence on the industry, but there are also larger, conventional reservoirs used for extraction in Oklahoma. Additionally, regarding injection wells in the United States related to disposal and enhanced recovery after petroleum extraction, 40% of those wells that have been spatiotemporally associated with earthquake activity are located in Oklahoma (Weingarten *et al.*, 2015). These circumstances necessitate significant research regarding the connection between injection and seismicity in Oklahoma.

In the U.S., three primary unconventional methods of fluid extraction and disposal used by the oil industry are fracking, enhanced oil recovery (EOR), and disposal of wastewater through SWD wells (Ellsworth, 2013; Rubinstein and Mahani, 2015). While vertical wells may utilize the method of fracking, a newer method of directional drilling involves drilling wells first vertically, then horizontally, and injecting a combination of water and a sand or chemical proppant (which is used to keep the fractures open) under high pressure to propagate cracks through the rock or to stimulate slip along preexisting faults (Figure 5; McGarr, 2014; Scanlon *et al.*, 2014). These fractures increase the contact area of the formation with the wellbore so operators can extract the maximum amount of gas or oil (Scanlon *et al*, 2014). Operators then remove the fluids, and, due to pressure gradients, oil, gas, and co-produced brine trapped in the same pore space flow readily into the well (McGarr, 2014; Rubinstein and Mahani, 2015).

Concurrent with increased petroleum production by this method has been increased co-production of brine from these producing formations, necessitating higher volumes and rates of salt-water disposal (Murray, 2015). SWD wells involve fluid injection of this brine and variable amounts of spent hydraulic fracturing fluid back into subsurface formations (Figure 6; EPA, 2016). Often saltier than seawater, this brine can also contain toxic metals and radioactive substances, which makes it both difficult and expensive to treat. Therefore, operators must inject this wastewater into formations well below oil and gas-producing formations (often at other sites and isolated from groundwater sources) into porous, confined sedimentary strata (e.g., limestone) above the basement (McCurdy, 2011; Rubinstein and Mahani, 2015; Walsh and Zoback, 2015). In Oklahoma, operators drill almost all SWD wells above the basement, though the exact distance between the bottom of each well and the basement below is not known for individual wells (Tello, 2016).

Enhanced oil recovery, on the other hand, is a secondary extraction method that involves injecting water into the producing formation and saturating pore space to encourage more oil and gas extraction than would otherwise come out naturally or during the fracking process (Murray, 2013; Weingarten *et al*., 2015). The U.S. EPA classifies both EOR and SWD wells as Class II Underground Injection Control (UIC) wells, which are wells injecting waste fluids associated with oil and gas production (EPA, 2016). The EPA either regulates these directly or grants state regulatory agencies primacy over wells in their states. Additionally, SWD wells usually involve the injection of much higher volumes of fluid over longer periods of time than both hydraulically fractured and EOR wells (Weingarten *et al*., 2015).

1.2 Oklahoma Geology

The main producing shale play in Oklahoma is the Woodford shale, which was deposited during the Mississippian (323-359 Ma) and is primarily drilled unconventionally for tight reserves of natural gas (Figure 4; Johnson, 2008; Murray, 2015). Other producing formations in Oklahoma located within sedimentary basins include permeable limestones (Figure 4). While operators drill into shale plays using unconventional methods for oil and gas extraction, these more permeable carbonates can be drilled both conventionally and unconventionally for oil extraction (Murray, 2015). These carbonate formations include the Mississippian limestone, or "Mississippi lime", in north central Oklahoma and the Hunton Lime Play, which is one of the largest co-producers of brine in the United States. Like extraction from shale plays, these carbonates also necessitate subsurface disposal of their co-produced brines (Walsh and Zoback, 2015). The primary disposal formation for Oklahoma is the Arbuckle Group, which is a limestone and dolomite formation located within the Cherokee Platform and Anadarko Shelf provinces in the central and northern portions of the state and extending north into southern Kansas (Figure 7; Murray, 2013, 2014; Walsh and Zoback, 2015). The Arbuckle Group accounts for more than 50% of the statewide total SWD injection volume and is the main disposal zone because it is highly permeable and underlies the producing zones, yet is sufficiently shallow to make drilling of SWD wells relatively inexpensive (Murray, 2015; Walsh and Zoback, 2015). In addition, it is underpressured and therefore has a capacity to accept waste fluids without immediately observable increases in pressure (Murray and Holland, 2014).

Underlying the Arbuckle Group is the basement, which consists primarily of Cambrian sandstone overlying Pre-Cambrian granites and rhyolites that characterize the basement of much of the southern continental interior of the U.S. (Denison, 1981; Murray, 2015). Not much is known about the basement structure, presence of fluid pathways, pore pressure, and other geophysical characteristics, as most of the wells drilled into it are concentrated in areas where they are overlain by petroleum-producing formations and extend into the basement only very shallowly.

1.3 Injection-Induced Seismicity

The phenomenon of induced seismicity has been recognized since the late 19th century as resulting from a variety of activities, including mining, petroleum production involving the withdrawal and injection of fluids into the subsurface, and reservoir impoundment (McGarr *et al*., 2002; Ellsworth, 2013). Over the past three decades, induced seismicity in the United States has been largely attributable to wastewater disposal in porous sedimentary strata (Ellsworth, 2013). Studies show that there are more $M \geq 3.0$ injection-induced earthquakes thought to be a result of SWD wells than as a result of EOR or of fracking wells (Frohlich, 2012; Horton, 2012; Keranen *et al.*, 2013; Keranen *et al.*, 2014; Kim, 2013; Weingarten *et al.*, 2015). This may be because SWD injection causes a net-positive reservoir pressure change whereas EOR and fracking employ injection and extraction operations simultaneously to balance reservoir pressures (Weingarten *et al.*, 2015).

The ability to influence the stress state of the subsurface by injecting fluid may be, in part, a result of the fact that intraplate crust is "critically-stressed." In situ stress measurements from deep drilling and induced seismicity experiments in a variety of tectonic environments support this conclusion (Hubbert and Rubey, 1959; Zoback and Healy, 1992; Brudy *et al.*, 1997; Townend and Zoback, 2000; McGarr *et al.*, 2002). Critically-stressed rock is very close to the point of fracture, and any level of increased stress might cause it to fracture. In addition, critically-stressed faults have high permeability, and the ambient pore pressure is near hydrostatic, facilitating fluid movement (Townend and Zoback, 2000). Fault failure, or slip, can occur because the stress loading on the fault increases, and/or the strength of the fault is reduced. In the case of fluid injection, fault failure can result from four different mechanisms (Rubinstein and Mahani, 2015).

The first mechanism is the increase in pore pressure along a fault, which occurs as injected fluid fills surrounding pores, decreasing the effective normal stress on the fault, reducing the shear resistance, and resulting in fault strength reduction and slip (McGarr, 2002; Segall and Lu, 2015). The second mechanism for fault failure is the interaction between compression or extraction of fluids within pore spaces and solid deformation of host rock that causes poroelastic deformation. A recent study provides evidence for this mechanism by demonstrating that simultaneous injection and extraction (as part of an effort to balance reservoir pressures and prevent induced earthquakes) can actually enhance seismicity rates through poroelastic stressing (Chang and Segall, 2016).

The last two mechanisms are thermoelastic deformation, which results from injected fluid being much colder than the host rock, and the addition of mass to the injection formation by injected fluid, both of which have been studied very little (Rubenstein and Mahani, 2015). Fluid can affect a fault's behavior by one or all of these mechanisms without the fluid having to travel the entire distance from the injection point to the fault, as changes in fluid pressure can be transmitted to farther distances than the fluid itself. While it is thought that direct pore pressure changes are the dominant effect in destabilizing faults, recent work does suggest that poroelastic deformation through the transmission of pressure may contribute a more significant proportion of failure stresses on faults compared to pore pressure increases alone (McGarr *et al.*, 2002; Segall and Lu, 2015; Chang and Segall, 2016; Barbour *et al.*, 2017). This mechanism might result in the effects of fluid injection extending to greater distances than might be expected based on just direct pore pressure changes. Although all of these mechanisms could contribute to well-injection inducing earthquakes, the nature of induced seismicity is largely dependent on the very specific relationships between fault geometry, well operations, and background stressing, which will dictate the failure mechanisms at work in the subsurface (Chang and Segall, 2016).

1.4 Forecasting Injection-Induced Seismicity

Although there exists strong evidence for injection-induced earthquakes in Oklahoma, the specifics of the geophysical mechanisms that result in these earthquakes and their spatial and temporal patterns are less well understood (Ellsworth, 2013; Keranen *et al.*, 2013, 2014; Hough and Page, 2015; Walsh and Zoback, 2015; Weingarten *et al.*, 2015; Petersen *et al.*, 2016, 2017). However, evidence suggests that the Arbuckle Group has a hydraulic connection with the underlying basement rock, as the majority of induced earthquakes in Oklahoma occurr in relatively shallow basement faults below the injecting formation (Walsh and Zoback, 2015). Therefore, pore pressure changes resulting from wastewater disposal in the Arbuckle may propagate to depth, either directly by fluid migration into basement rock or indirectly by poroelastic deformation. Thus, these pore pressure changes may be what eventually triggers injection-induced slip on critically stressed faults in the basement. How long it takes for the increase in pressure to propagate to basement faults is yet unknown and would likely be dependent upon permeability of the injection formation, injection rate, natural pore pressure, the amount of fluid pressure required to trigger fault failure in the injection formation in question, as well as stratigraphy and basement fault characteristics such as their location, orientation, and how close they are to critical failure (Ellsworth, 2013; Holland, 2013; Rubinstein and Mahani, 2015). Higher permeability formations with high natural pore pressure and therefore a lower amount of required fluid pressure to trigger fault failure would be considered to have a higher likelihood of hosting injection-induced earthquakes. Theoretical models can estimate the extent of these effects, but measured data regarding these effects are not currently available to the public, and no in-situ or statistical investigations have been conducted to test these relationships (McGarr *et al.*, 2002). Additionally, fault failure can result not just from an increase in pore pressure along a fault, but also from any of the other three possible mechanisms, which may have a different effect on the spatial and temporal patterns of these earthquakes. It is for these reasons that the ability to forecast which areas are more susceptible to induced earthquakes based on geology and characteristics of injection operations is limited.

1.5 Correlation of Mapped Faults with Induced Seismicity in Oklahoma

Although analysis of the distribution of mapped faults in Oklahoma might seem to be one of the most straightforward indicators of where induced seismicity will tend to occur, such an approach turns out not to be as straightforward as it might seem to be. The Oklahoma Geological Survey (OGS) is building a comprehensive subsurface Quaternary fault database that documents fault locations and orientations from their surface exposures and focal mechanisms of earthquakes that have occurred on them (Figure 8A; Holland, 2013; Darold and Holland, 2015; Marsh and Holland, 2016). The OGS assigns each orientation a likelihood of generating earthquakes in the current stress field as a way to better identify potential earthquake hazards in Oklahoma, with optimally-oriented faults presumed to be the most likely to host earthquakes (Holland, 2013).

As this database has yet to be utilized in investigations of the effect of fault geometry on patterns of induced earthquakes, a preliminary analysis as part of the background for this thesis study is presented here to better understand spatial patterns of these injection-induced earthquakes in Oklahoma as they relate to basement fault locations and orientations. This analysis illustrates that the available fault database is not of sufficient quality to discern whether or not the actual pattern of seismicity confirms the hypothesis that optimally-oriented faults are the most likely to host earthquakes in this environment. Although this hypothesis is, of course, expected to be true in principle, it is not necessarily the case that the mapped fault database adequately represents the complete picture of the orientation of the faults underlying the study area.

These analyses involved sectioning Oklahoma into square grid cells of equal areas and calculating the total number of earthquakes (earthquake density) and total number of optimally-oriented faults (fault density) for each cell (Figure 8). The resulting data are not normally-distributed, and there are some cases of zero values of each variable, so they do not satisfy the assumptions of standard regression (or even the assumptions of non-parametric methods of measuring association, such as the Spearman rank method) necessary to find possible correlation between the two variables (Figure 9). Therefore, an exploratory analysis of this database was the only possibility.

This exploratory data analysis involved separating the grid cells into categories of those with ≤ 20 faults and those with > 20 faults and calculating the frequency of grid cells for different ranges of earthquake densities for each category (Figure 10). If there is any pattern at all, it is a very slight negative relationship between earthquake and fault density, i.e. a (counterintuitively) low percentage of earthquake density is associated with higher fault density values (Figure 9). Even ignoring cells with zero earthquakes, these analyses reveal very little about the possible relationship between faults that have been mapped and induced earthquake frequency, and, if anything, suggest that areas with high densities of optimally-oriented faults have not been shown to be more likely to see more earthquakes (Figures 9 and 10).

These results highlight the fact that the available data may be insufficient for these kinds of analyses, as it includes only faults exposed at the surface and surely excludes an unknown number of active faults that are not exposed at the surface, as is common in these types of fault mapping studies. Additionally, much of the well injection and earthquakes occur north of the densest region of mapped faults, suggesting that many earthquakes in the last several years have been occurring on un-mapped faults or may have occurred along newly formed faults or fractures as a consequence of injection (Figure 8A). Therefore, data on the location, orientation, and density of the naturally-occurring faults in any given area that have been so far mapped are not sufficient for the methods of this project. This negative result is not surprising given the general lack of known correlations between mapped faults and earthquakes (either natural and/or induced) in the CEUS (e.g., Kafka, 2000).

1.6 Other Factors That Affect Injection Induced Seismicity

The reported wellhead pressures, well depths, and different or changing injection rates and volumes of fluid injected into rock are also key parameters regarding injection-induced seismicity, and some work has been done throughout the CEUS to understand spatial and temporal patterns of induced earthquakes in the context of these (Weingarten *et al.*, 2015; Barbour *et al.*, 2017). Current evidence shows no strong correlation between wellhead pressures and the likelihood of injection being associated with earthquakes, nor is there current evidence for a strong correlation between well depth and this likelihood (Weingarten *et al*., 2015). However, this lack of correlation may result from possibly unreliable reported pressures, the inability to couple wellhead pressure data with pore-pressure conditions of the injecting formation, and the lack of detailed stratigraphic knowledge surrounding the injection interval. Changing injection rate and different monthly and annual injection volumes could also affect the likelihood of inducing earthquakes (Weingarten *et al.*, 2015; Barbour *et al*., 2017).

Evidence shows that the likelihood of an SWD well being associated with earthquakes increases with higher injection rates (Weingarten *et al.*, 2015). However, no strong trend of increasing SWD well association as a function of increasing cumulative injected volume (or the total volume injected over the entire lifetime of a well) exists. These results suggest that SWD wells injecting higher volumes in a shorter amount of time are more likely to be associated with seismicity than wells injecting the same volume or less over a longer amount of time. In addition, Barbour et al. (2017) show that a model simulation of a variable rate well (changing its injection rate, in bbls/month, over a period of three years) and a constant rate well (keeping its injection rate constant over the same period), in which the total injected volume is the same for both wells, predicts that variable rate wells experience more than an order of magnitude increase in seismicity rate above background rates compared to constant rate wells.

One last factor to consider is the highly debated possibility that earthquakes, either induced or natural, are fundamentally unpredictable (Main, 1999; Koronovski and Naimark, 2012). It is possible, especially in a critically stressed environment, that very small changes in the stress and/or material properties (from some unpredictable source) at some point on the fault surface could trigger an earthquake. Such a level of complexity in the process means that predicting the causative parameters that result in an induced earthquake and/or whether a specific well was directly responsible for an earthquake outside of some general pattern of spatial and temporal association may be currently out of reach (such as that investigated in this study).

1.7 Spatial and Temporal Patterns of Injection-Induced Seismicity

Just how far in space and time an induced earthquake can be from its associated injection well activity is still an open question. However, Davis and Frohlich (1993) established common criteria for an earthquake induced by wastewater disposal, which include a change from historical seismicity, correlation between injection parameters (such as injection volume and reservoir pressure increases or decreases) and seismicity, proximity to wells, and expected effect of fluid injection on the stress regime. Results of several site-specific case studies agree with some of these criteria and suggest that induced earthquakes are likely to occur very close in both space (within several km) and time (within about a year) to their associated injection wells (Healy *et al.*, 1968; Rayleigh *et al.*, 1976; Hseih and Bredehoeft, 1981; Nicholson *et al.*, 1988; Ake *et al.*, 2005; Horton, 2012; Frohlich *et al.*, 2011; Kim, 2013). More specifically, Davis and Frohlich (1993) along with more recent, broader-scaled studies posit that earthquakes can be considered induced if they occur within about 5-15 km of a well and if that well is actively injecting wastewater at the time of the earthquake (Ellsworth, 2013; Weingarten *et al.*, 2015). Findings from all of these studies therefore motivate the first hypothesis of this study. However, both of these assumptions may not hold true for all cases, as induced seismicity has been found tens of kilometers from injection wells (Keranen *et al.*, 2014) and years to decades after injection has terminated (Herrmann *et al.*, 1981; Keranen *et al.*, 2013).

A case study of the 2011 Mw5.7 earthquake in Prague, Oklahoma suggests that the "time scale considered diagnostic of induced seismicity" necessitates reconsideration because the earthquake occurred nearly 20 years after the initiation of injection (Keranen *et al.*, 2013). Another case study, this time of the 2011 earthquake swarm in Jones, Oklahoma, shows that the swarm was linked to injection and occurred up to 35 km away from the disposal wells, "much further than previously considered in existing criteria for induced seismicity" (Keranen *et al.*, 2014). These findings outline the need for further testing of previously held spatial and temporal assumptions regarding injection-induced seismicity in the CEUS and motivate this study's use of MCS analysis as a new tool for spatiotemporal investigation.

Weingarten et al. (2015) posed similar research questions to those presented here, and one of their objectives involved determining differences in the percentage of wells associated with earthquakes for operationally distinct wells. This study also seeks to determine differences among wells of different parameters, but there are several key differences in the methods, assumptions, and objectives between their study and this one. Weingarten et al. (2015) conducted analyses on all SWD and EOR wells in the CEUS, while this study is limited to SWD wells in Oklahoma. This work involves studying these patterns, in great detail, over a seven-year time period (during which the OCC database is of particularly high quality), while Weingarten et al. (2015) studied wells over a 41 year time span. Additionally, this study uses MCS to investigate whether earthquakes are associated with wells, while Weingarten et al. (2015) used a spatiotemporal filter to find wells associated with earthquakes. Lastly, the crux of these analyses involves testing two spatial and temporal assumptions made by Weingarten et al. (2015) to conduct their comparisons of operationally distinct wells. Their spatial assumption involves the evaluation of a radius of 15 km as a conservative distance from any given earthquake within which a well should be considered as "associated" with that earthquake. They also explored the sensitivity of their results to the choice of radius, using additional radii of 5 km and 10 km. This study provides a parallel exploration of that sensitivity, but uses the MCS method to explore finer details of the effect of distance from the well's location on the likelihood that a well will be associated with seismicity.

The temporal assumption of the Weingarten et al. (2015) study is that wells would be considered to be associated with earthquakes only if the well was actively injecting at the time of the earthquake. This study tests that assumption by investigating the extent of association of both active wells and those that have ceased injection, testing their association with earthquakes that occur in the same year as well as several years later.

The results of these analyses explore whether patterns in space and time indicate higher or lower percentages of earthquakes "near" (in an MCS sense) injection wells and/or close in time to when the wells were initiated and active, while those of Weingarten *et al.* (2015) elucidate differences in the likelihoods of different categories of wells to induce earthquakes given the spatial and temporal assumptions listed above. The use of MCS as a tool for the systematic exploration of spatial and temporal patterns of wastewater injection-induced seismicity in Oklahoma and how those patterns differ among operationally distinct wells should provide complementary insight to the findings of Weingarten et al. (2015).

1.8 Going Forward

Despite some success in discerning which injection parameters and what underlying geology indicate conditions favorable to inducing earthquakes, no comprehensive method can adequately forecast where and under what conditions injection-induced seismicity is likely to occur. This thesis study is, therefore, one attempt at exploring the spatial and temporal patterns of injection wells and seismicity in Oklahoma, in the hope of elucidating the wastewater injection-induced earthquake phenomenon that is currently occurring in that region.

2.0 METHODS

2.1 Oklahoma Disposal Wells

The wells analyzed in this study are disposal wells only, which include SWD, 2D, 2DNC and 2DCm wells from 2010-2016 (acronyms defined in Table A.2.1) and mostly salt water wells from 2006-2009 (refer to Appendix A.1 for further description of these well classifications). Because all of these well types involve saltwater disposal, catalogs in this study reference all wells as SWD. For 2010-2016, monthly values from each well were summed into yearly values, and separate datasets of wells from each year were created. For 2006-2009, wells were also compiled into separate yearly databases, but these years are used only as references for filtering of wells in 2010-2016 for one of the time progression analyses (outlined in section 2.3.4.2) and not as individual catalogs to be used in MCS analyses. This is because the OCC organized well data by fluid type, not well type, during those years, and both SWD and EOR wells inject salt water or brackish water. Therefore, the OCC does not differentiate between SWD and EOR wells for these years. API numbers of wells from the year 2010 that are labeled as EOR and match numbers in the datasets from previous years could be removed, but that does not account for wells that were active from 2006-2009 but inactive in later years. Additionally, records of Class II UIC wells are also believed to be unreliable and incomplete before the year 2009 due to the nature of regulation during that time (Murray, 2014). Therefore, to insure that this study compares across consistent and uniform datasets, it excludes the years 2006-2009 as separate catalogs for analyses.

2.2 Oklahoma Earthquakes

This study uses earthquake data in the state of Oklahoma from the Advanced National Seismic System Comprehensive Earthquake Catalog (ANSS ComCat) run by the U.S. Geological Survey (USGS) according to parameters listed in Table 1. In order to use a catalog that, in theory, contains all earthquakes above a given magnitude in the geographic region of interest (i.e. to maintain magnitude completeness) and to limit the scope to earthquakes more likely to have been induced by wastewater injection as opposed to fracking and extraction, a Gutenberg-Richter analysis was conducted to determine the lowest magnitude at which the values appear to be completely reported (Figure 11). Based on a linear fit to the Gutenberg-Richter relation and the aforementioned criteria, a conservative minimum magnitude of 3.0 was chosen.

2.3 Modified Cellular Seismology Analysis

2.3.1 Original CS and Modification

The original CS method involves plotting two catalogs of earthquakes on a map of a specified region. The first catalog contains "previously-occurring" earthquakes (or the "Pre-CAT"), denoted by "+" signs on the map of hypothetical examples shown in Figure 3. Circles are drawn around these points, and their radius is varied relative to the size of the map area such that the interiors of the circles occupy a given percentage of map area (often 33%, see Kafka 2002, 2007). The second catalog contains "later-occurring" earthquakes (or the "Post-CAT"), denoted by the red crossed circles on the same map (Figure 3). The essence of the original CS method is to systematically explore the extent to which the Post-CAT earthquakes occur "near" the Pre-CAT earthquakes, operationally defined as being within the green zones shown in Figure 3.

In the MCS method, the "+" signs of Figure 3 become the locations of injection wells (referred to as the "Well-CAT"), and the green circles of Figure 3 are zones defined by a given radius surrounding those wells. In this MCS variation, the method involves varying the to test the distance from a well within which an earthquake can be considered to be potentially induced and is not necessarily analyzed in terms of the percentage of map area. The red crossed circles in Figure 3 are earthquakes that occurred at various times after the initiation of injection of wells in the Well-CAT. For this repurposed MCS method, the term "Quake-CAT" replaces the term "Post-CAT", to emphasize the investigation of the relationship between well locations (Well-CATs) and earthquake locations (Quake-CATs). In both CS and MCS, when a Post-CAT (or Quake-CAT) earthquake occurs within a green circle, it is referred to as a "hit." For MCS analyses, any earthquake that is a “hit” would then be considered “potentially induced.” Two examples of actual MCS map analyses from this study are shown in Figure 12 for comparison with the hypothetical examples in Figure 3 and also to show the slight variation in map symbol notation used for the actual analyses. Appendix B contains a more complete set of representative examples of MCS map analyses.

The proportion of hits relative to the total number of Quake-CAT earthquakes is calculated and referred to as the “hit percentage”, which is denoted by $\hat{p}$. This hit percentage is also referred to here as a measure of the “CS Predictability”, which is used here as an operational definition of the extent to which injection wells are associated with induced earthquakes (Chambless and Kafka, 2017). Therefore, higher hit percentages (i.e., higher values of $\hat{p}$) indicate higher CS Predictabilities. Wells in a given catalog that have higher CS Predictabilities then have a higher likelihood of being associated with future potentially induced earthquakes.

2.3.2 Spatial and Temporal Analyses using MCS

The MCS analysis was designed to investigate hypotheses regarding spatial and temporal patterns of different sub-catalogs of wells in Oklahoma that have undergone various modes of filtering and/or cataloging based on various parameters (amended from Chambless, 2015 and Kafka, 2002, 2007). MCS analyses include both “spatial” and “time progression” analyses. Each will be further defined in the sections below, but their purpose is to test different Well-CAT radii and Quake-CAT times after Well-CAT injection year regarding the likelihood of wells in a particular catalog to be associated with future potentially induced earthquakes. The four examples of actual MCS map analyses from this study shown in Figure 12 represent two different Well-CAT radii and two different possible Quake-CAT times after injection for the MCS method.

Before any filtering or categorization, Well-CATs initially include all SWD wells in Oklahoma that are active during a particular year (and might also be active in other years). These exclude wells in Osage county (as they are regulated by the U.S. EPA) and those with recorded injection volumes of zero bbls likely due to errors in compiling these data from Form 1012a (*pers. comm.*, Phillip Bailey). These Well-CATs are created from the yearly well datasets described in section 2.1 and Appendix A.1 and include only the following information: year of activity, API, longitude, latitude, total yearly volume (in bbls), and packer depth (originally reported in feet but converted to meters for these analyses). Because the OCC has not yet compiled and made publicly available the well data for 2017, wells from this year are not used in this study. Quake-CATs were created for each of the years 2010-2017 and include all earthquakes of minimum magnitude 3.0 ($M \geq 3.0$). The earthquake catalog for 2017 is incomplete, as it only includes earthquakes up to 10/20/2017 (Table 1). Table 2 lists the sample sizes of these non-filtered Well-CATs and Quake-CATs.

2.3.3 Spatial Analyses

These MCS spatial analyses test the hypothesis that earthquakes induced by well injection generally tend to occur within at most 15 km from the well(s) with which they are associated (Davis and Frohlich, 1993; Weingarten *et al.*, 2015). These analyses involve calculating $\hat{p}$ values using a Well-CAT of all active SWD wells in Oklahoma from 2010-2015 and progressively later Quake-CATs for up to five years after the Well-CAT year in question for radii of all whole numbers between one and 15 kilometers. The

$\hat{p}$ values, which are inherently cumulative with increasing radius, were then averaged across all Well-CAT years and compared against radius. Various degree polynomial models were initially applied to those plots of cumulative $\hat{p}$ against radius in an attempt to find the inflection points of those curves. That point would, in principle, represent the radius above which $\hat{p}$ values begin to be less dependent on the likelihood of wells in the Well-CAT to be associated with earthquakes and more a product of the larger Well-CAT radius itself. In other words, a large enough radius would result in higher hit percentages that may not necessarily reflect a proportionally higher likelihood of earthquake association. The curve fitting procedure was not able to model the shape of the variation of cumulative $\hat{p}$ against radius, likely because the data did not cover a wide enough range of radius values. Thus, this study analyzed non-cumulative $\hat{p}$ values across the same range of radii for each non-filtered Well-CAT from 2010-2015 and Quake-CATs for up to five years after the Well-CAT year in question without basing the analyses on curve fitting.

These non-cumulative $\hat{p}$ values represent the proportion of hits from the total number of Quake-CAT earthquakes for every 1 km interval between 1 and 15 km. For example, the non-cumulative $\hat{p}$ value for a radius of 3 km is calculated from the number of hits that occur between 2 and 3 km from the injection well. A yearly-averaged non-cumulative $\hat{p}$ was calculated for each radius interval and compared against radius. The primary peaks of these plots represent the distance from the well at which the highest number of hits occurs, and secondary peaks indicate a second, smaller cluster of hits. The distance intervals at which these average primary and secondary peaks occurred as well as the peak $\hat{p}$ values themselves were then compared across time (i.e. the number of

Quake-CAT years after the Well-CAT year) in order to determine if the location of these peaks as well as their average values changed over time.

2.3.4 Time Progression Analyses

The next set of MCS analyses explore how close in time induced earthquakes are to the time the well with which they are spatially associated was active. These analyses are referred to here as "time progression analyses." "Close" has been defined slightly differently by different studies of this topic, but here, it is defined it as within the same year as active injection, i.e. essentially concurrent with injection (Weingarten *et al.*, 2015). Therefore, the hypothesis tested here is that earthquakes associated with injection are more likely to occur within the same year of active injection than to occur in later years. If no relationship between time after well injection and $\hat{p}$ values exists, then earthquakes associated with any particular well site have the same potential to occur during the same year as active injection as they do for several years after injection. This component of the study explores the notion that the effects of injection on inducing earthquakes would presumably decrease as time increases after the injection activity.

For each of the well catalogs created for these MCS analyses, $\hat{p}$ values were calculated for each Well-CAT year and each progressively-later Quake-CAT (0-7 years after active injection, depending on the Well-CAT in question) using radii of 5 and 10 km. These are previously-tested estimates of the distance from wells within which earthquakes are likely to be induced (Davis & Frohlich, 1993; Weingarten *et al.*, 2015). Each $\hat{p}$ value calculated for each of the two radii, then, has an associated MCS map created to determine that value (e.g., Figures 3 and 12 and Appendix B). Two of the maps show wells from 2010 with 5 and 10 km radii and with earthquakes from the same year, and the other two show the same wells but with earthquakes from 2015, which is the year in which seismicity peaked in this region (Figure 2). For all Well-CATs from 2010-2015 and for both radii, these $\hat{p}$ values were compared against time after injection. In order to evaluate evidence of linear trends over time, regression statistics were calculated for each of these radii for all of the Well-CATs from 2010-2012.

2.3.4.1 Non-filtered Well-CATs

The first MCS time progression analysis uses the initial, non-filtered Well-CAT and Quake-CAT data to calculate $\hat{p}$ values. Subsequent MCS analysis create progressively-later Quake-CATs that include multiple years of earthquakes to calculate $\hat{p}$ values for each Well-CAT year. The purpose of creating these multi-year Quake-CATs is to evaluate, in various ways, the effect of time on the potential to induce earthquakes and to further investigate the results from the previous, non-filtered time progression analysis.

2.3.4.2 Filtered Well-CATs

Filtering of Well-CATs for different MCS analyses involves separating well catalogs by activity status, i.e., whether or not a well is active in previous and/or consecutive years relative to the Well-CAT year in question. The initially non-filtered Well-CATs from 2010-2015 underwent different degrees of filtering to spatially and temporally isolate the effects of injection in order to search for other patterns that may have been obscured in the non-filtered catalogs. First, Well-CATs were filtered to include only wells that ceased injection after the Well-CAT year in question and were more than 1 km away from other wells active in that year and consecutive years (referred to as “no post” Well-CATs). However, these Well-CATs include wells that may have been active in previous years or were within 1 km of wells that may have been active in previous years. The $\hat{p}$ values were again analyzed against the series of time-progressive Quake-CATs.

The next MCS time progression analysis involves Well-CATs filtered to include *only wells that were inactive both prior to and after the active year in question* (referred to as "unique year" Well-CATs). Wells within 1 km of any given well in the original Well-CAT that were active outside of the year in question are also filtered out. By removing the effects of injection that occurred before and after the year in question, including the effects of surrounding wells, this analysis of wells active for only one year may better reveal the direct effects of any possible time-dependency of injection-induced seismicity. The $\hat{p}$ values for all "unique year" Well-CATs were compared against the time-progressive Quake-CATs.

2.3.4.3 Categorized Well-CATs

Categorization of Well-CATs involves separating wells by their volume and by depth. The volume values are total annual injection volumes listed in barrels (bbls). The depth values represent depth to the packer. While the packer is not necessarily at the same location as the zone within which injection occurs (i.e. the permitted injected bottom depth), it is generally located directly above or below that zone, and we assume that its depth is an acceptable "proxy" for this permitted injection bottom depth (Murray, 2015). A regression analysis of packer depth and permitted depth to the bottom of the injection zone for wells active in 2015 with recorded depth values above zero supports this assumption (Figure 13). As procedures relating to the packer remain constant through time, this study assumes this relationship is the same for previous years (*pers. comm*, Phillip Bailey). Lastly, the injection bottom depth values represent only permitted values rather than actual measured values, though operators do generally drill up to the permitted depth (*pers. comm*, Phillip Bailey).

The non-filtered Well-CATs were separated by volume ranges to compare tests of the time dependence of the potential for injection wells to induce earthquakes for low versus high volume wells. Low volume wells are defined here as those injecting ≤120,000 bbls/year, and high volume wells are those injecting ≥3.6 Mmbbls/year, based on similar classifications in Weingarten *et al*. (2015). The resulting low volume and high volume Well-CATs were analyzed with the series of time-progressive Quake-CATs. However, the catalog of low volume wells is significantly larger than that of high volume wells, resulting in what might be a "catalog sample size bias". In the original version of CS, radii of circles drawn around Pre-CAT points vary among catalogs so that every Pre-CAT occupies the same percent of the map area (often 33%). In effect, larger catalogs have smaller radii and smaller catalogs have larger radii. In MCS analyses, however, the radius drawn around wells in each catalog remains the same due to our intent of investigating the effect of radius on spatial patterns of induced earthquakes. Therefore, larger catalogs are inherently more likely to produce more hits, for their wells cover a larger percentage of the total map area. In order to correct for this bias, a random sample of low volume wells was extracted for the same number of wells as that of the high volume wells data for each year, and the same MCS analysis was conducted on these sampled low volume Well-CATs. This analysis was then used to compare to the high volume Well-CATs.

Additionally, the non-filtered Well-CATs were separated by depth ranges to compare the time dependence of the potential for injection wells to induce earthquakes for shallow versus deep wells. Shallow wells are defined here as those with packer depths $\leq$ 305 m, and deep wells are those with packer depths $\geq$ 1,220 m. The resulting shallow and deep Well-CATs were analyzed with the series of time-progressive Quake-CATs. However, the same catalog sample size bias exists for the deep wells, as there are more deep wells than there are shallow wells. Again, a random sample was taken from the deep Well-CAT for each year to match the size of the shallow Well-CAT, and the same MCS analyses were conducted.

2.3.5 Further Analysis of Wells Active for only a Single Year

A unique feature of this study is filtering of the injection well database to isolate, as much as possible, the effect of specific well injection on the potential to induce earthquakes. In order to further explore the effects of wells most spatially and temporally isolated from other active wells, both spatial and time progression analyses were performed on a single well from each of the "unique year" well catalogs. Wells from each year that were associated with the highest number of hits within 5 km of that well's location were chosen, out of all the wells in the catalog, to emphasize those wells that are most likely suspected of inducing earthquakes. Following the MCS procedure for spatial analyses, plots for both cumulative and non-cumulative $\hat{p}$ value against radius were made for each Well-CAT from 2010-2015 and each Quake-CAT year after the Well-CAT, as well as a series of MCS maps zoomed in to the well in question.

2.4 Finding Average Trends Across Well-CATs

The frequency distribution of all of the slopes from the time progression regression analyses were then analyzed, and a 95% confidence interval about the mean was calculated to investigate the *overall* trend of hit percentage over time for all well catalogs. Additional analyses were made from frequency distributions of slopes categorized by only those calculated using a 5 km Well-CAT radius, only those calculated using a 10 km radius, only those with a p-value less than 0.2, and only those with a p-value of less than 0.1 in order to fully explore possible deviations from this trend.

Additionally, total changes in hit percentage over the time interval (five to seven years, depending on the Well-CAT year in question) were calculated from all of the time progression regression slopes, and the resulting values were also compiled into a frequency histogram to determine a 95% confidence interval about the mean change over time. Additional histograms were created using only change in $\hat{p}$ over a five year time period, only change in $\hat{p}$ over a six year time period, and only change in $\hat{p}$ over a seven year time period to determine possible differences in that change over different lengths of time.

3.0 RESULTS

3.1 Spatial Analyses

All of the plots of yearly-averaged cumulative $\hat{p}$ values against all whole number radii from 1 to 15 km for non-filtered Well-CATs from 2010-2015 and Quake-CATs of the same year to up to five years after injection generally follow a sigmoid-shaped curve, as a higher map area coverage inherently results in a higher probability of having a hit (Figure 14). While some variation across Well-CAT years exists, each year generally follows the same curve as the yearly-averaged values (Figure C1). No quantitatively-defined inflection points exist in these yearly-averaged plots indicating a definitive “threshold” radius. The quadratic curve fit gave estimates of $\hat{p}$ values that were above 100%, and higher degree polynomial curve fits estimated too much curvature in the fitted function to match the observed curvature. Nonetheless, it is clear from Figure 14 that in all cases 100% hits is reached by about 12 to 15 km. This result is consistent with the general conclusion that injection well induced seismicity generally extends to about 15 km from the associated wells.

In the analogous non-cumulative plots of $\hat{p}$ values against time, however, two peaks correspond to distances from the wells in which the highest number of hits occur (Figure 15). Again, scatter does exist across Well-CAT years, but each year generally follows the same pattern as the yearly-averaged plot (Figure C2). A well-defined peak in $\hat{p}$ of 17.6% occurs at an average of 3.5 km from the injection wells. The secondary peak, which is not as clearly defined, occurs at an average of 11.3 km from the injection wells with an average 4.25%. These results suggest that the most frequently observed distance of spatially associated earthquakes in Oklahoma is between about 2.5 to 3.5 km away from a well, and that between about 10.3 to 11.3 km away from a well, there is another (albeit not as clearly defined) cluster of earthquakes.

In determining whether there was a change in the average peak $\hat{p}$ values and/or a change in the radius at which these peaks occur, evidence shows that the primary peak radius increases exponentially over time and that the primary peak $\hat{p}$ value decreases linearly over time (Figure 16). It also shows that the secondary peak radius increases linearly over time, and the corresponding secondary peak $\hat{p}$ values decrease linearly over time (Figure 17). These results suggest that the MCS method has identified the effects of injection-induced seismicity expanding in distance from the wells over time, and has also identified a decrease over time in the effects of injection on inducing earthquakes.

Generally, a 5 km radius has been regarded in previous studies as the "distance of association", and a 10 km radius has been shown to be an estimate of typical spatial uncertainty in CEUS epicenter locations, and, therefore, 15 km is a more conservative estimate of association distance (Davis and Frohlich, 1993; Weingarten *et al.*, 2015). These estimates of the primary and secondary peaks in $\hat{p}$ match these previous estimates relatively well, but the MCS analysis provides additional detail on the way that this effect varies with distance. Based on the above analysis, the time progression analyses use 5 and 10 km as radii. Refer to Figure 12 for examples of MCS maps that use Well-CAT radii of 5 km versus 10 km.

3.2 Time Progression Analyses

3.2.1 Non-filtered Well-CATs

With variations across non-filtered Well-CATs 2010-2015 and between the two Well-CAT radii of 5 and 10 km, $\hat{p}$ generally decreases from the first to the last year after injection (Figure 18). Linear regression statistics on Well-CAT years 2010-2012 show an average decrease of 1.6%/year for a Well-CAT radius of 5 km and an average decrease of 0.68%/year for 10 km, though all of the r values are low to moderate and the p-values high for these years (Figure 19; Table C1). Over the average period of 6 years for each Well-CAT from 2010-2012, $\hat{p}$ decreases by an average total of 9.1% for a radius of 5 km and by 4.2% for a 10 km radius (Table C1).

Similarly for Well-CATs 2010-2015 and multi-year Quake-CATs, $\hat{p}$ generally decreases from the first to the last year after injection for both radii (Figure 20).

Regression statistics performed on Well-CATs 2010-2012 show an average decrease of 0.71%/year for a 5 km radius and 0.73%/year for a 10 km radius. However, Well-CAT 2011 shows a positive relationship between $\hat{p}$ and time (Figure 21). Generally, the strength and significance of these relationships are high (Table B1). $\hat{p}$ decreases by an average total of 3.2% over an average time period of 6 years for a radius of 5 km and by 3.8% for a 10 km radius (Table B1).

3.2.2 Filtered Well-CATs

For "no post" Well-CATs 2010-2015, it is difficult to see any average change in $\hat{p}$ from the first to the last year after injection for both radii (Figure 22). Regression statistics performed on Well-CATs 2010-2012 show an average decrease of 0.77%/year for a 5 km radius, but an increase of 0.08%/year for a 10 km radius (Figure 23). However, only Well-CAT 2010 shows a negative relationship between $\hat{p}$ and time for both radii, but it is low enough that the average slope is negative for a 5 km radius and close to 0 for a 10 km radius (Table C1). Additionally, all the r values are low to moderate and the p-values high (Table C1). $\hat{p}$ decreases by an average of 5.5% over an average period of six years for a radius of 5 km and by 0.85% for a 10 km radius (Table C1).

For "unique year" Well-CATs 2010-2015, it is again difficult to see any average change in $\hat{p}$ from the first to the last year after injection for both radii (Figure 24). Regression statistics show very weak or no significant linear relationships between $\hat{p}$ and time for Well-CATs 2010-2012 for both 5 and 10 km radii (Figure 25; Table B1). Assuming weak linear relationships with low significance, $\hat{p}$ increases by an average of 0.02%/year for a 5 km radius and 0.07%/year for a 10 km radius (Table C1). Over an averaged period of six years, $\hat{p}$ increases by 0.15% for a 5 km radius and by 0.09% for a 10 km radius (Table C1). This analysis is, of course, not optimal because it is based on very small samples of wells. However, a tradeoff exists here between having to be satisfied with a less-than optimal statistical analysis and what (to our knowledge) is the is the only broad statistical investigation of the effect of unique wells, during unique times of activity, on the potential for inducing earthquakes.

3.2.3 Categorized Well-CATs

3.2.3.1 Volume

For low volume wells ($\leq$120,000 bbls/year), $\hat{p}$ generally decreases from the first to the last year after injection for Well-CATs 2010-2015 for both radii (Figure 26). Linear regression statistics on Well-CAT years 2010-2012 show an average decrease of 2.2%/year for a radius of 5 km and an average decrease of 4.4%/year for 10 km, and the strength and significance of these relationships across Well-CAT years is relatively high (Figure 27; Table C1). Over the average period of six years, $\hat{p}$ decreases by an average total of 14% for a radius of 5 km and by 26% for a 10 km radius (Table C1).

For high volume wells ($\geq$3.6 Mmbbls/year), $\hat{p}$ generally decreases from the first to the last year after injection for Well-CATs 2010-2015 for both radii (Figure 28). Linear regression statistics on Well-CATs 2010-2012 show an average decrease of 2.4%/year for a radius of 5 km and an average decrease of 3.8%/year for 10 km (Figure 29; Table C1). The strength and significance of these relationships is more variable than those of low volume wells, tending toward relatively lower (Table C1). Over an average period of six years, $\hat{p}$ decreases by 13% for a radius of 5 km and by 21% for a 10 km radius (Table C1).

For the random sample of low volume wells, it is difficult to see any average change in $\hat{p}$ from the first to the last year after injection for Well-CATs 2010-2015 for both radii (Figure 30). Linear regression statistics on Well-CATs 2010-2012 show an average decrease of 0.07%/year for a radius of 5 km and an average increase of 0.35%/year for 10 km (Figure 31; Table B1). Only Well-CAT 2010 shows a negative relationship between $\hat{p}$ and time for both radii, but it is low enough that the average slope for a 5 km radius is negative, and the 2011 and 2012 slopes are high enough that the average slope for a 10 km radius is positive (Table C1). $\hat{p}$ decreases by an average of 0.66% over an average period of six years for a radius of 5 km and increases by an average of 1.4% for a 10 km radius (Table C1).

3.2.3.2 Depth

In determining whether the packer is a good proxy for injection depth, analyses show a significant, positive linear relationship between the two, meaning that deeper injection bottom depths correlate with deeper packer depths (Figure 13).

For shallow wells ($\leq$ 305 m to the packer), it is difficult to see a general change in $\hat{p}$ from the first to the last year after injection for Well-CATs 2010-2015 and a 5 km radius, but $\hat{p}$ generally increases for a 10 km radius (Figure 32). Linear regression statistics on Well-CATs 2010-2012 show an average increase in $\hat{p}$ by 0.1%/year for a 5 km radius and by 1.2%/year for a 10 km radius (Figure 33; Table C1). Only Well-CAT 2010 with a 5 km radius showed a decrease in $\hat{p}$ over time. $\hat{p}$ increases by an average of 0.46% over an average period of six years for a radius of 5 km and by 7.5% for a 10 km radius (Table C1).

For deep wells ($\geq$1,220 m to the packer), $\hat{p}$ clearly decreases from the first to the last year after injection for Well-CATs 2010-2015 for both radii (Figure 34). Linear regression on Well-CATs 2010-2012 show an average decrease in $\hat{p}$ by 2.8%/year for a 5 km radius and by 1.6%/year for a 10 km radius (Figure 35; Table C1). Well-CAT 2010 actually shows a decrease in $\hat{p}$ over time, but the other two years have such a high rate of increase with relatively high strength and significance that the average is an increase (Table C1). $\hat{p}$ decreases by an average of 15% over an average time period of six years for a radius of 5 km and by 4.5% for a 10 km radius (Table C1).

For the sample of deep wells, it is difficult to see any average change in $\hat{p}$ from the first to the last year after injection for Well-CATs 2010-2015 for both radii (Figure 36). Regression statistics on Well-CATs 2010-2012 show an average increase in $\hat{p}$ by 1.2%/year for a 5 km radius and by 0.12%/year for a 10 km radius (Figure 37; Table C1). However, there exists considerable variation in the nature of the slopes across Well-CATs 2010-2012, and their strengths and significance are relatively low (Table B1). $\hat{p}$ increases by an average of 8.0% over an average period of six years for a radius of 5 km and by 1.2% for a 10 km radius (Table C1).

3.3 Further Analysis of Wells Active for a Single Year

Plots of yearly-averaged, cumulative $\hat{p}$ values calculated from a single well from each Well-CAT year exhibit a steady increase in hit percentage with increasing radius (Figure 38). However, the curves are not “S”-shaped like the plots of yearly-averaged, cumulative $\hat{p}$ against radius for non-filtered Well-CATs (Figure 14). The $\hat{p}$ values for the single “unique year” wells averaged across Well-CATs do show some indication of leveling-off near 15 km for most of the Well and Quake-CAT combinations, but not to the extent seen in the plots from the non-filtered Well-CATs. This difference for the single wells from the “unique year” Well-CATs might be an artifact of their much smaller sample sizes.

All plots of yearly-averaged, non-cumulative $\hat{p}$ values from the single “unique year” wells show significantly more scatter in spatial distribution with increasing distance from the well than do those values calculated from the non-filtered (and largest) well catalogs (Figure 39). Again, this additional scatter might be a result of the smaller sample sizes for the single “unique year” cases. Maps of a single well from Well-CATs 2010-2015 shown with circles of 5 and 10 km radii and Quake-CAT hits from 2013 to 2017 depict the migration of earthquakes within and around the zones inside the 5 and 10 km radii of the well site (Figures A11-A16). Plots of $\hat{p}$ values against time after injection and the calculated regressions are much the same as those from the “unique year” Well-CAT, as the single wells chosen from each Well-CAT year hosted about 87% of all the total hits hosted within 10 km of wells in the full “unique year” well catalog. They are, therefore, not shown here.

3.4 Comparing Slopes between Two Radii

The two radii of 5 and 10 km were used for all of the time progression analyses to determine if the slope values changed between these two distances, which would suggest a change in the relationship between $\hat{p}$ values and time when considering different distances within which earthquakes are considered to be associated. The linear regressions for the non-filtered Well-CATs from 2010 to 2012 in Figure 19 show that with increasing radius, the negative slopes increase for all years. The regressions calculated for non-filtered Well-CATS and multi-year Quake-CATs show that again the slopes generally increase with increasing distance for all years (Figure 21). Regressions calculated from catalogs of "no post" wells show an increase in slope values with distance for all Well-CATs (Figure 23). The regressions calculated from the "unique year" Well-CATs show an increase in slope with distance for 2010 and 2012 but a decrease in slope with distance in 2011, although those results are based on very low percentage values that are close to zero (Figure 25). The regressions calculated from non-sampled low volume and high volume Well-CATs show a decrease in slope with distance for all years (Figures 27 and 29), while regressions calculated from sampled low volume Well-CATs show a decrease in 2010 but an increase in 2011 and 2012 (Figure 31). Regressions calculated from the shallow Well-CAT show an increase in slope with distance for all years, with Well-CAT 2010 changing from a negative to a positive slope (Figure 33). For the non-sampled deep Well-CAT 2010, the slope decreases with distance, and for 2011 and 2012, the slope increases with distance (Figure 35). Finally, the sampled deep Well-CATs, regression analyses show a change from a positive to a negative slope for 2010, a decrease in slope for 2011, and a change from a negative to a positive slope in 2012 (Figure 37).

3.5 Finding Average Trends Across Well-CATs

The above results show considerable scatter in the relationship between $\hat{p}$ values and time and that the implied change is both slow and variable across wells of different conditions, ranging from a total decrease of 26% to a total increase of 8% over the five to seven years covered by this study. Nonetheless, within that scatter is a subtle but consistent signal of a general decrease in CS Predictability over time after well injection.

Although analyzed in different ways for different selection criteria, frequency histograms of various categories of linear regression slopes (Figures 40-42) all show a negative mean slope, with the 95% confidence interval bounds not including zero. These results suggest that any given well's likelihood of being associated with earthquakes decreases over time. For all time progression analyses, the average decrease in $\hat{p}$ is 5.4% over a period of five to seven years (Figure 43), or an average of 0.93% decrease per year (Figures 40-42).

4.0 DISCUSSION

This study explores the use of MCS to investigate spatial and temporal patterns of possible induced earthquakes by evaluating their occurrence in space and time around Class II SWD wells listed in the Oklahoma well database. By separating wells into catalogs of various activity status and operational parameters, these analyses also explored patterns among different classes of wells to determine how specific characteristics of injection might be used to forecast the extent over time to which earthquakes are associated with activity of injection wells, represented by the "CS Predictability," $\hat{p}$.

These analyses across the different catalogs of wells have revealed general patterns of CS Predictability over space and time. Spatial analyses show that, on average and at any given time up to 5 years after the start of injection, earthquakes are most likely to occur (or have the highest CS Predictability) 2.5-3.5 km from any given well (Figure 15). The distance at which the primary peak occurs increases exponentially over time, and the primary peak $\hat{p}$ values decrease linearly over time (Figure 16). However, there are only six years over which to fit a curve to the data, and the radius does not begin to increase until four years after the initiation of injection. Therefore, a database including more time between the Well-CAT and Quake-CAT would be necessary to determine if this change in distance from the well at which the primary peak in $\hat{p}$ occurs over time is actually exponential. Considering, however, that the radius of this primary peak increases and that the primary peak $\hat{p}$ values decrease with time after injection, this suggests that the distance of the primary peak CS Predictability not only migrates farther from the well over time, but the extent of a given well's association with earthquakes at that distance also decreases.

For the time progression analyses, evidence generally shows a lot of scatter in the relationship between CS Predictability and time after any given Well-CAT year. However, the amount of scatter and the nature of this relationship (i.e. the rate of change and the direction of the slope) varies among different well catalogs and different Well-CAT years (from 2010-2012). Analyses show some indication within those highly scattered results that the percentage of associated earthquakes decreases (on average) as a function of time such that the percentage of associated earthquakes generally decreases by about 0.9% per year (Figure 40), or about 5.4% over a period of five to seven years for any given well (Figure 43). These results agree with those of the spatial analyses, as the CS Predictability of any given well catalog is expected to slowly decrease over time (Figure 16).

In examining how the relationship between CS Predictability and time would change when considering a greater distance from the well within which earthquakes are considered to be "hits", the slope values calculated from the time progression regressions for all Well-CATs from 2010 to 2012 using a 5 km radius were compared to those using a 10 km radius (which, in these cases, include *all* earthquakes within these radii). Evidence shows that the majority of time progression analyses (18 out of 30, or 60%) show an increase in the slope of the linear relationship between CS Predictability and time with increased distance from the injection well (Table C1). This suggests that at farther distances from the well, CS Predictability may either decrease at a slower rate or increase at a faster rate over time. For two instances, CS Predictability decreases over time at 5 km from the well, but increases over time at 10 km from the well (Table C1). This majority also agrees with the fact that the slope of the linear regression of secondary (i.e., further from the well) CS Predictability peaks is higher than that of the linear regression of primary (i.e., closer to the well) CS Predictability peaks (Figures 16 and 17). However, this change in relationship with distance is for a small majority of cases (i.e., 60%), as a significant number of Well-CATs (12/30, or 40%) show a decrease in the slope with increased distance. It is therefore still difficult to attribute an overall trend in how this relationship changes with distance. Additionally, the average r value (i.e., a measure of the amount of scatter in the relationship between CS Predictability and time) is approximately 0.48 for a Well-CAT radius of 5 km and is approximately 0.54 for a 10 km radius, suggesting that the strength of the relationship increases with distance (Table B1). These results suggest that, after about five to seven years, the effect of injection inducing earthquakes begins to abate within 5 km of any given well, but not necessarily within 10 km, and that there exists less scatter in the relationship over time when considering greater distances within which an earthquake can be considered induced.

In specifically comparing the relationships between CS Predictability and time of well injection activity for different operational parameters, differences in wells of different volumes and depths exist, averaged over Well-CAT years 2010 to 2012. For a 5 km radius, the high volume wells experienced a slightly higher rate of decrease in CS Predictability over time than did the low volume wells (Table C1). However, for a 10 km radius, high volume wells experienced a lower rate of decrease than the low volume Well-CATs. The sampled low volume catalog experienced a much smaller rate of decrease than did the high volume catalog for a 5 km radius, and it actually showed an increase in CS Predictability for a 10 km radius (Table C1). In comparison to both the sampled and non-sampled low volume catalogs, the high volume catalog shows more scatter in the relationship between CS Predictability and time. Additionally, the $\hat{p}$ values for the sampled low volume catalog are lower than those of the high volume catalog, which suggests that low volume wells have a lower CS Predictability in any given year after injection than do high volume wells. The need to use sampled data for low volume wells (to avoid a sample size bias) may bias these results regardless. However, this approach was necessary to properly apply the statistical comparison analysis.

In comparing the change in CS Predictability over time for shallow and deep wells, the difference is greater than observed for low versus high volume wells. For both 5 and 10 km radii, shallow wells exhibit an average increase in CSP over time, but a decrease over time for deep wells (Table C1). Additionally, that decrease occurs at a higher rate than the increase over time for shallow wells. On the other hand, for the sample of deep wells, evidence shows an increase over time, but at a higher rate than shallow wells for a 5 km radius and a lower rate than shallow wells for a 10 km radius. Lastly, $\hat{p}$ values for the sampled deep well catalog are generally higher than those of the shallow well catalog, which suggests that deeper wells have a higher CS Predictability in any given year after injection than do shallow wells. This seems intuitively reasonable, because the deeper wells are closer to the zones at depth where most of the earthquakes are occurring and thus would be expected to be more likely to induce earthquakes.

In order to discern further structure that might be occurring in this temporal pattern, the effects of specific well injection on the potential to induce earthquakes were isolated by filtering the catalog of wells such that only wells uniquely active for one year were analyzed. The characteristics of wells in this catalog were further narrowed by also filtering out wells that were within 1 km of other wells active in previous or consecutive years. This was done in an effort to, as much as possible, isolate the direct effects of well injection on inducing earthquakes. Only a very low percentage (<1%) of earthquakes in the database were found to be directly associated with the wells in this "unique year" catalog, and only one or two wells in each of the Well-CATs were associated with earthquakes, as shown by some of the MCS maps from the time progression analyses (Figure B3). While the regression calculations for this catalog show no significant linear relationship for $\hat{p}$ values over time (Figure 25), each catalog, especially in 2010, does not host hits until at least a year after the start of injection. The $\hat{p}$ values peak at some year after the start of injection and then decrease back down to either zero or a lower $\hat{p}$ value. Furthermore, qualitative evidence shows this pattern of a peak (or multiple peaks) and then a subsequent decrease in $\hat{p}$ at least a year after the start of injection in several of the other time progression regression plots. Even in analyses establishing a significant linear relationship, like the regression statistics calculated on the deep Well-CAT 2011 for 10 km (Figure 32), this pattern of a lag and then peak in CS Predictability can be observed. The selection of one well from each "unique year" Well-CAT from 2010 to 2012 on which to perform spatial analysis does not show a distance at which the majority of associated earthquakes occur, and maps in Figures B10-B15 do not qualitatively show any particular spatial distribution pattern over time. These results may be a product of the small sample size, and a larger sub-catalog of “unique year” wells is necessary to find overall spatial and temporal patterns for these isolated wells.

5.0 CONCLUSIONS

This exploration of earthquakes associated with injection wells in Oklahoma has revealed a few key spatial and temporal patterns, both generally (i.e. for any type of injection well operational parameters) and specifically for wells of certain operational parameters. Evidence shows that while any earthquake within 15 km of a well is considered (as previously found by others) to be associated with injection from that well, the majority of these associated earthquakes occur within about 2.5-3.5 km of any given well. Evidence also shows that this peak distance begins to increase three years after the start of injection, while the CS Predictability at these peak distances decreases over time, suggesting that the effect of injection may migrate farther from the well over time at the same time that the overall effect of injection decreases.

On average across all well catalogs, any given well’s likelihood of being associated with an earthquake (i.e., its CS Predictability) within 5 or 10 km of the well slowly decreases over time (by ~1%/year), though the nature of this relationship among the different well catalogs exhibits a relatively high amount of variability. For most well catalogs, this relationship also tends to change when considering associated earthquakes at a greater distance (i.e. 10 instead of 5 km). However, it cannot be said with confidence whether or not this change in CS Predictability over time tends to increase or decrease with distance from any given injection well in any given subset of cases, as only a small majority (about 60%) indicated an increase in the change in CS Predictability over time.

In support of previous claims that high volume wells increase the probability of inducing an earthquake, evidence shows that low volume wells are less likely to be associated with earthquakes than high volume wells (Figures 28 and 30; Ellsworth, 2013; Weingarten *et al.*, 2015). Analyses have also suggested that deep wells are more likely to be associated with earthquakes than are shallow wells (Figures 32 and 36). Lastly, analyses on the most spatially and temporally isolated wells reveal that there may be a lag of at least a year before any given well is likely to be associated with earthquakes, and that this lag can be observed qualitatively in the plots of $\hat{p}$ over time for other cases of wells analyzed.

These spatial and temporal patterns for wells of various operational parameters have been elucidated through the exploration of these larger-scale spatial and temporal patterns of wastewater injection-induced earthquakes in Oklahoma. The amount of scatter in these results necessitates more of these MCS analyses using more Well-CAT years and longer Quake-CAT times after injection in order to determine how these patterns hold up when analyzing over longer periods. However, this study has shown that, within the very scattered and variable pattern of injection wells and earthquakes in Oklahoma, a subtle signal exists indicating underlying process of fracking-related wastewater injection inducing earthquakes. Most significantly: 1. The induced earthquakes appear to be primarily occurring between 2.5 to 3.5 km from any given well. This distance appears to increase over time with continued injection activity, and the associated CS Predictability generally decreases over time, 2. The potential of any given well to induce earthquakes decreases by an average of about 1% per year or by about 5% over five to seven years, 3. High volume and/or deeper wells have an overall higher potential of being associated with induced seismicity than low volume and/or shallower wells, and 4. Evidence exists for a lag of at least a year before a spatially and temporally isolated well is associated with earthquakes. Extracting this signal from the noise, however, required the very high quality database available for Oklahoma (a level of quality that is not generally available elsewhere). Thus, while it is clear that fracking-related well injection is inducing earthquakes, unravelling the specifics of the process by which that is happening will remain a major challenge.

6.0 TABLES

Table 1. The geographic area and criteria for earthquakes analyzed in this study. *Data from the ANSS ComCAT run through the USGS Earthquake Hazards program.*

OKLAHOMA EARTHQUAKE CATALOG	
Parameter	**Value**
Geographic coordinates (in decimal degrees)	Northern boundary: 37.000 °N Southern boundary: 33.797 °N Western boundary: 102.063 °W Eastern boundary: 94.439 °W
Minimum Moment Magnitude	3.0
Minimum Depth (in km)	0
Start date	01/14/2010
End date	10/20/2017

Table 2. Number of wells in each Well-CAT and the number of earthquakes in each Quake-CAT from 2010-2017. Well-CATs include only wells active in OK (reporting injection volumes >0 bbls) during that year. Quake-CATs include all earthquakes of M≥3.0 in OK.

WELL AND QUAKE-CAT SIZES							
	Quake-CAT	Non-Filtered	"No Post"	"Unique Year"	Low Vol	High Vol	Sampled Low Vol
Year	# of EQs in Quake-CAT	# of wells in Well-CAT					
2010	41	3312	393	13	2419	37	37
2011	63	2569	47	2	1804	27	27
2012	35	2846	59	3	1942	34	34
2013	103	2888	70	5	1873	54	54
2014	585	2949	138	6	1865	75	75
2015	888	2686	213	7	1647	84	84
2016	639	N/A	N/A	N/A	N/A	N/A	N/A
2017	214	N/A	N/A	N/A	N/A	N/A	N/A
	Quake-CAT	Shallow	Deep	Sampled Deep			
Year	# of EQs in Quake-CAT	# of wells in Well-CAT					
2010	41	402	674	402			
2011	63	283	597	283			
2012	35	301	733	301			
2013	103	285	793	285			
2014	585	295	854	295			
2015	888	27	445	27			
2016	639	N/A	N/A	N/A			
2017	214	N/A	N/A	N/A			

7.0 FIGURES

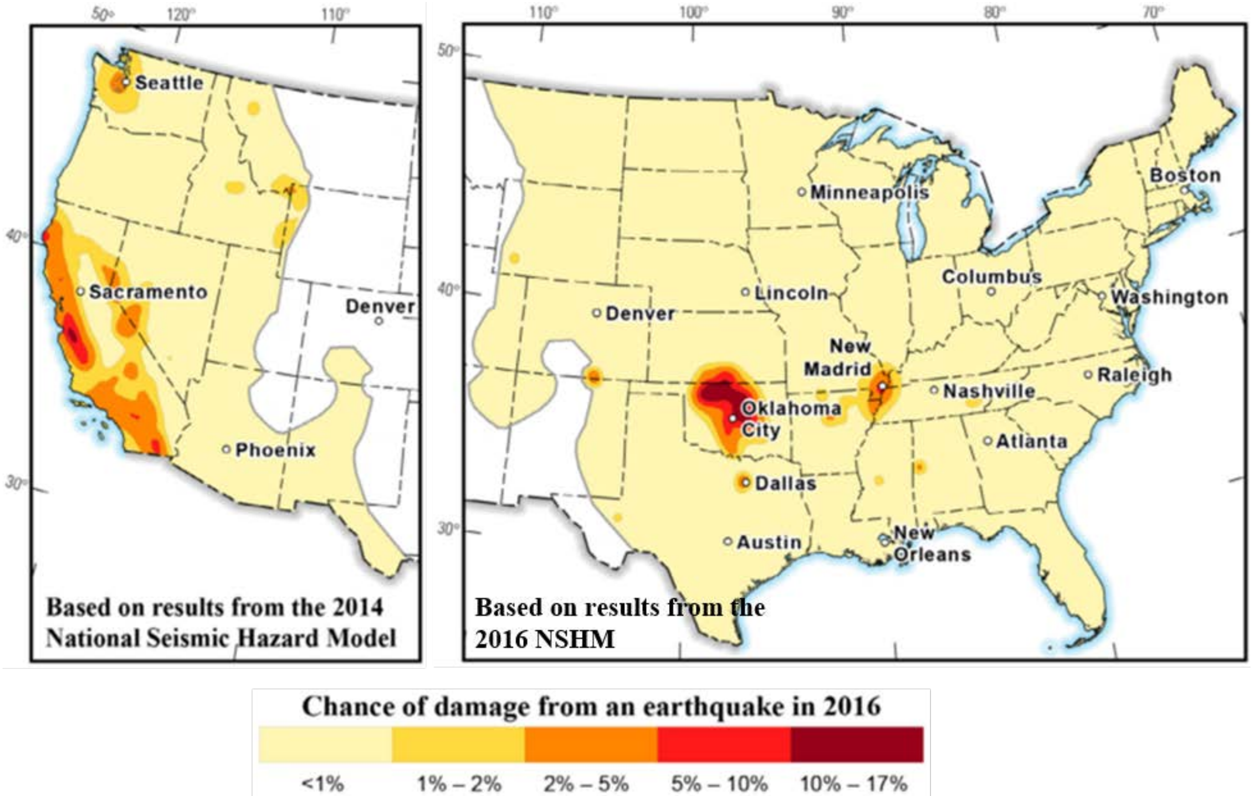

Figure 1. National Seismic Hazard Map (NSHM) displaying the forecasted chance of damage from an earthquake in 2016 based on peak ground accelerations. The left portion is based on results from the long-term 2014 NSHM model that includes data from only natural earthquakes. The right portion is based on results from the 2016 1-year NSHM model that includes data from both natural and induced earthquakes. *Figure modified from Peterson et al., 2016.*

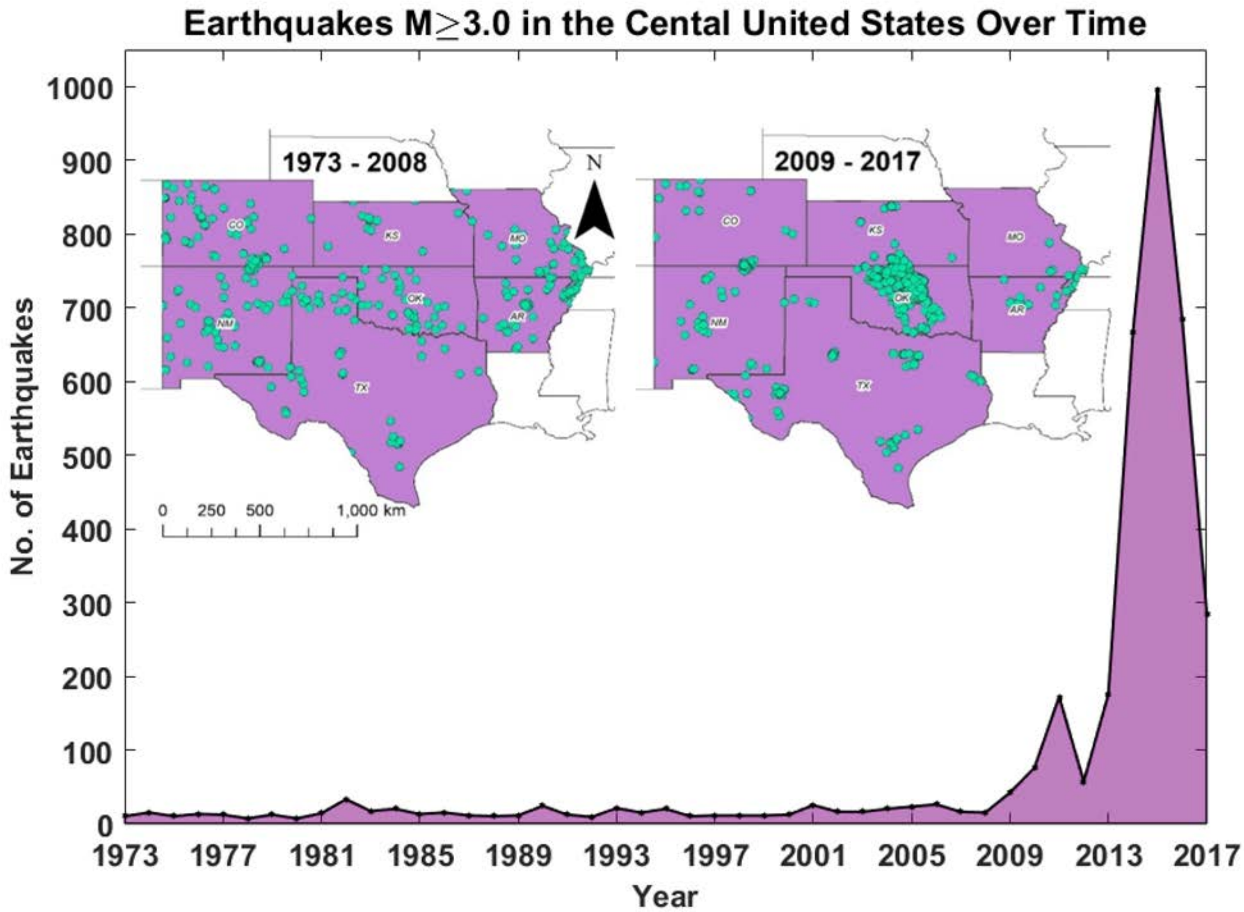

Figure 2. Annual frequency of earthquakes of M≥3.0 that have occurred in the Central United States (CUS) from 1973 to 2017. States included in this plot are highlighted on the map in purple. Earthquakes (teal dots) from 1973 to 2008 are shown on the left map, while those from 2009-2017 are shown on the right. *Data are from the ANSS ComCat.*

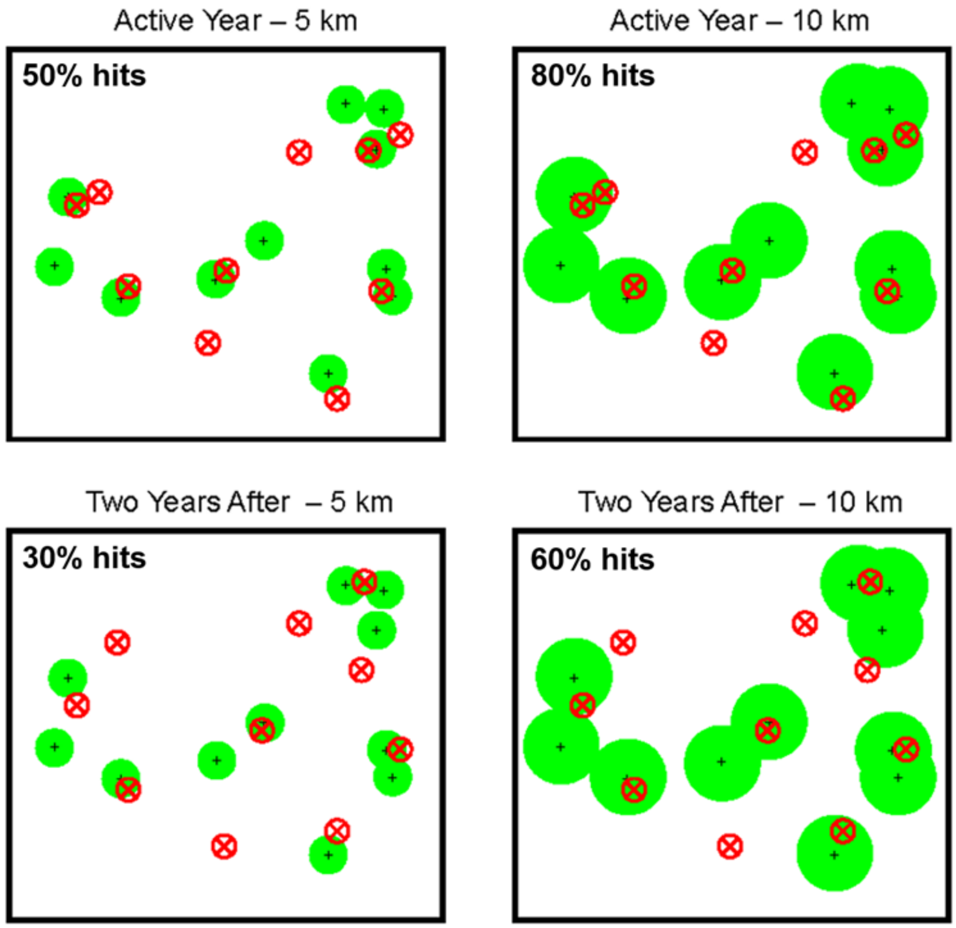

Figure 3. Hypothetical illustration of how this study repurposed the "Cellular Seismology" (CS) method and representation of the layout of MCS maps for each set of analyses in this study. For the MCS method, the "+" signs are locations of injection wells (referred to as the Well-CAT), the filled green circles are zones (defined by a given radius) surrounding those wells, and the open circles with "x" signs are the "Quake-CAT" earthquakes that occurred at various times after the initiation of injection at well locations in the Well-CAT. When a Quake-CAT earthquake occurs within a green Well-CAT zone, it is referred to as a "hit." The four hypothetical situations shown here represent different Well-CAT radii (5 and 10 km) and different Quake-CAT times after injection (earthquakes that occurred one year and two years after injection) for the MCS method. Hit percentages, or the number of hits over the total number of earthquakes, are also shown. This figure uses red crossed circles (as opposed to the red dots used in the actual MCS analyses) as better visuals for understanding and calculating hypothetical hit percentages.

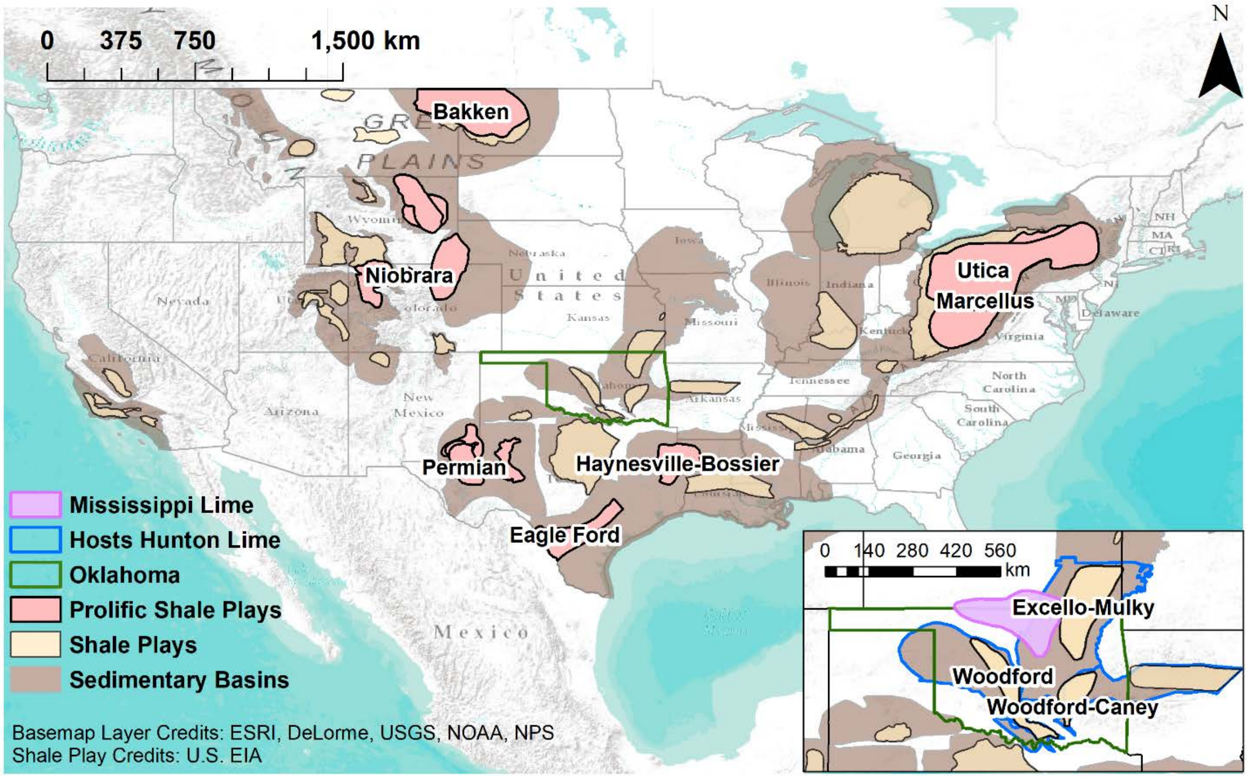

Figure 4. Map of all current tight oil and gas shale plays and sedimentary basins in the lower 48 states of the U.S (last updated June 2016). All sedimentary basins within which shale plays are found are shown in brown, and shale plays are shown in beige. The seven most prolific plays, according to the U.S. EIA, are highlighted in light pink and labeled by name. In addition, Oklahoma is outlined in green, and an enlarged image of the reservoirs in this state are shown in the lower right corner of the map. The main shale plays are labeled, and the sedimentary basins (Anadarko, Ardmore, Arkoma, Cherokee Platform, and Marietta) that also contain a conventional reservoir, the Hunton Lime, are highlighted in blue. Additionally, the Mississippi Lime, another conventional reservoir, is shown in purple. *Credits for base map and shale play data are given in the lower left corner of the map. Information on limestone reservoirs in OK is from Rottman et al., 2000.*

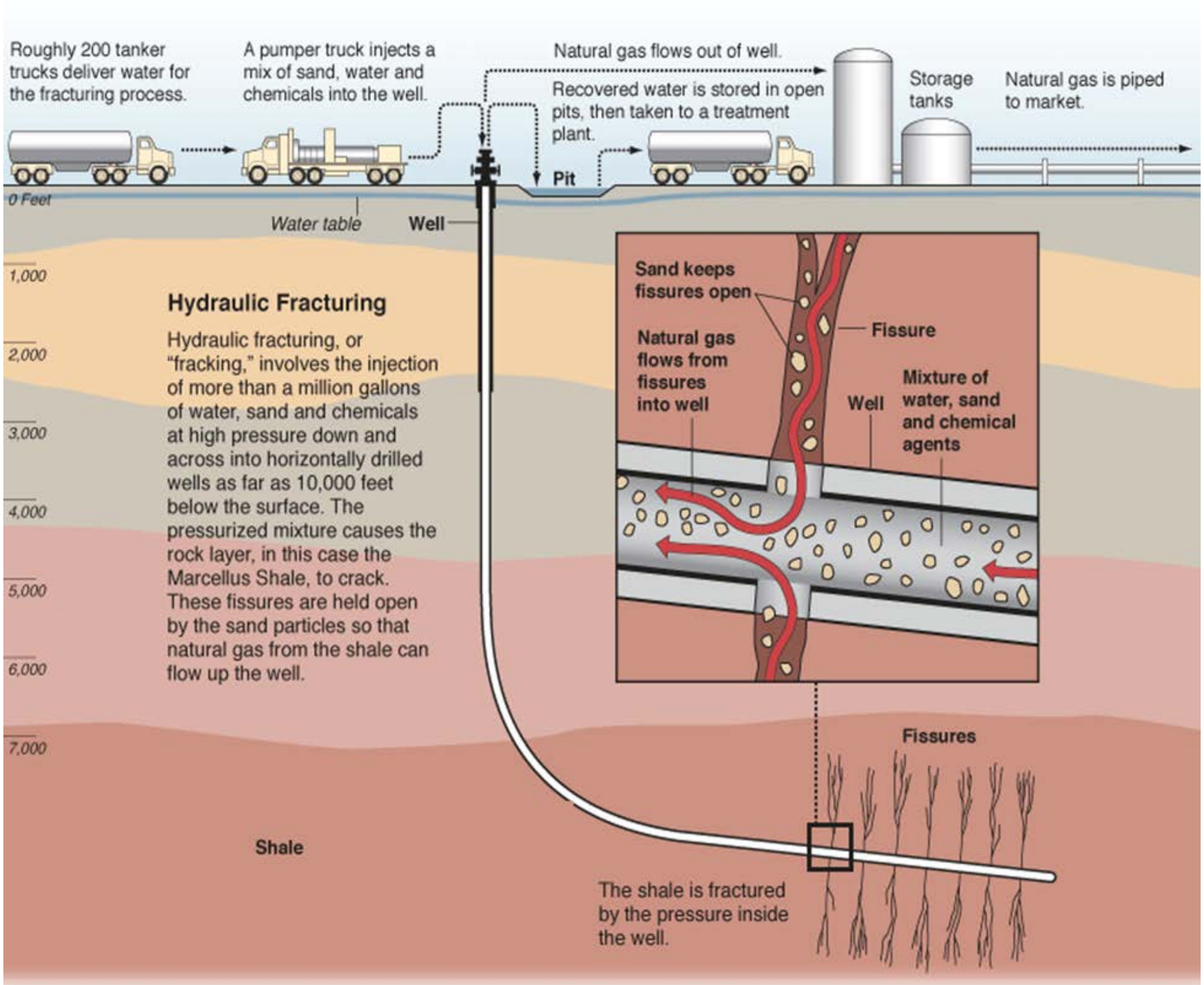

Figure 5. Diagram outlining the use of unconventional, horizontal fracking to extract tight oil and gas reserves in shale plays, with text explaining each step of the process. After operators recover oil and gas from the well, they store the produced water in open pits until it is later later taken to a treatment plant or, most often, taken to other sites to be re-injected into the subsurface by salt water disposal (SWD) wells.
Figure edited from https://www.propublica.org/special/hydraulic-fracturing-national.

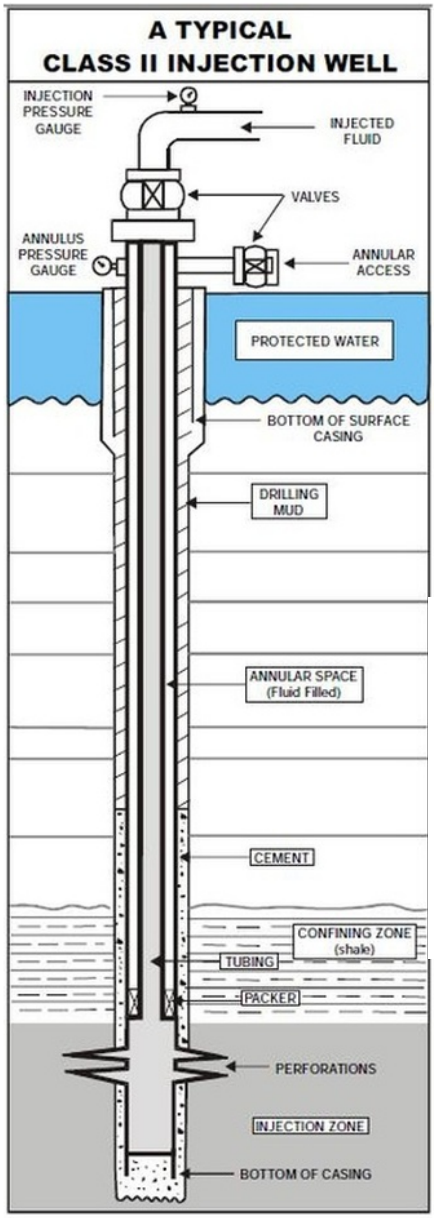

Figure 6. Diagram of a typical Class II SWD injection well (left). Photograph of a Class II injection well in Oklahoma (above) *Diagram taken from* http://www.highlanddiw.com/disposal-injection-well-construction.html. *Photograph taken from* http://kfor.com/2016/01/25/report-oklahoma-disposing-oil-wastewater-for-other-states/.

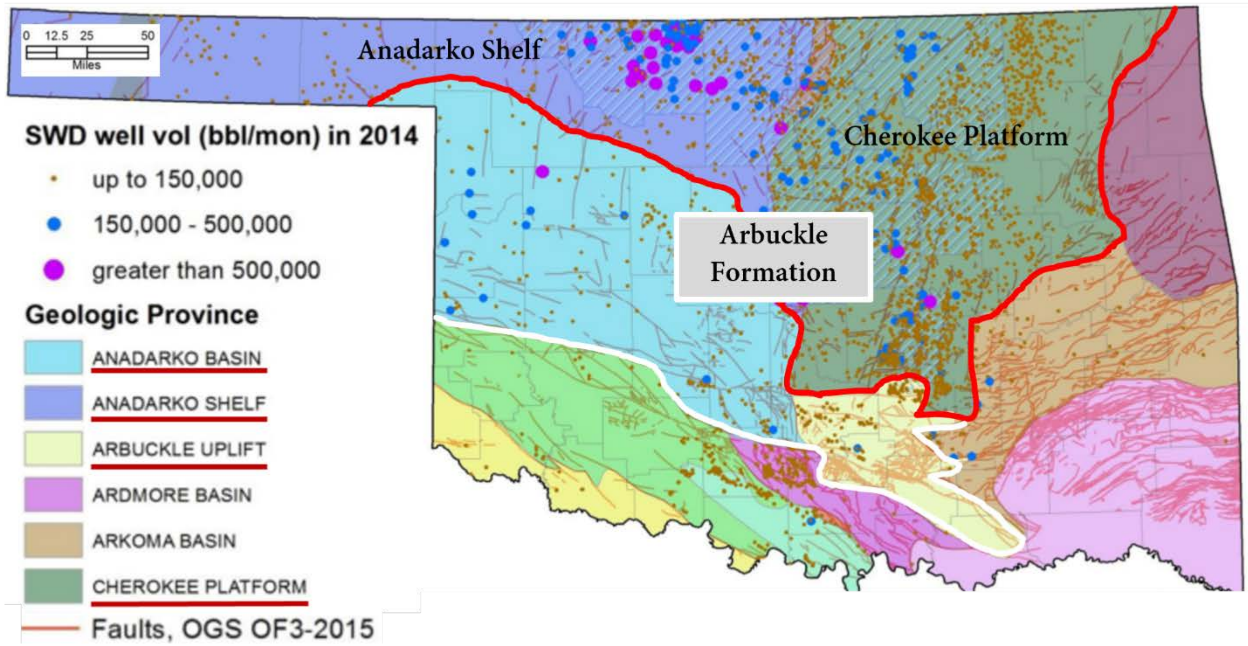

Figure 7. Main geologic provinces in Oklahoma overlain by points marking SWD well locations and lines marking known basement fault locations. The Arbuckle Formation, which is a sedimentary basin and the main disposal formation in the state, is located within the provinces outlined in red and white. The majority of SWD wells are located within the Anadarko Shelf and Cherokee Platform, outlined in red on the map, though the formation extends down to the Anadarko Basin and the Arbuckle Uplift, outlined in white on the map. These geologic provinces of the Arbuckle Uplift are also underlined in the legend. *Figure is edited from Murray (2016).*

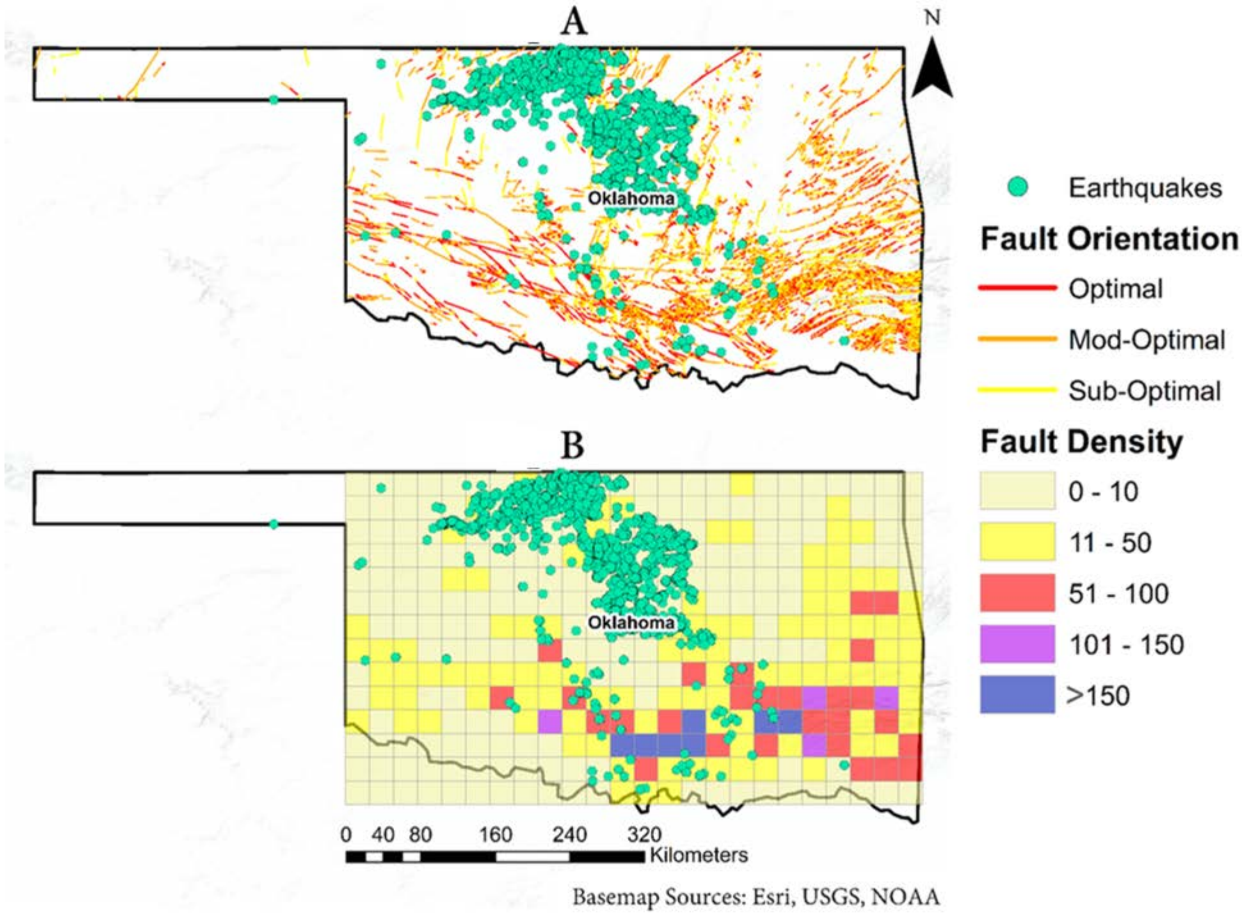

Figure 8. (A) Earthquakes in Oklahoma of M> 3.0 from 3/17/1974 to 4/07/2017 and all Quaternary active basement faults in Oklahoma that have surface exposures. The faults in this database were located and characterized from 688 focal mechanisms calculated between 2010 and 2015 as well as mapped surface exposures and focal mechanisms from previous studies. Their azimuths were calculated in order to determine their likelihood of having an earthquake within the contemporary stress field (N85°E). Faults optimally-oriented for slip (red) have azimuths 45°-60°, 105°- 120°, and 135°-150°. Those moderately optimally-oriented for slip (orange) have azimuths 15°-45°, 60°-75°, 90°-105°, and 120°-135°. Those sub optimally-oriented for slip (yellow) have azimuths 0°-15°, 75°-90°, and 150°-180°. **(B)** Oklahoma divided into grid cells of equal area (~103 km^2). Grid cells are symbolized by the number of optimally-oriented faults within them. The same earthquake catalog from Map A is also shown in Map B. *Earthquake data for these maps were taken from the ANSS ComCAT, and fault data were taken from Darold and Holland, 2015.*

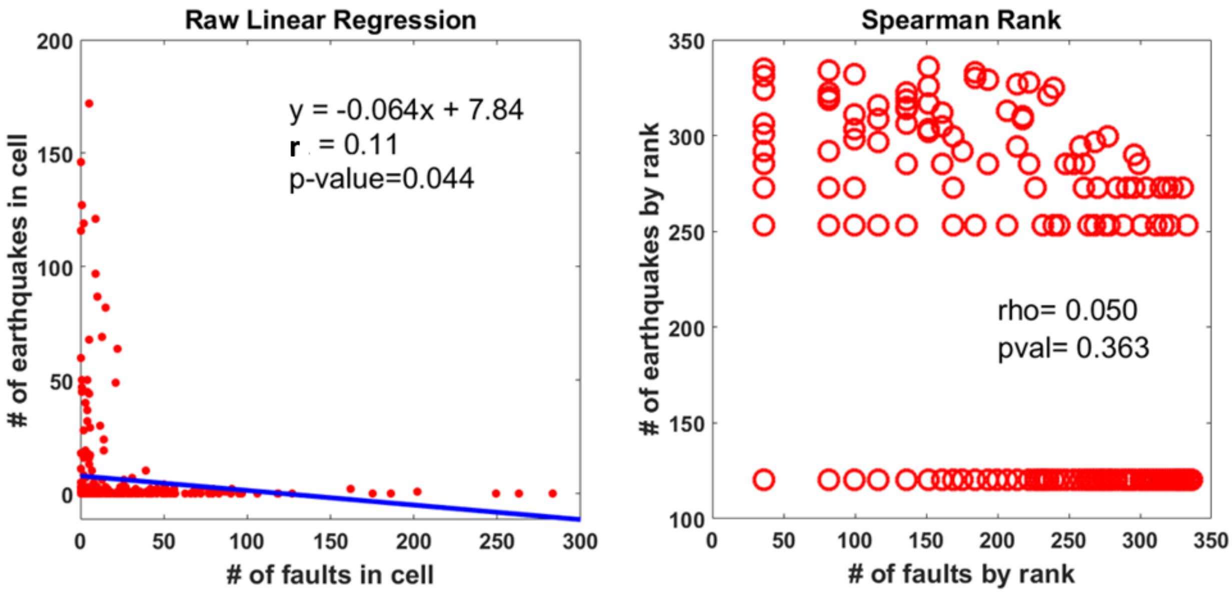

Figure 9. The number of earthquakes in each grid cell, i.e. earthquake density, against the number of faults in a cell, i.e. fault density (left). A linear regression analysis was performed on these data, and the best-fit line (in blue), its equation, the correlation coefficient (R) and statistical significance (p-value) are shown on the plot as well. The plot on the right shows the non-parametric analysis of correlation, with ranked earthquake density plotted against ranked fault density. The Spearman rank correlation coefficient (rho) and p-value were calculated and shown on the plot as well. *Data from the ANSS ComCat from the USGS and Darold and Holland (2015).*

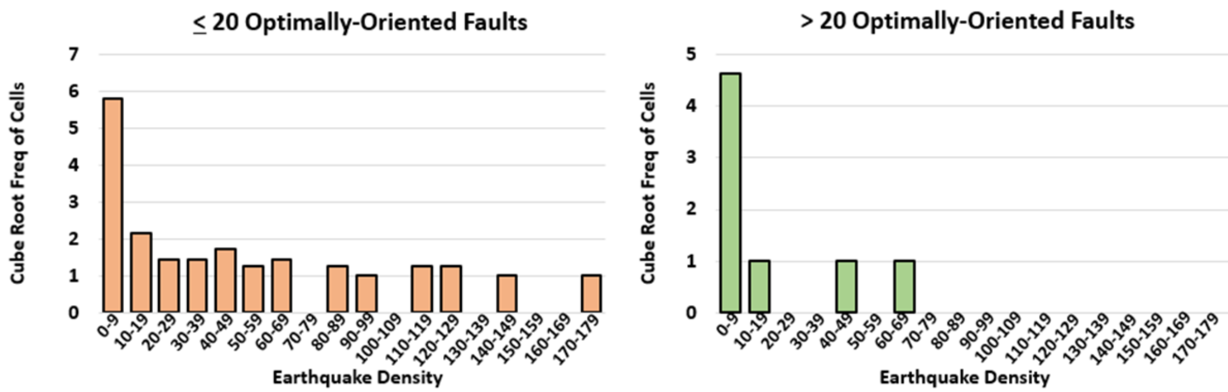

Figure 10. Frequency histograms of the cube root of the number of cells with a particular range of earthquake density for cells with ≤ 20 optimally-oriented faults (histogram on the left) and for cells with > 20 optimally-oriented faults (histogram on the right). The cube root of the frequency was calculated in order to better visualize the histograms, and to avoid problems with transformation to log (frequency) when some of the values are zero.

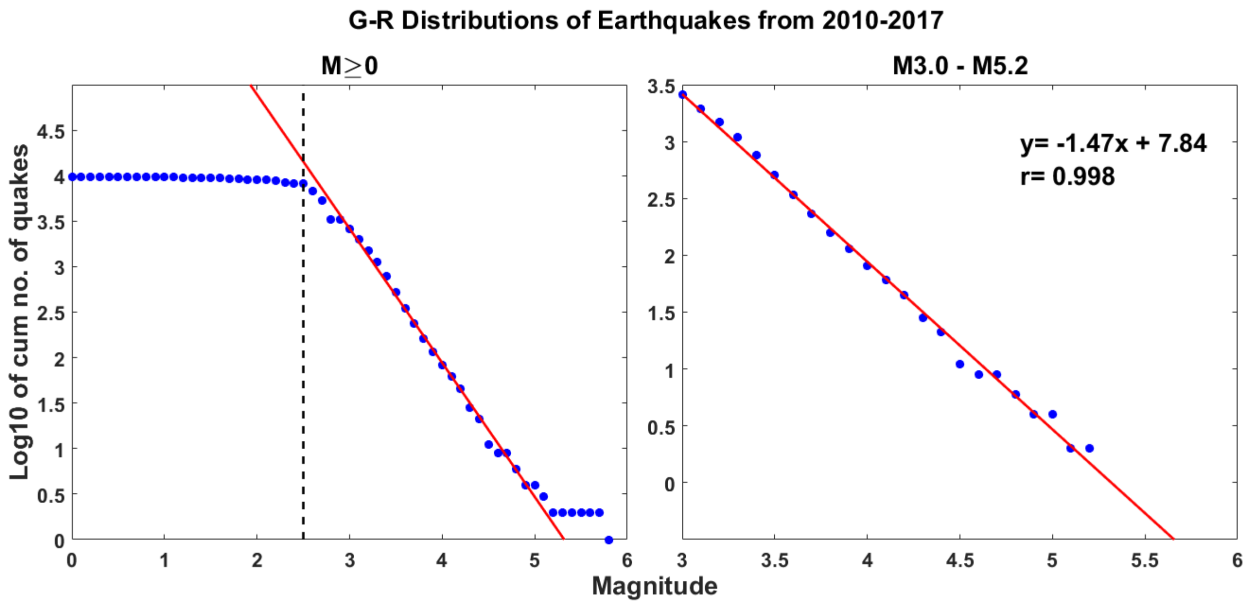

Figure 11. Gutenberg-Richter distributions of two different catalogs of earthquakes in Oklahoma from 2010-2017. On the left is a catalog of earthquakes of M≥0, and on the right is a catalog of earthquakes of M≥3.0. The linear regression for the M≥3.0 catalog distribution is shown as a red line in both plots, and the statistics are shown in the right plot.

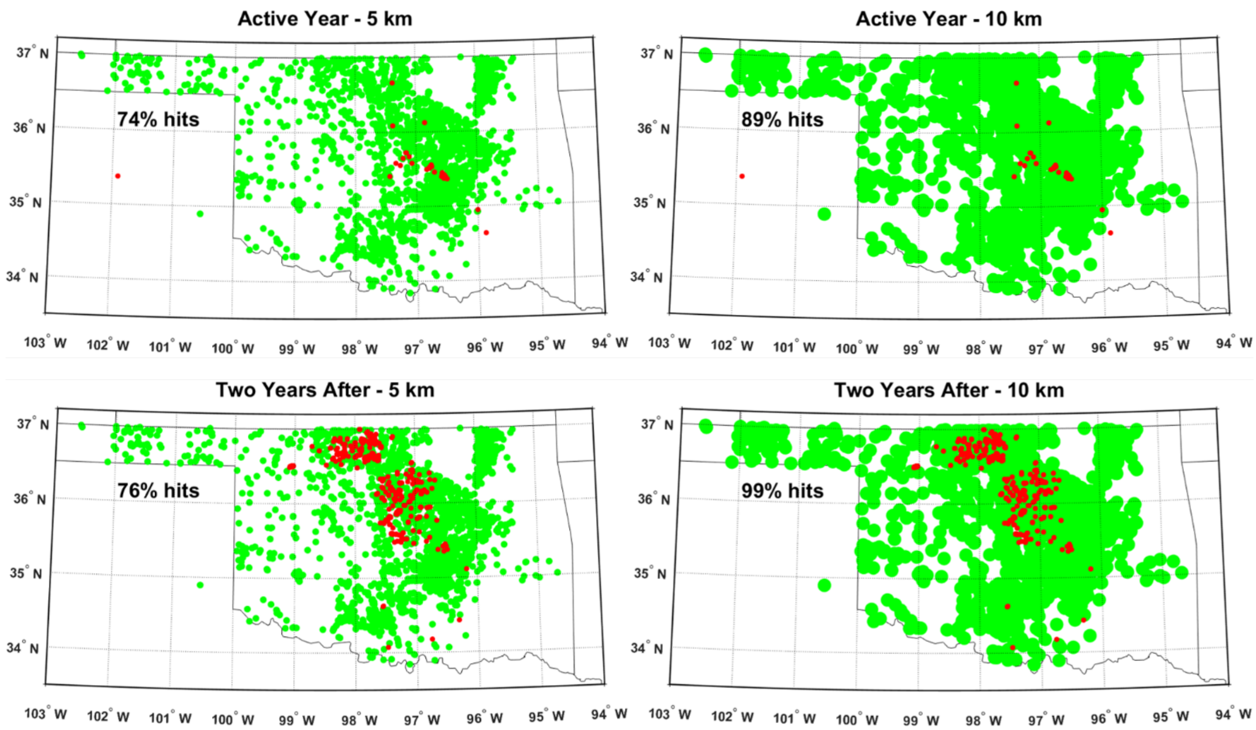

Figure 12. Representative examples of MCS maps from this study using the non-filtered Well-CAT from 2012 and Quake-CATs from 2012 (top two maps) and 2014 (bottom two maps). Maps were made using Well-CAT radii of 5 km (left two maps) and 10 km (right two maps). The layout of this figure is the same as that of Figure 3, but the symbols used in our MCS analyses for the Quake-CATs are red dots, while those used for the hypothetical example in Figure 3 are red crossed circles. The red crossed circles were used as better visuals for understanding and calculating hypothetical hit percentages.

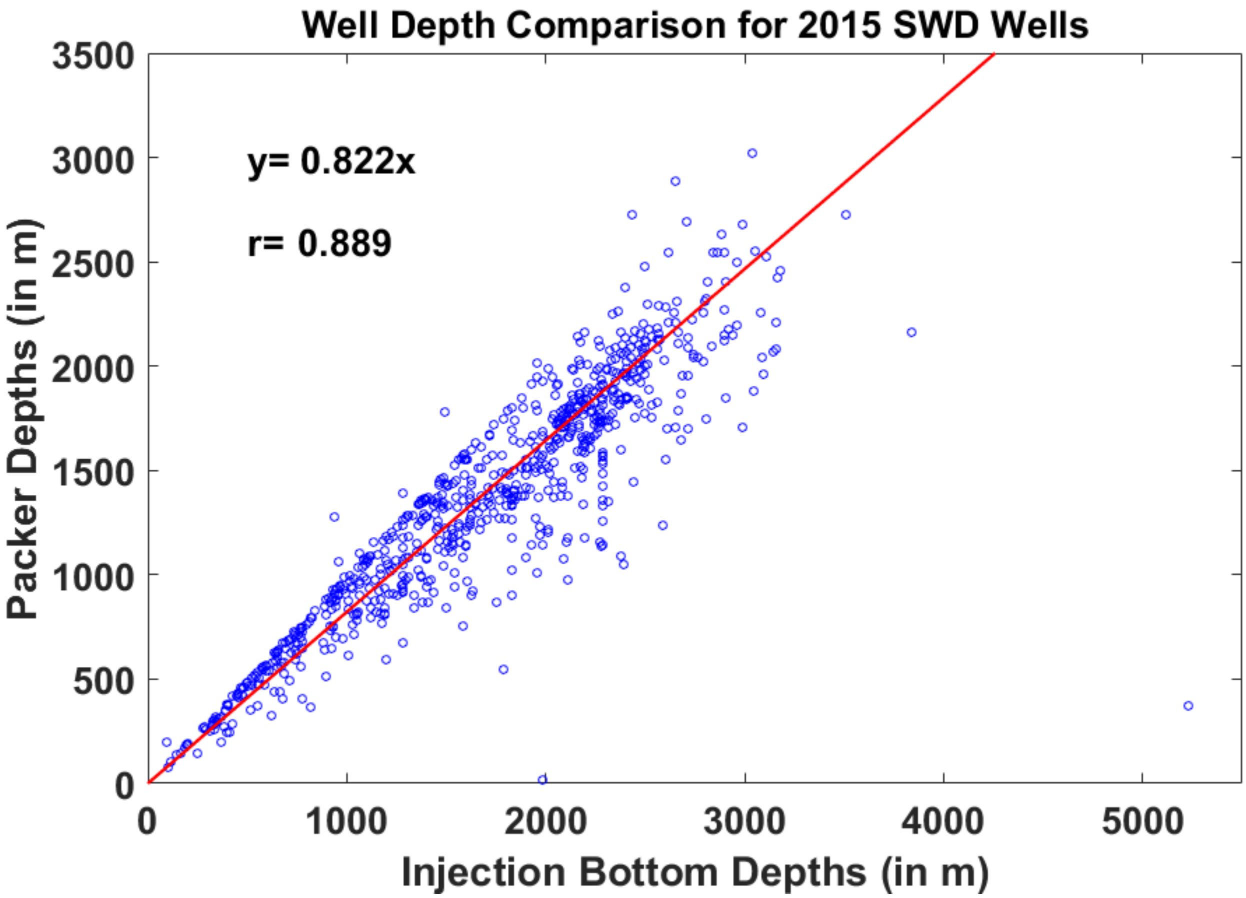

Figure 13. Packer depth (in m) plotted against the permitted injection bottom depth (in m) for all SWD wells active in 2015. Wells with both recorded depth values (some wells in 2015 had either no recorded depth or a recorded depth of zero) were used. The regression line (forced through the origin) shows a strong, positive relationship between these two depth values.

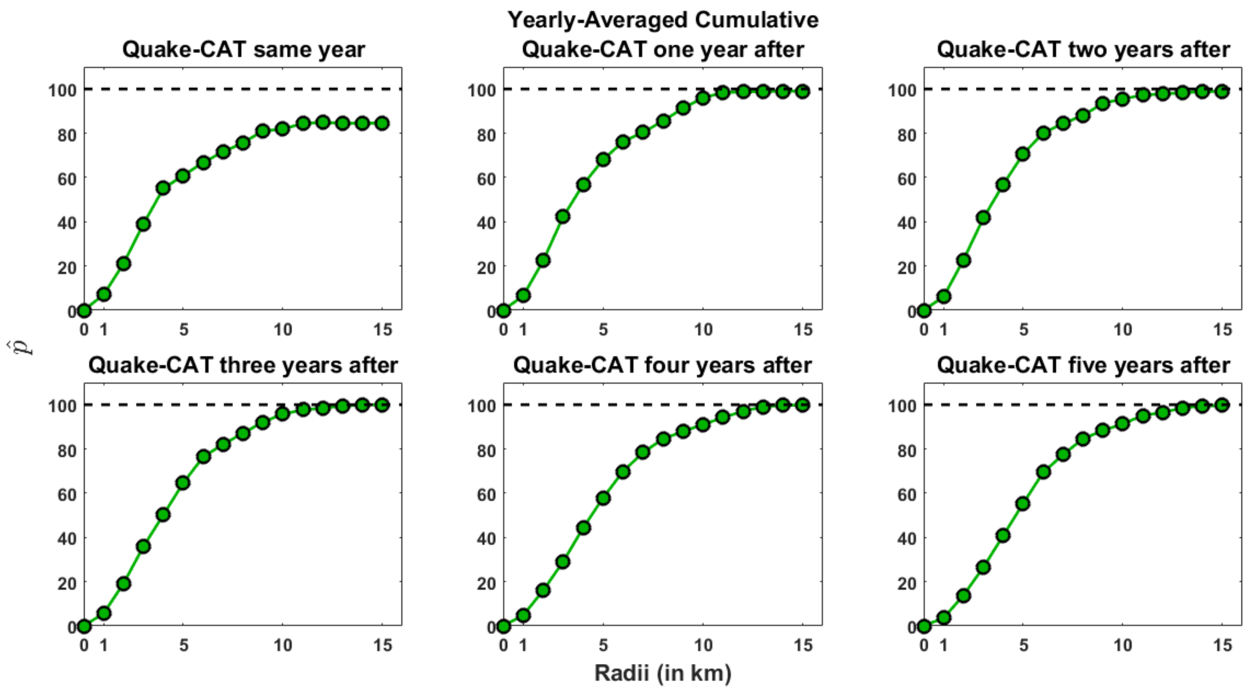

Figure 14. Yearly-averaged, cumulative hit percentage ($\hat{p}$) against MCS radii, or distance from a well site within which an earthquake is considered to be a "hit", or induced, for all active SWD wells in Oklahoma. Each $\hat{p}$ is the average of all $\hat{p}$ values calculated from each of the Well-CAT years in question, and each is calculated from Well-CATs and Quake-CATs from the same year to Well-CATs and Quake-CATs that are five years apart.

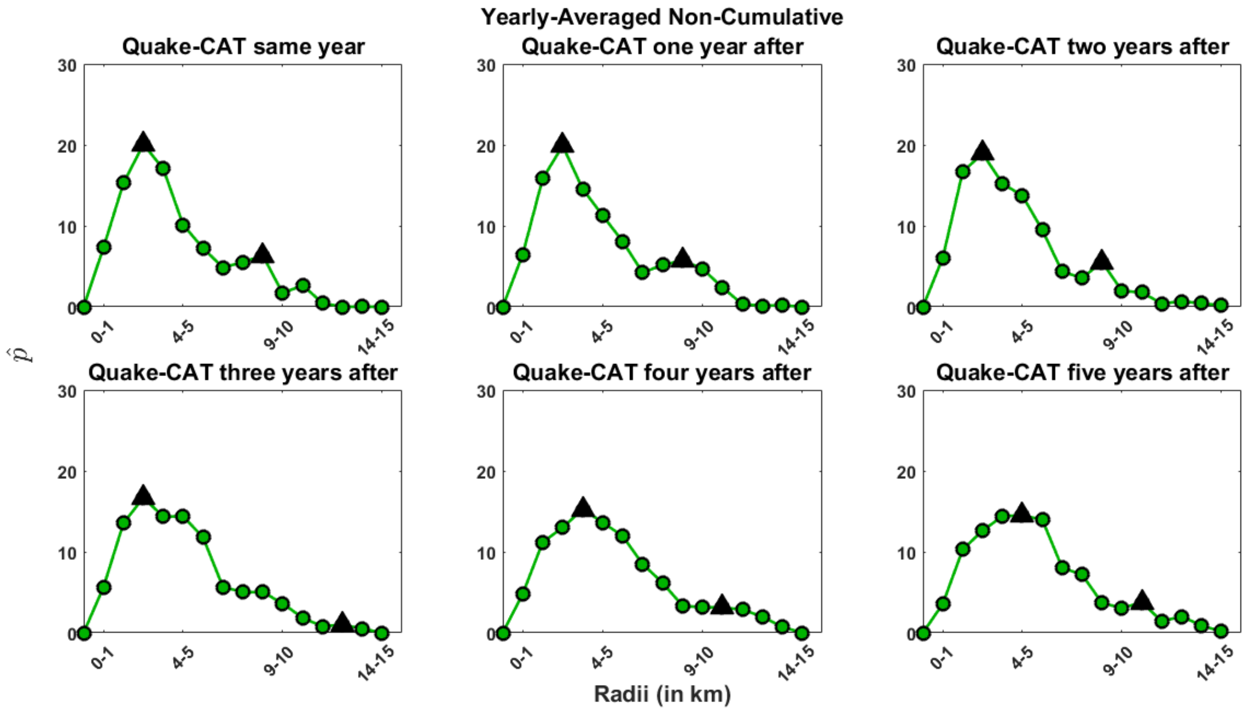

Figure 15. Yearly-averaged, non-cumulative hit percentage ($\hat{p}$) against MCS radii for all active SWD wells in Oklahoma. Each $\hat{p}$ is the average of all $\hat{p}$ values calculated from each of the Well-CAT years in question. Subplots show $\hat{p}$ values calculated from Well-CATs and Quake-CATs from the same year to Well-CATs and Quake-CATs that are five years apart. The primary and secondary peaks in $\hat{p}$ are shown by the black triangles.

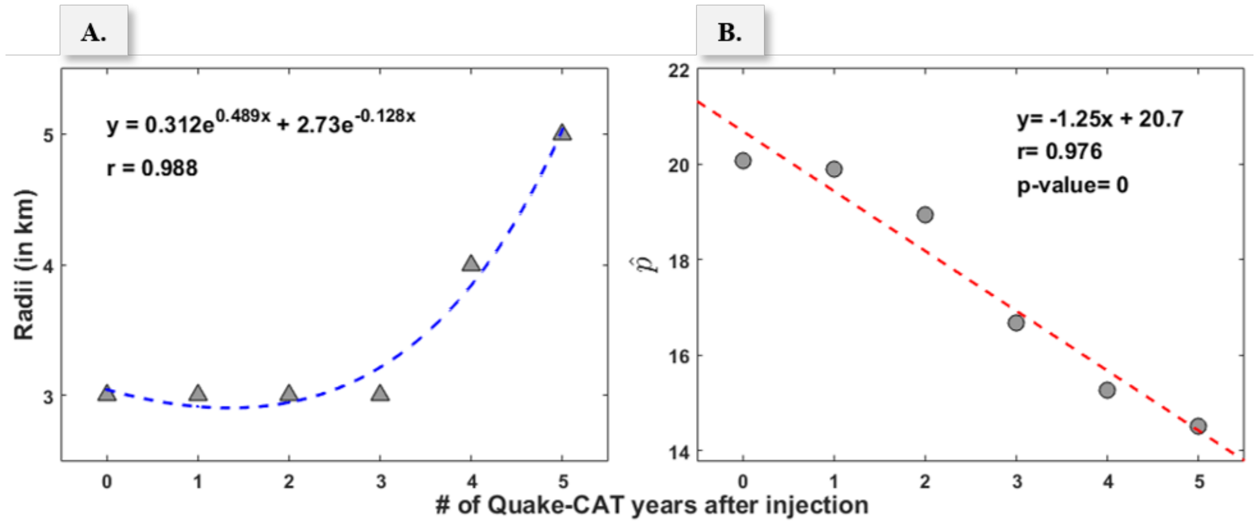

Figure 16. Each point on subplot (A) represents the yearly-averaged radius (taken from all Well-CAT years) for each of the 0 to 5 Quake-CAT years after injection at which there is a primary peak in $\hat{p}$. A second-degree exponential curve is fit to the data and its equation and r value are displayed. Each point on subplot (B) represents the yearly-averaged, primary peak $\hat{p}$ value for each year from 0 to 5 Quake-CAT years after injection. A linear regression is calculated and the statistics are displayed on the plot.

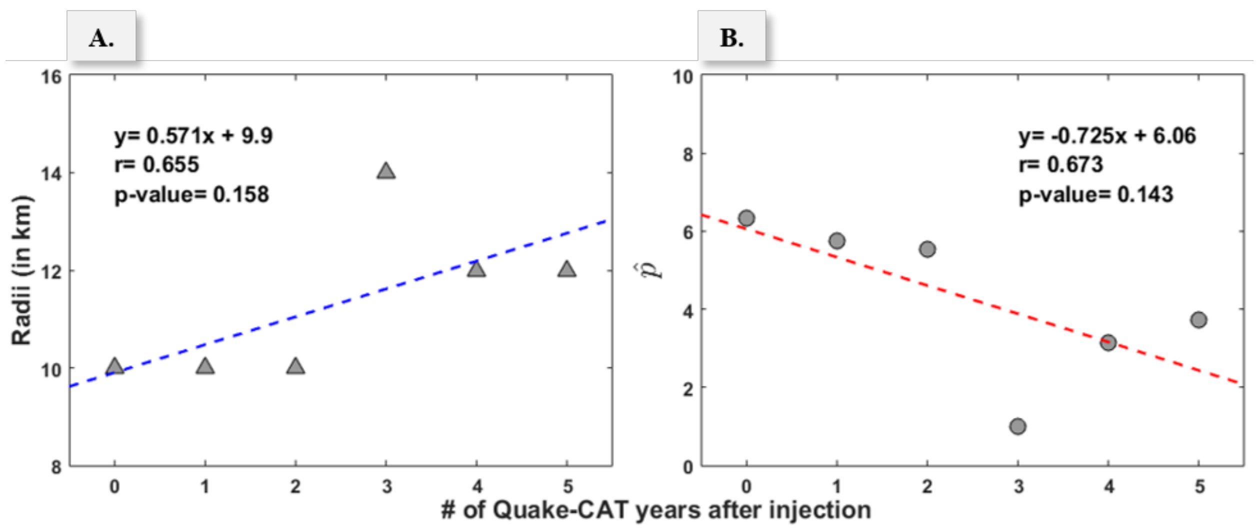

Figure 17. Each point on subplot (A) represents the yearly-averaged radius (taken from all Well-CAT years) for each of the 0 to 5 Quake-CAT years after injection at which there is a secondary peak in $\hat{p}$. A linear regression is calculated for the data and its equation, r, and p-values are displayed. Each point on subplot (B) represents the yearly-averaged, secondary peak $\hat{p}$ value for each year from 0 to 5 Quake-CAT years after injection. A linear regression is calculated and the statistics are displayed on the plot.

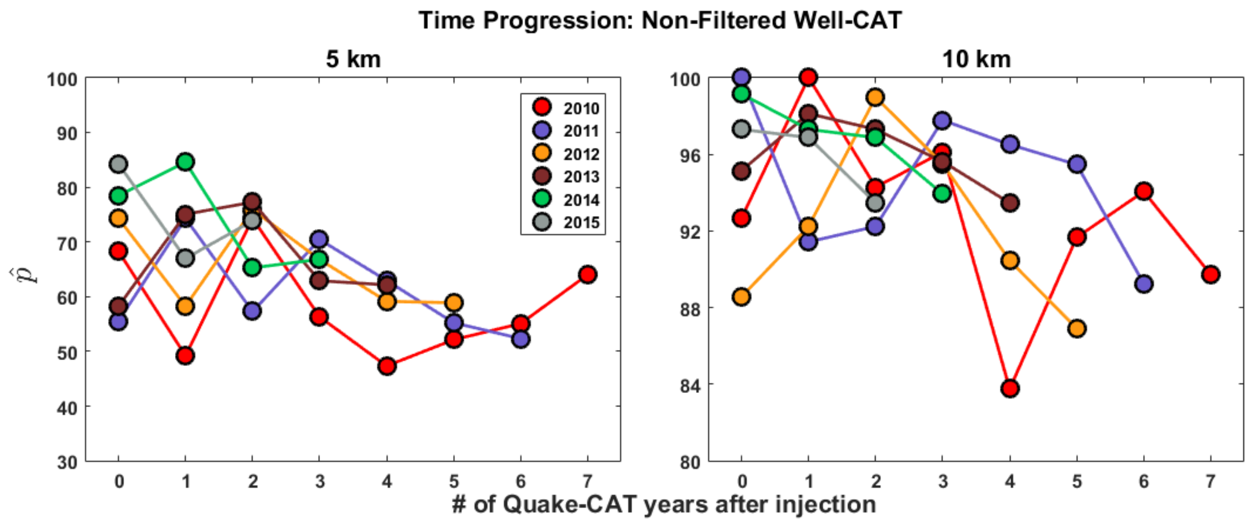

Figure 18. CS Predictability ($\hat{p}$) plotted against the number of Quake-CAT years after injection for the non-filtered Well-CATs. The $\hat{p}$ values are calculated for Well-CATs 2010-2015, which are not filtered and therefore include all SWD wells in Oklahoma that have recorded volume values above zero. Quake-CATs are also not filtered and therefore include all earthquakes of M≥3.0 that have occurred within the geographic coordinates listed in Table 1. The plot on the left shows $\hat{p}$ values calculated using a Well-CAT radius of 5 km for all years, and the plot on the right shows $\hat{p}$ values calculated using a 10 km radius.

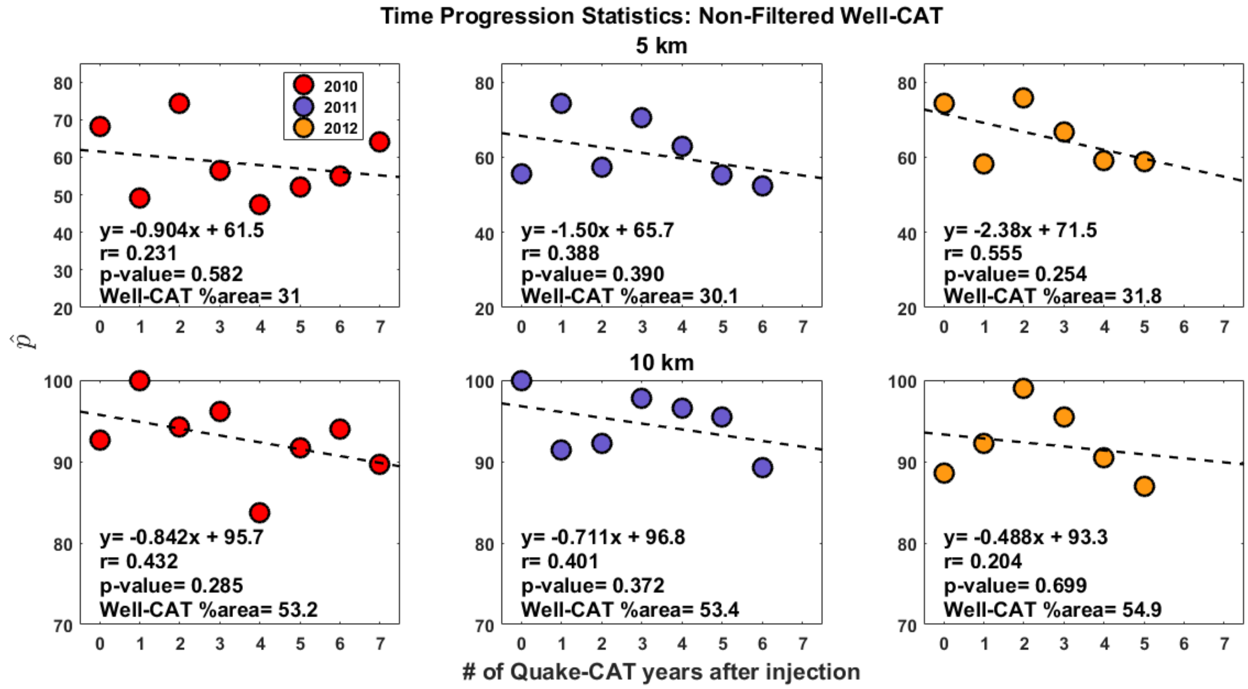

Figure 19. CS Predictability ($\hat{p}$) plotted against number of Quake-CAT years after injection for Well-CAT years 2010-2012. Well-CATs and Quake-CATs are not filtered, and values for each Well-CAT year are displayed on individual plots in order to calculate their linear regressions, as well as correlation coefficients (r) and their statistical significance (p-value). The three top plots show $\hat{p}$ values calculated using a Well-CAT radius of 5 km, and the three on the bottom show $\hat{p}$ values calculated using a 10 km Well-CAT radius, which applies to all regression plots.

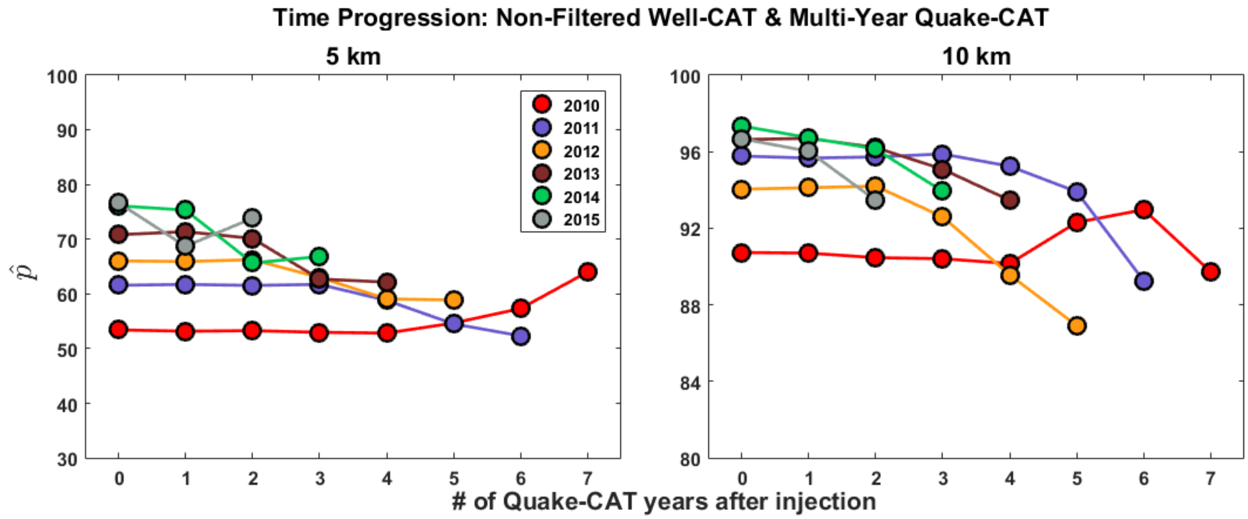

Figure 20. $\hat{p}$ against the number of Quake-CAT years after injection for non-filtered Well-CATs CATs and multi-year Quake-CATs of 2010 to 2015. Quake-CATs include all earthquakes from multiple years, from the starting Quak-CAT year until the year 2017 (e.g. for 0 years after injection, Quake-CAT includes the Well-CAT year to 2017, and for 1 year after injection, Quake-CAT includes 1 year after the Well-CAT year to 2017, etc). The yearly-averaged percent change from the first to last $\hat{p}$ value is displayed in each plot.

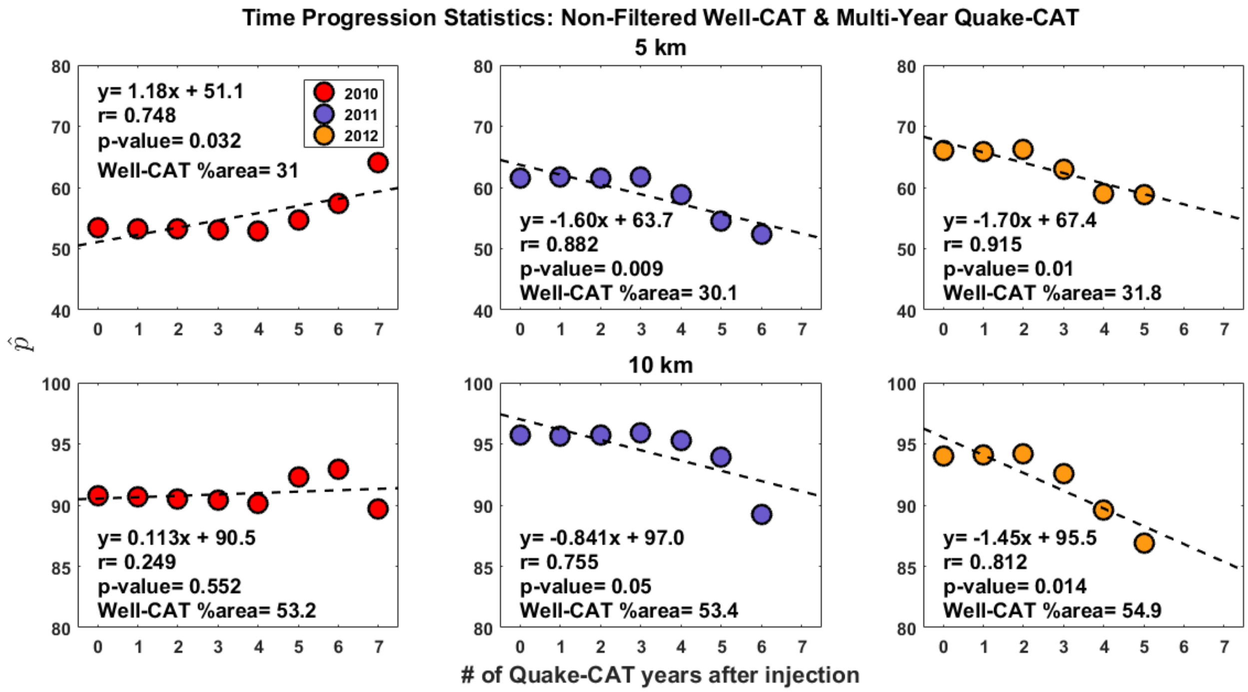

Figure 21. $\hat{p}$ against the number of Quake-CAT years after injection and regressions for non-filtered Well-CAT and nulti-year Quake-CAT years 2010- 2012. Quake-CATs include earthquakes from multiple years.

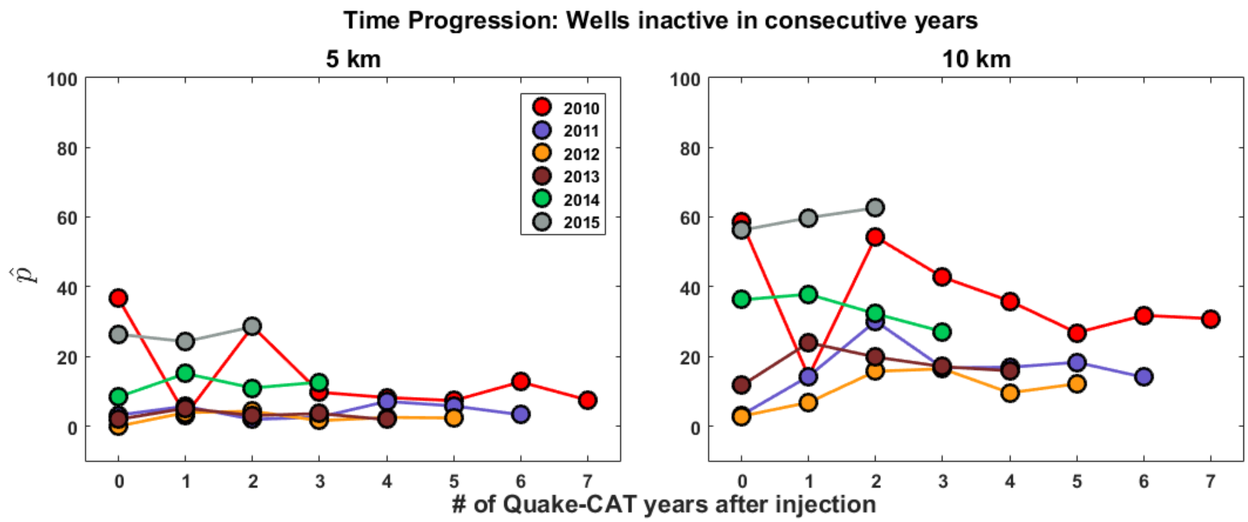

Figure 22. p̂ number of Quake-CAT years after injection for "no post" Well-CATs of 2010-2015. Well-CATs are filtered to include only wells that are not active in the years following the Well-CAT year in question. Additionally, this catalog filters out wells within 1 km of other wells active in consecutive years. Quake-CATs are not filtered. The left plot shows $\hat{p}$ values calculated using a 5 km Well-CAT radius, and the right plot uses a 10 km radius. The yearly-averaged percent change from the first to the last $\hat{p}$ value is displayed on each plot as well.

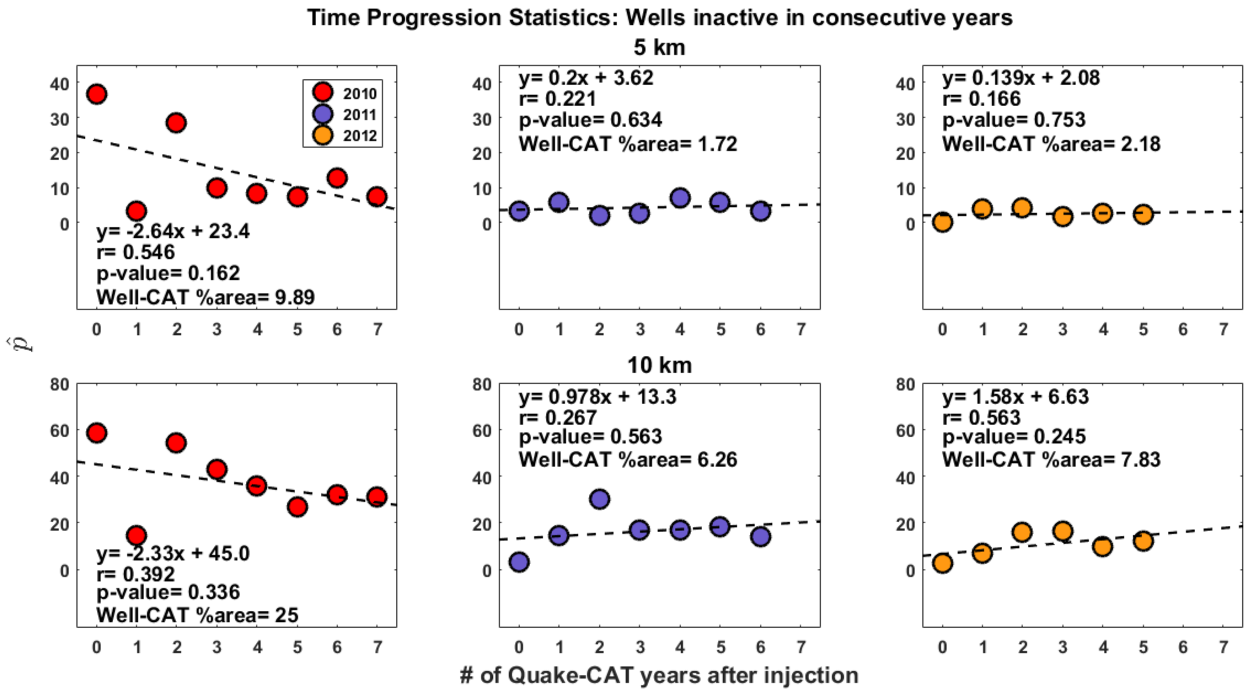

Figure 23. $\hat{p}$ against number of Quake-CAT years after injection and regressions for "no post" Well-CAT years 2010-2012. Well-CATs are filtered to include only wells that are not active in the years following the Well-CAT year in question and wells that are not within 1 km of other wells active in consecutive years.

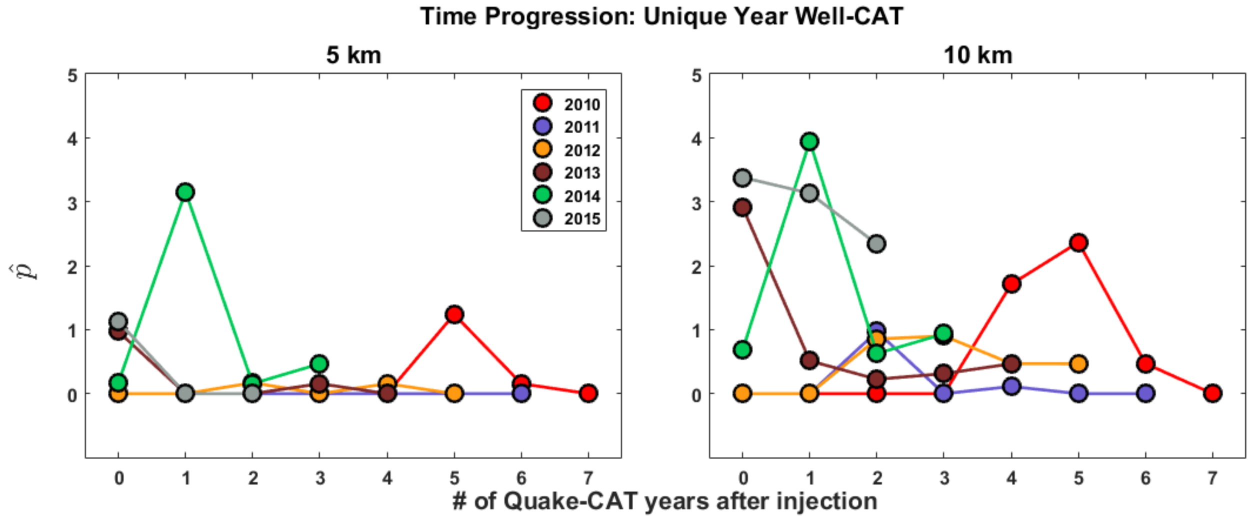

Figure 24. p̂ against number of Quake-CAT years after injection for "unique year" Well-CATs 2010-2015. Well-CATs are filtered to include only wells that are not active in the years prior to and following the Well-CAT year in question and wells that are not within 1 km of other wells active in prior and consecutive years. Quake-CATs are not filtered. The $\hat{p}$ values in the left plot were calculated using a 5 km Well-CAT radius, and the right plot uses a 10 km radius. The average percent change in $\hat{p}$ is not displayed as it is in the other time progression plots, for many of the $\hat{p}$ values calculated with Quake-CATs from the same year are zero.

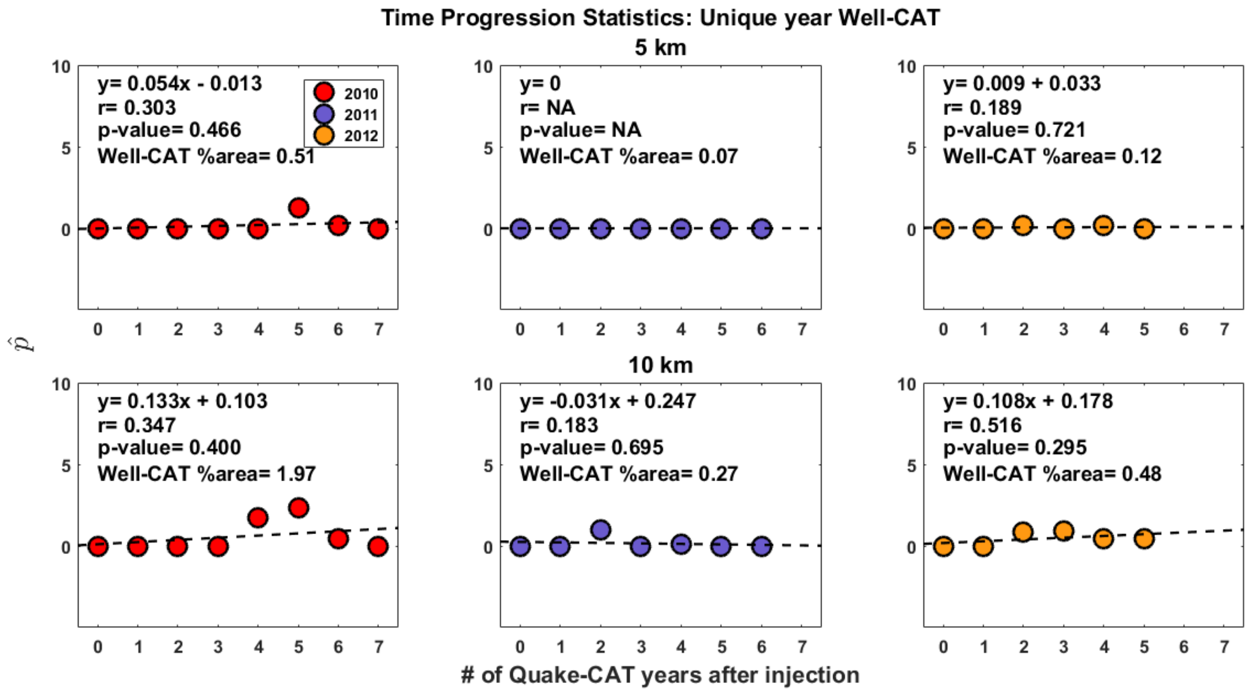

Figure 25. $\hat{p}$ against number of Quake-CAT years after injection and regressions for "unique year" Well-CAT years 2010-2012. Well-CATs are filtered to include only wells that are not active in the years prior to and following the Well-CAT year in question and wells that are not within 1 km of other wells active in prior and consecutive years.

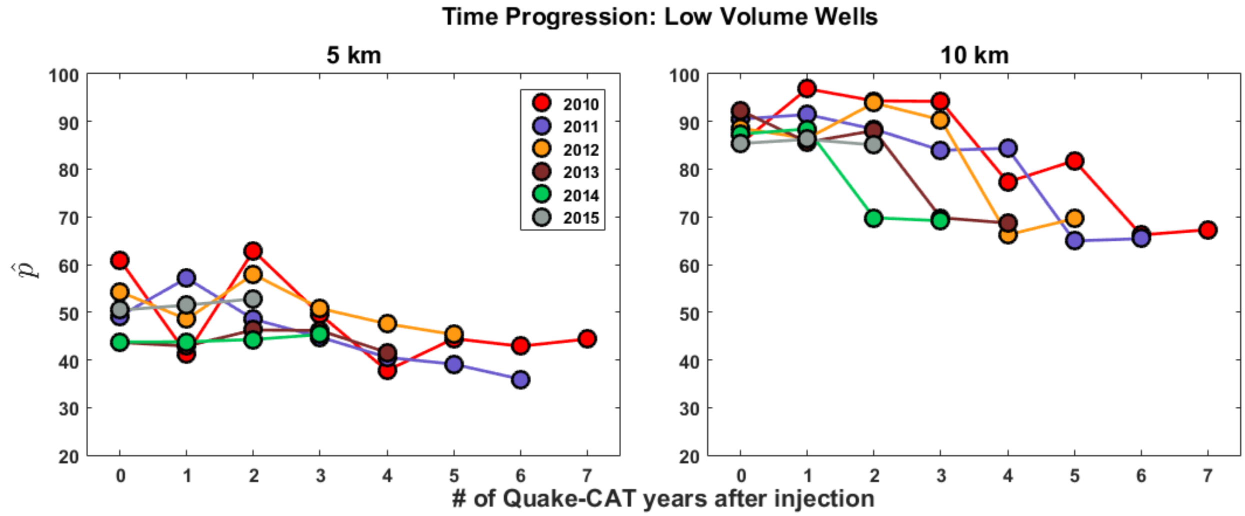

Figure 26. p̂ number of Quake-CAT years after injection for low volume Well-CATs 2010-2015. Well-CATs are filtered to include only low volume (i.e. injecting ≤ 120,000 bbls/year) wells. Quake-CATs are not filtered. The $\hat{p}$ values in the left plot were calculated using a 5 km Well-CAT radius, and the right plot uses a 10 km radius. The yearly-averaged percent change from the first to the last $\hat{p}$ value is also displayed.

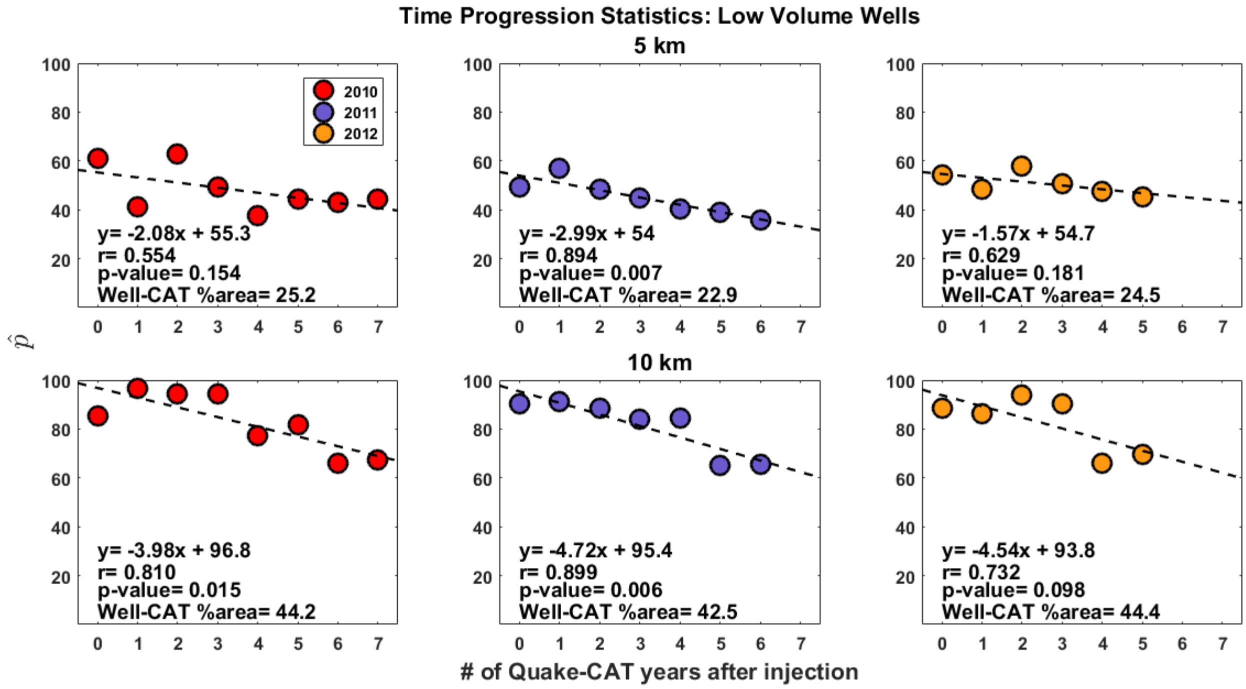

Figure 27. $\hat{p}$ against number of Quake-CAT years after injection and regressions for low volume Well-CATs from 2010-2012.

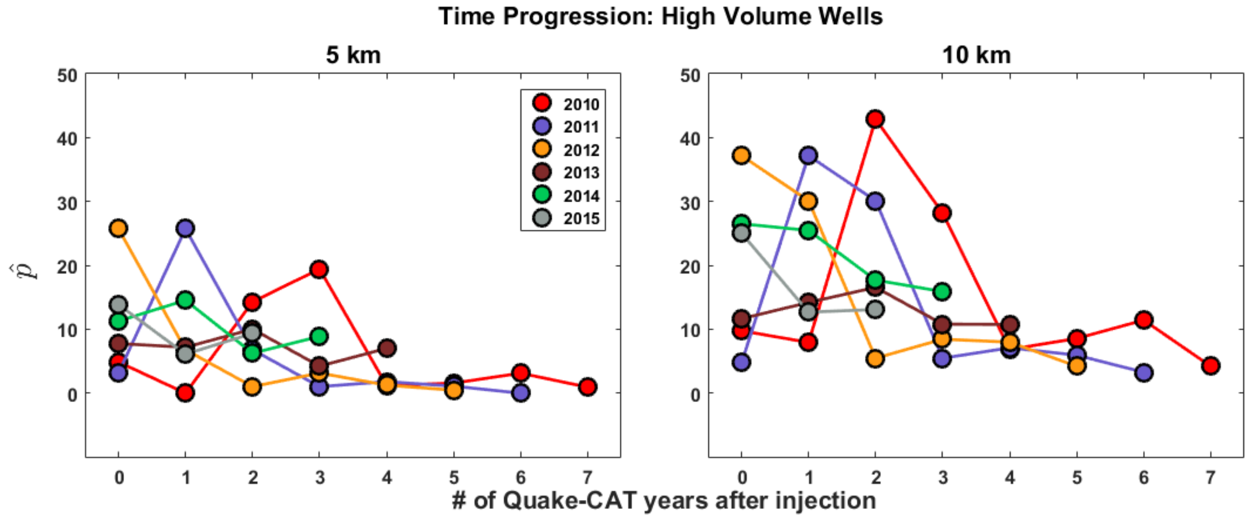

Figure 28. p̂ against number of Quake-CAT years after injection for high volume Well-CATs 2010-2015. Well-CATs are filtered to include only high volume (i.e. injecting ≥ 3.6 Mmbbls/year) wells. Quake-CATs are not filtered. The $\hat{p}$ values in the left plot were calculated using a 5 km Well-CAT radius, and the right plot uses a 10 km radius. The yearly-averaged percent change from the first to the last $\hat{p}$ value is also displayed.

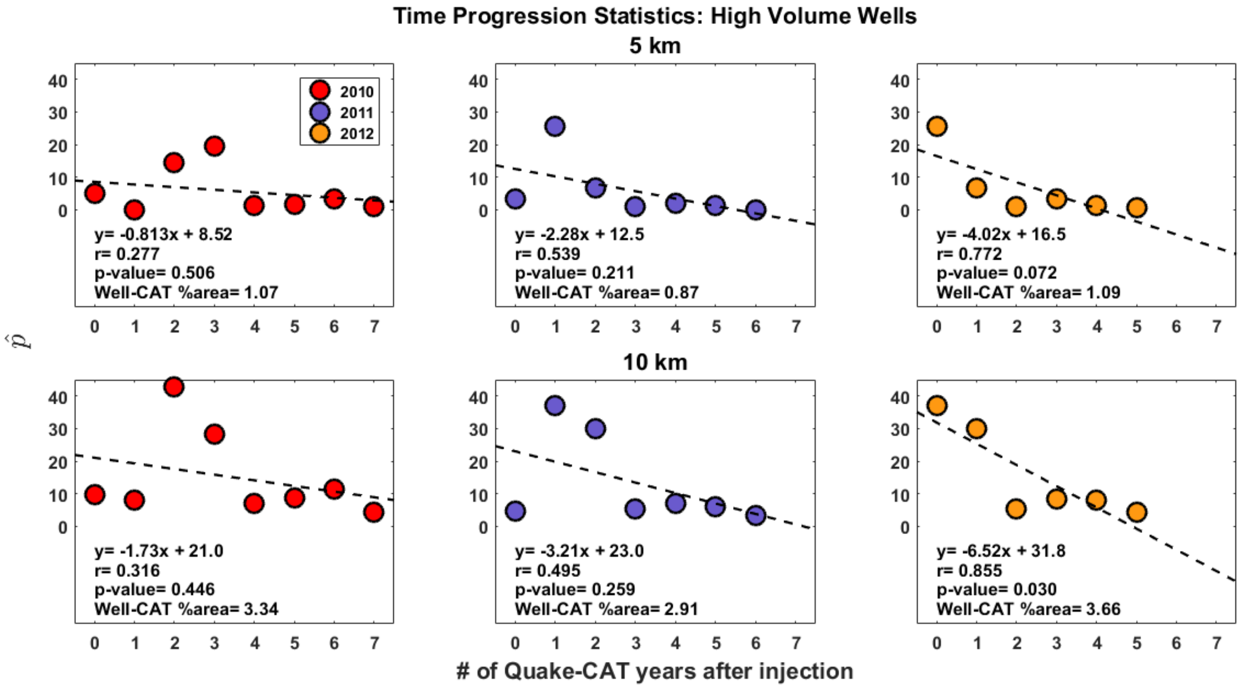

Figure 29. $\hat{p}$ against number of Quake-CAT years after injection and regressions for high volume Well-CATs from 2010-2012.

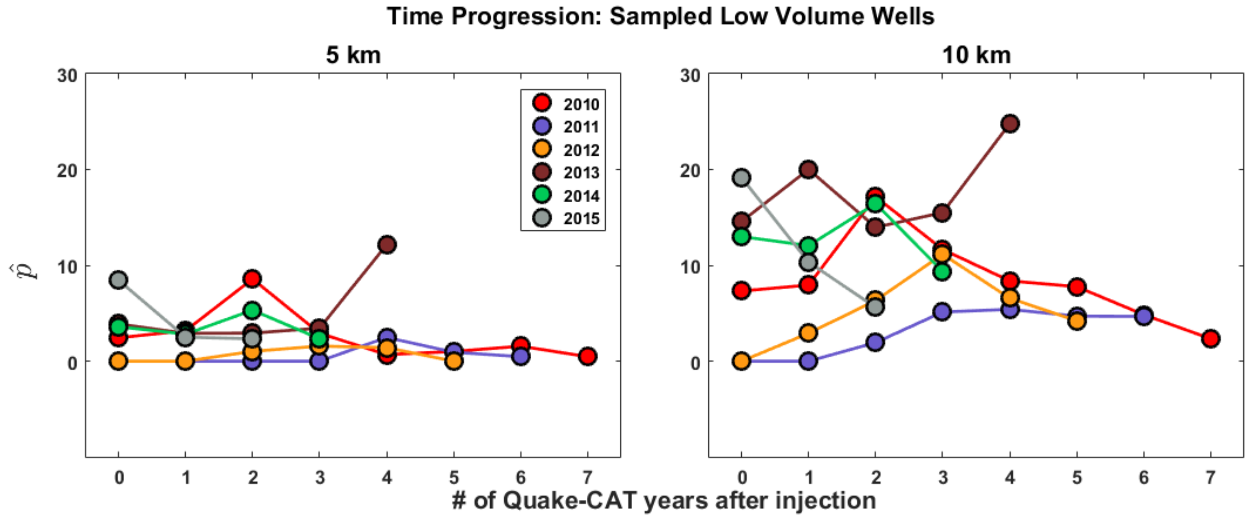

Figure 30. p̂ against number of Quake-CAT years after injection for sampled low volume Well-CATs 2010-2015. Well-CATs are filtered to include only a sample of low volume wells from each year. Quake-CATs are not filtered. The $\hat{p}$ values in the left plot were calculated using a 5 km Well-CAT radius, and the right plot uses a 10 km radius.

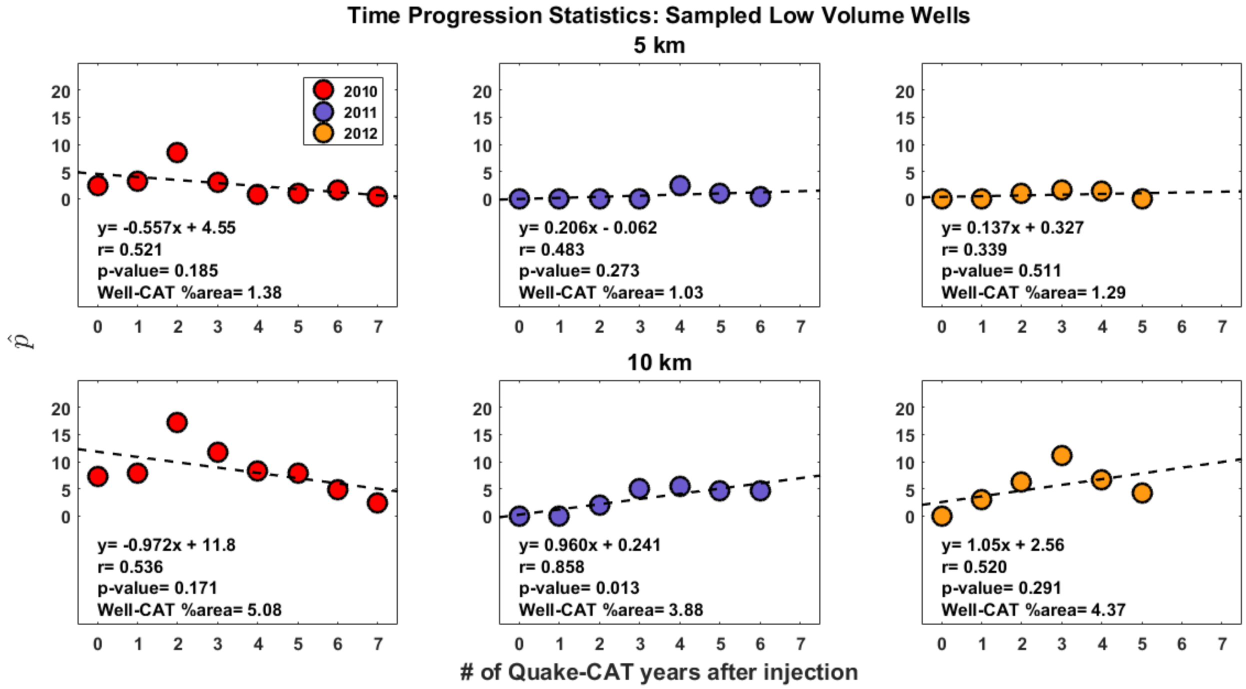

Figure 31. $\hat{p}$ against number of Quake-CAT years after injection and regressions for the sampled low volume Well-CATs from 2010-2012.

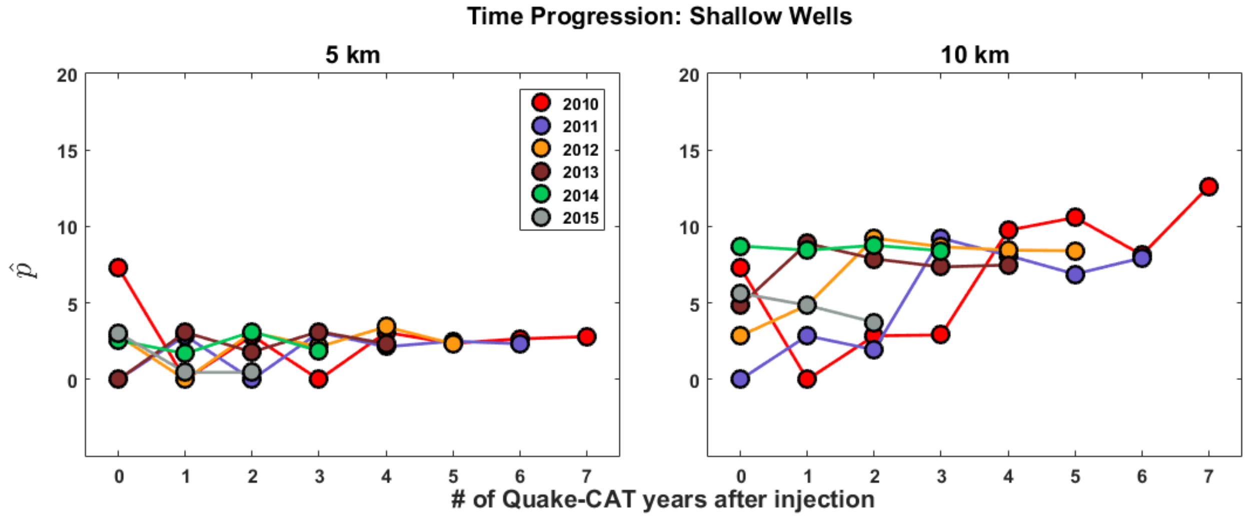

Figure 32. $\hat{p}$ against number of Quake-CAT years after injection for shallow Well-CATs 2010-2015. Well-CATs are filtered to include only shallow (≤ 305 m) wells. Quake-CATs are not filtered. The $\hat{p}$ values in the left plot were calculated using a 5 km Well-CAT radius, and the right plot uses a 10 km radius. The yearly-averaged percent change from the first to the last $\hat{p}$ value is also displayed.

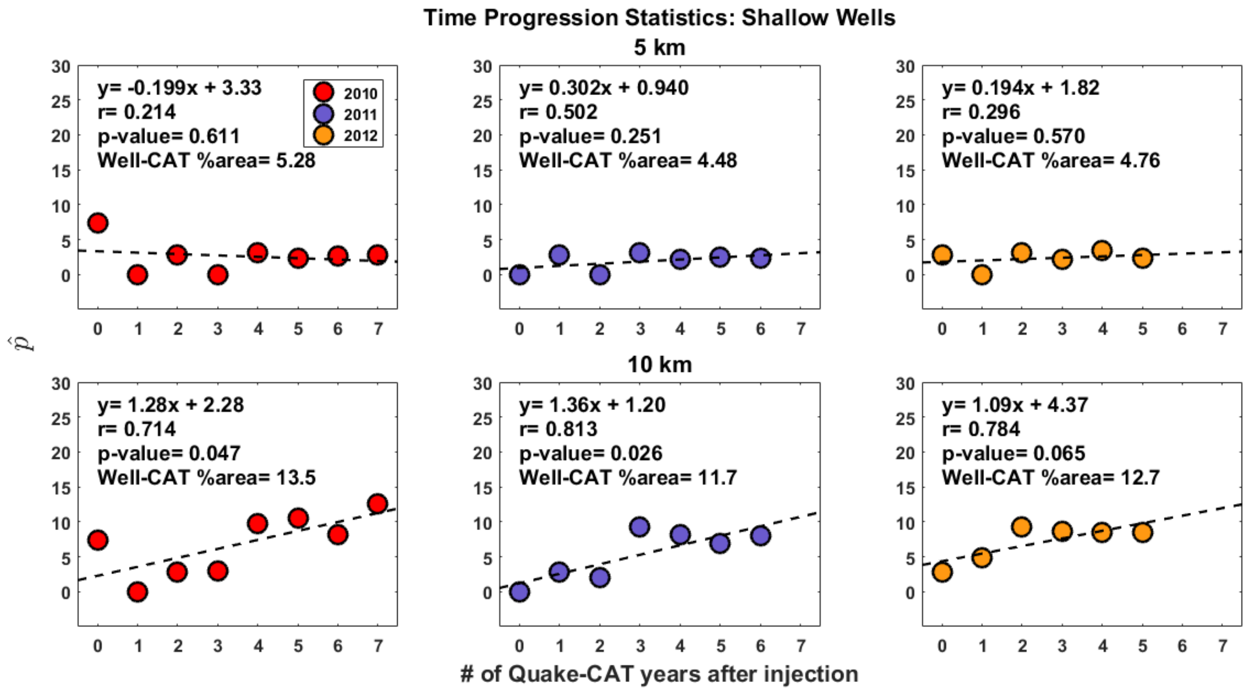

Figure 33. $\hat{p}$ plotted against number of Quake-CAT years after injection and regressions for shallow Well-CATs from 2010-2012.

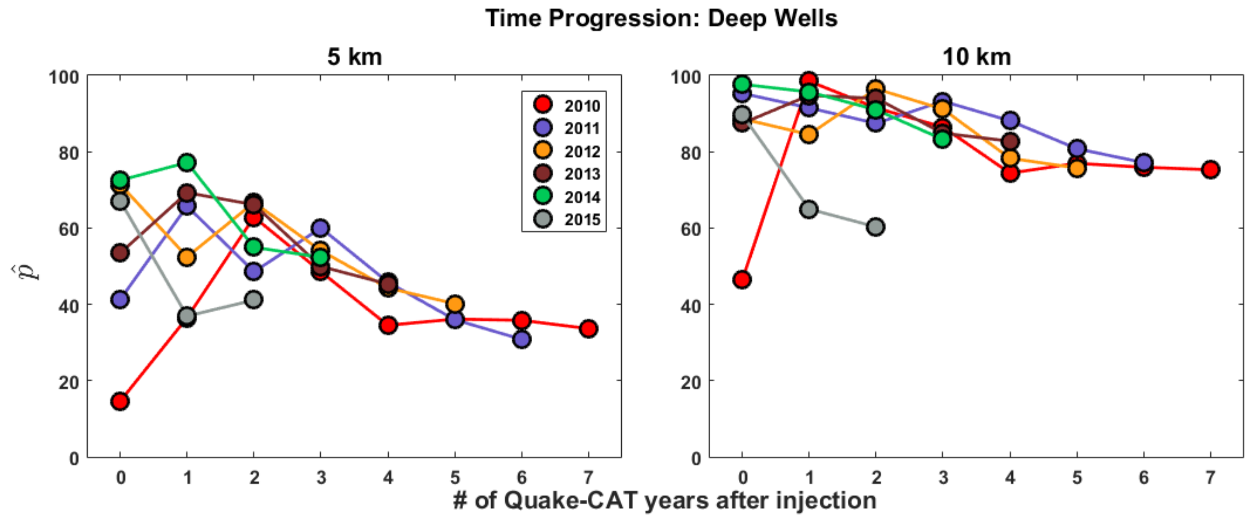

Figure 34. $\hat{p}$ against number of Quake-CAT years after injection for deep Well-CATs 2010-2015. Well-CATs are filtered to include only deep (≥ 1,220 m) wells. Quake-CATs are not filtered. The $\hat{p}$ values in the left plot were calculated using a 5 km Well-CAT radius, and the right plot uses a 10 km radius. The yearly-averaged percent change from the first to the last $\hat{p}$ value is also displayed.

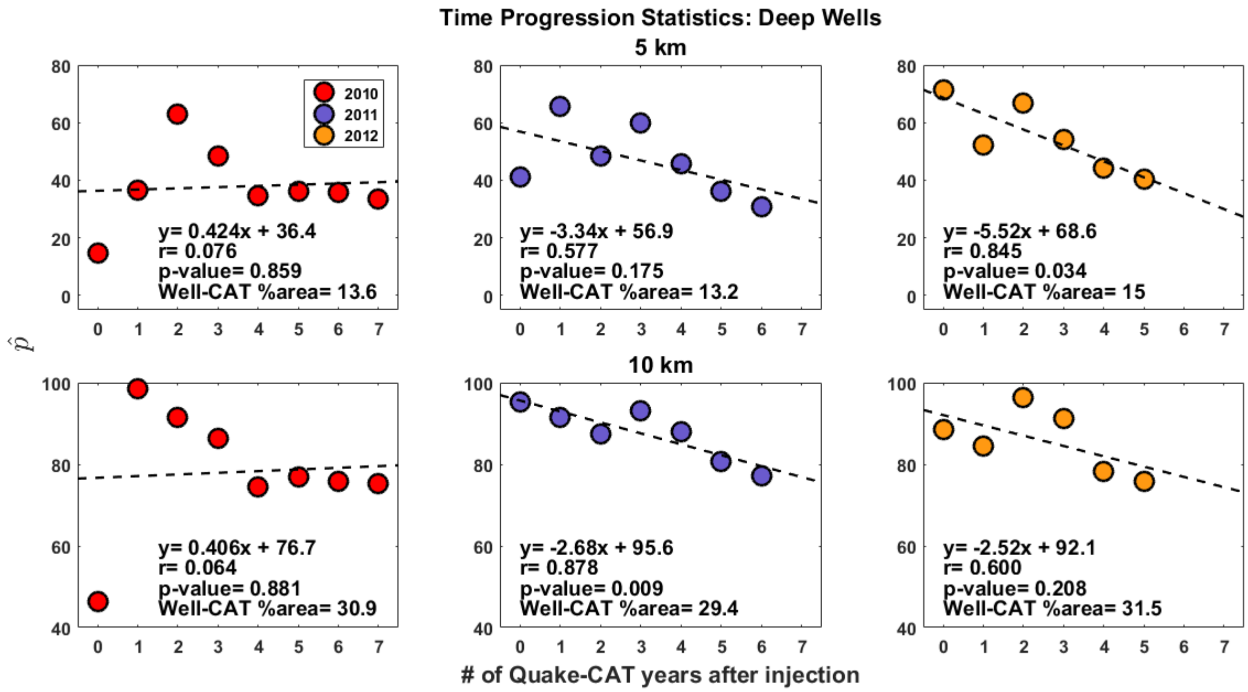

Figure 35. $\hat{p}$ against number of Quake-CAT years after injection and regressions for deep Well-CATs from 2010-2012.

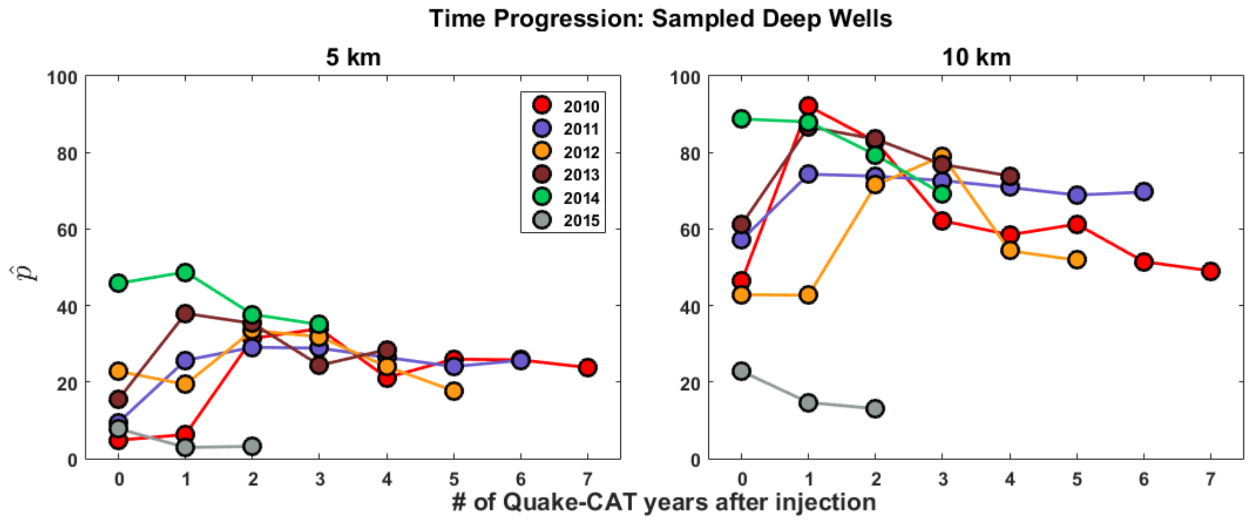

Figure 36. $\hat{p}$ against number of Quake-CAT years after injection for sampled deep Well-CATs 2010-2015. Well-CATs are filtered to include only a sample of deep wells. Quake-CATs are not filtered. The $\hat{p}$ values in the left plot were calculated using a 5 km Well-CAT radius, and the right plot uses a 10 km radius. The yearly-averaged percent change from the first to the last $\hat{p}$ value is also displayed.

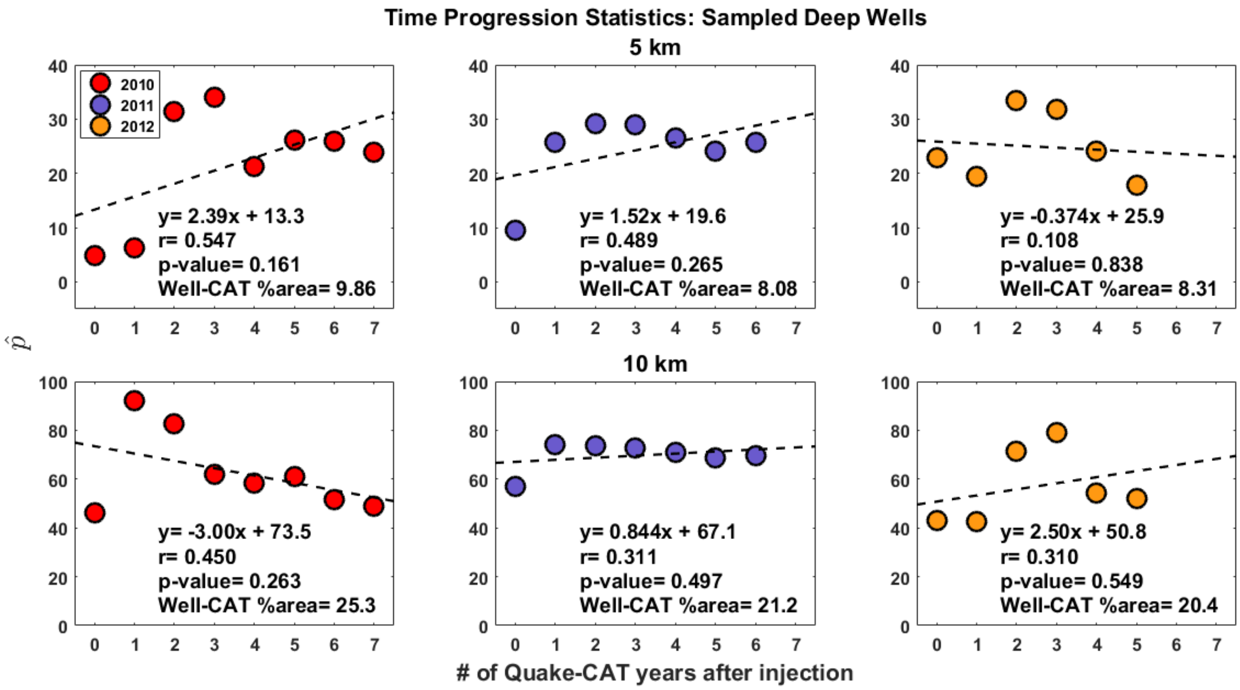

Figure 37. $\hat{p}$ against number of Quake-CAT years after injection and regressions for the sample of deep wells from 2010-2012.

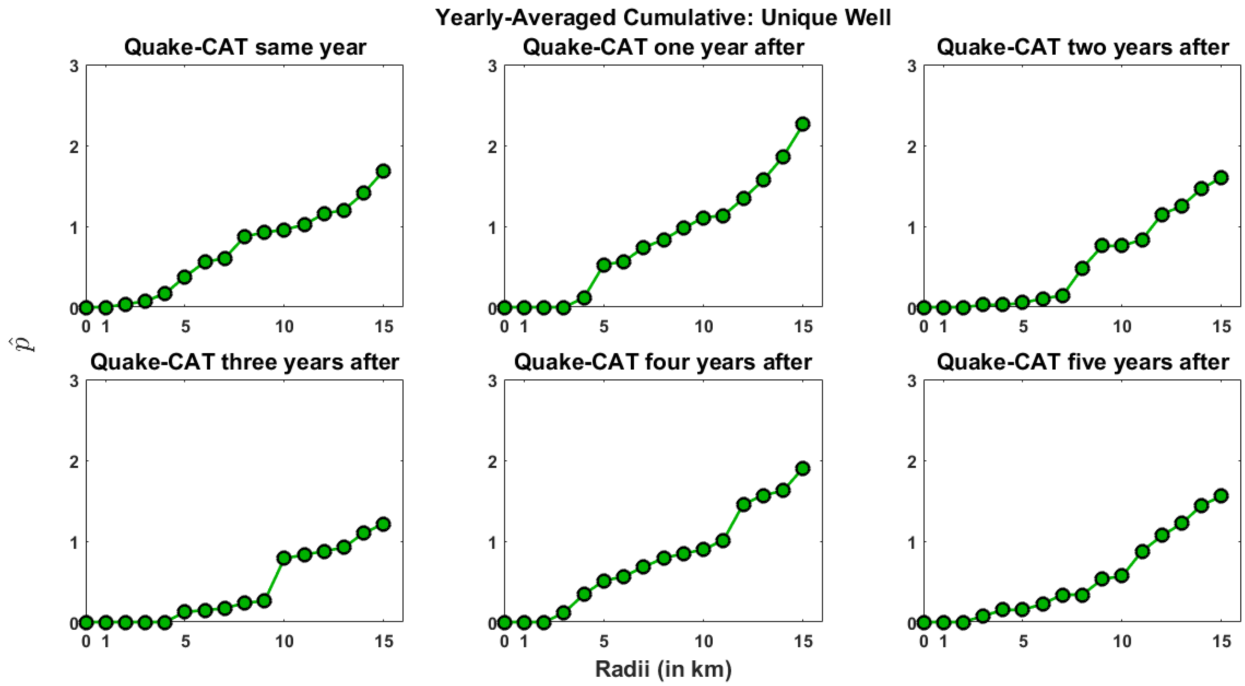

Figure 38. Yearly-averaged, cumulative hit percentage ($\hat{p}$) plotted against MCS radii, or distance from a well site within which an earthquake is considered to be a "hit", or induced, **for a single well** from each "unique year" Well-CAT. Subplots show $\hat{p}$ values calculated from Well-CATs and Quake-CATs from the same year to Well-CATs and Quake-CATs that are five years apart.

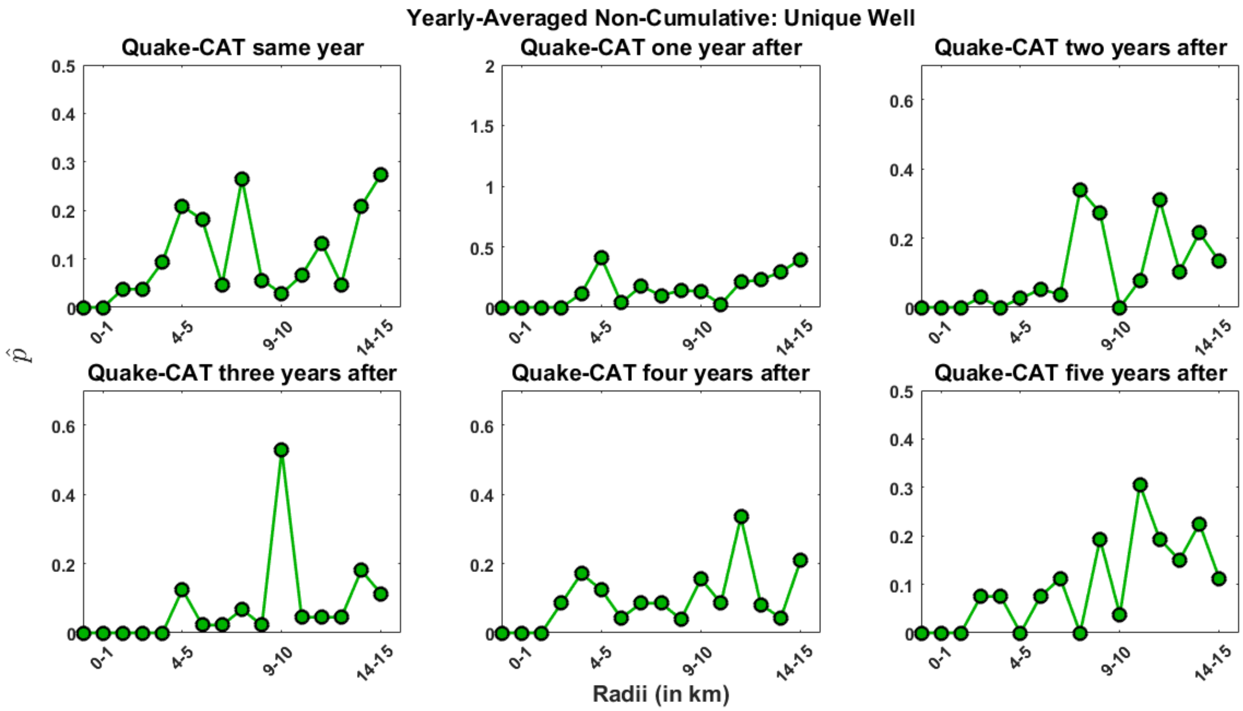

Figure 39. Yearly-averaged, non-cumulative hit percentage ($\hat{p}$) plotted against MCS radii, or distance from a well site within which an earthquake is considered to be a "hit", or induced, for **a single well** from each "unique year" Well-CAT. Subplots show $\hat{p}$ values calculated from Well-CATs and Quake-CATs from the same year to Well-CATs and Quake-CATs that are five years apart.

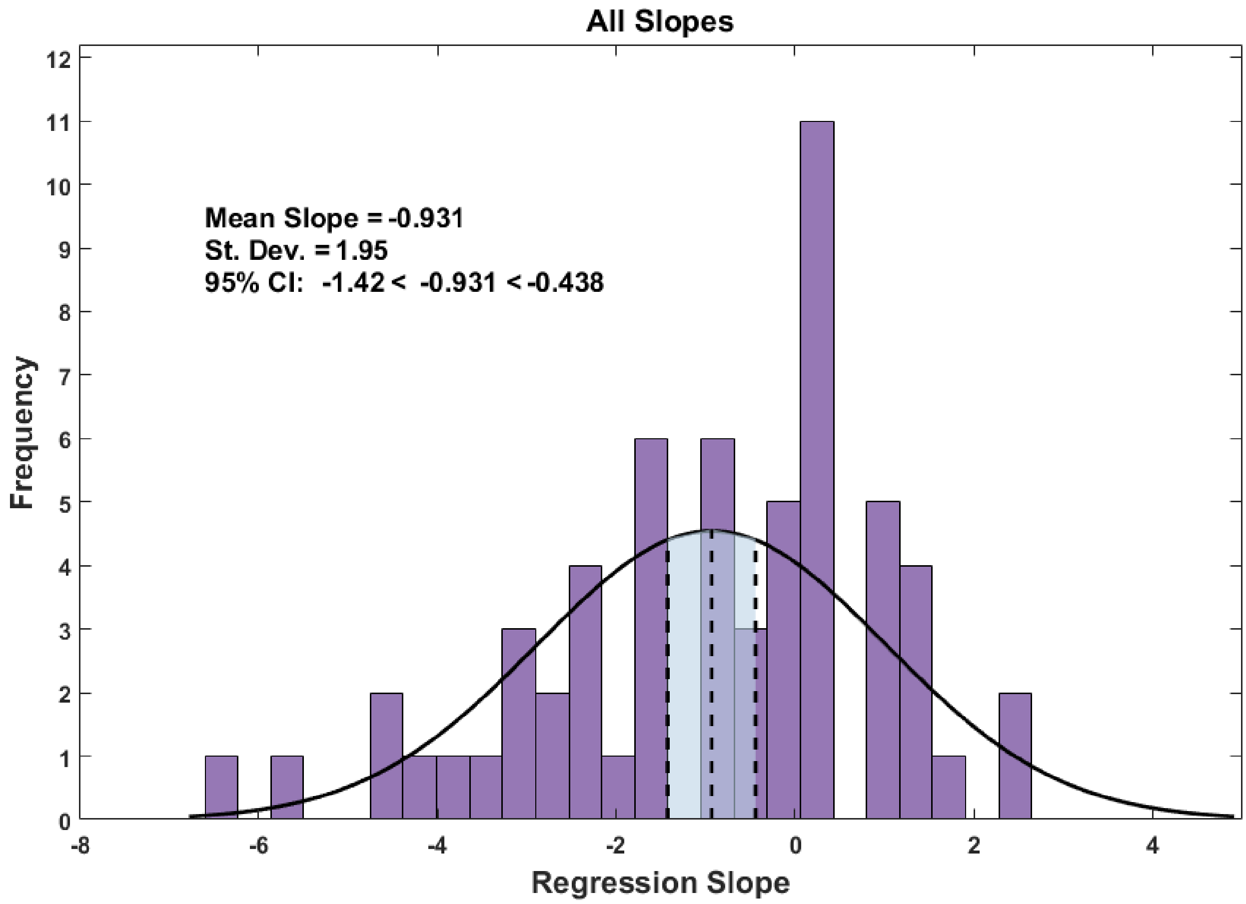

Figure 40. Frequency histogram of all 60 regression slopes from all time progression analyses conducted on Well-CATS 2010-2012. A normal probability distribution is fitted to the histogram, and the mean and 95% confidence interval bounds are also shown.

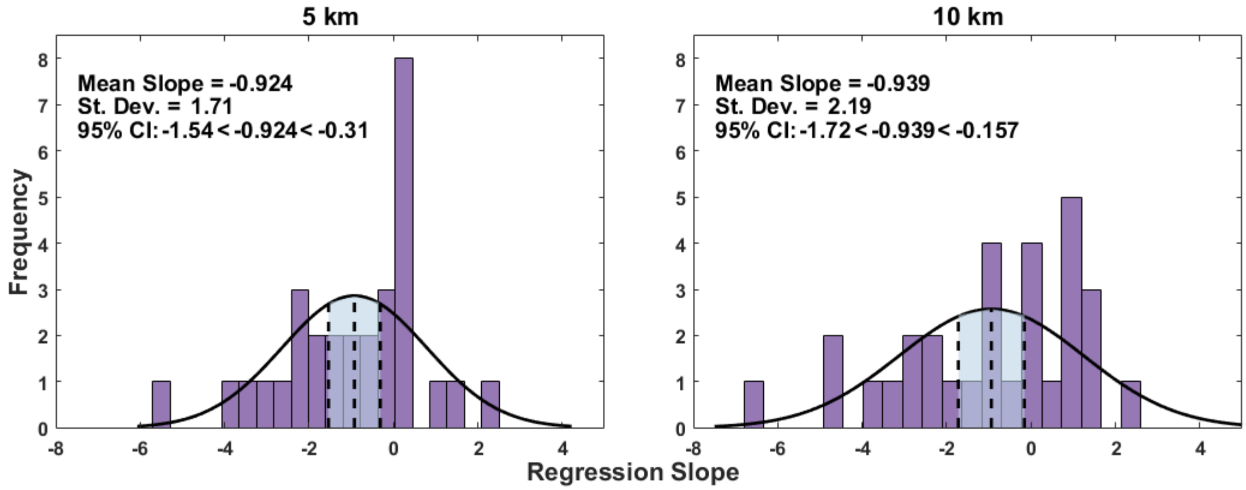

Figure 41. Frequency histograms of two groups of slopes categorized by the Well-CAT radius used to calculate them. On the left are slopes calculated from 5 km radii and on the right are those calculated from 10 km radii. These slopes are from time progression analyses conducted on Well-CATS 2010-2012.

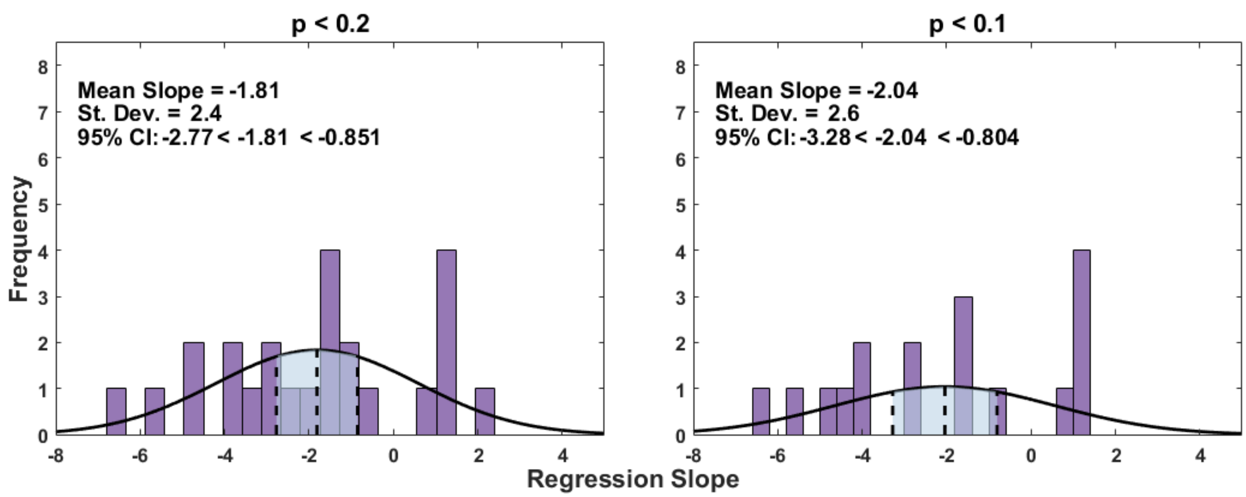

Figure 42. Frequency histograms of two groups of slopes categorized by their statistical significance. On the left are slopes with p-values < 0.2 and on the right are those with p-values < 0.1. These slopes are from time progression analyses conducted on Well-CATS 2010-2012.

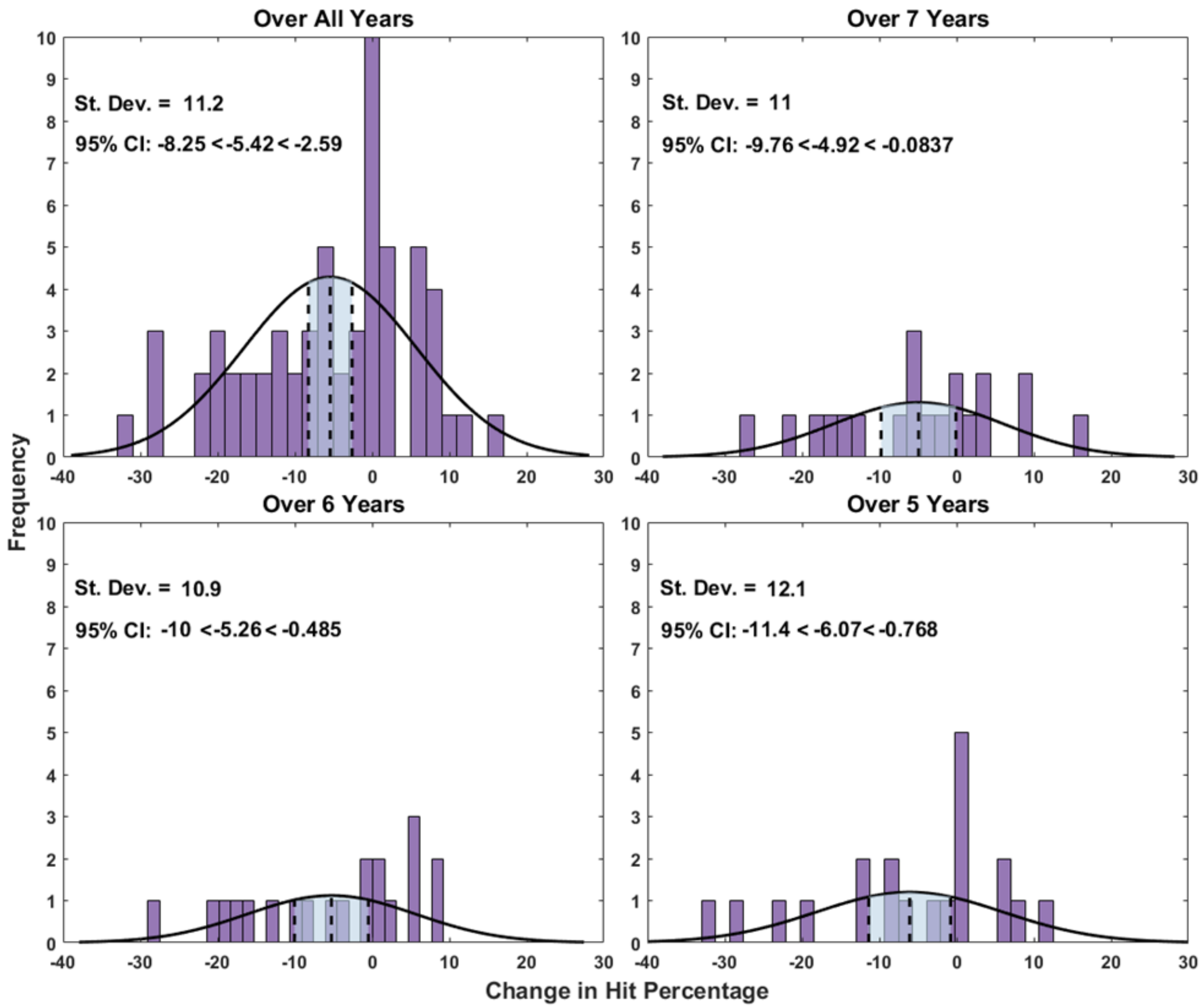

Figure 43. Frequency histograms of the total changes in p̂ calculated from Well-CATs 2010-2012 over periods of 5-7 years. The first plot shows the distribution and mean change in $\hat{p}$ calculated from the regression slopes for all time periods. The second shows the distribution of changes in $\hat{p}$calculated only over a time period of 7 years. The third and fourth plots are for time periods of 6 years and 5 years, respectively.

8.0 DATA AND RESOURCES

OCC. (2017). All Oklahoma UIC Wells: http://www.occeweb.com/og/ogdatafiles2.htm.

OCC. (2017). OCC Imaging Web Application: http://imaging.occeweb.com/.

OCC. (2017). OCC Well Data System: http://www.occpermit.com/WellBrowse/.

United States Geological Survey (USGS). Advanced National Seismic System (ANSS) Comprehensive Catalog (ComCat): http://earthquake.usgs.gov/earthquakes/search (accessed April 2016).

9.0 REFERENCES

Ake, J., Mahrer, K., O'Connell, D., & Block, L. (2005). Deep-injection and closely monitored induced seismicity at Paradox Valley, Colorado. *Bulletin of the Seismological Society of America*, *95*(2), 664–683. http://doi.org/10.1785/0120040072.

Barbour, A. J., Norbeck, J. H., & Rubinstein, J. L. (2017). The Effects of Varying Injection Rates in Osage County, Oklahoma on the 2016 Mw5.8 Pawnee Earthquake. *Seismological Research Letters*, *88*(4). http://doi.org/10.1785/0220170003.

Benz, H.M., McMahon, N.D., Aster, R.C., McNamara, D.E., & Harris, D.B. (2015). Hundreds of Earthquakes per Day: The 2014 Guthrie, Oklahoma, Earthquake Sequence. *Seismological Research Letters*, *86*(5), 1318–1325. http://doi.org/10.1785/0220150019.

Brudy, M., Zoback, M.D., Fuchs, K., Rummel, F., & Baumgartner, J. (1997). Estimation of the complete stress tensor to 8 km depth in the KTB scientific drill holes: Implications for crustal strength. *Journal of Geophysical Research*, *102*(B8), 18453–18457. http://doi.org/0148-0227/97/96JB-029425.

Chambless, H.E. (2015). A study of injection-induced seismicity from Class II wastewater wells and hydraulic fracturing operations, Senior Thesis, Boston College.

Chambless, H.E. & Kafka, A. L. (2017). Modified Cellular Seismology exploration of spatial and temporal patterns of injection wells and seismicity in Oklahoma, *Eastern Section Meeting, Seismological Society of America*, Norman, OK, 8–10 October, 2017.

Chang, K.W. & Segall, P. (2016). Seismicity on Basement Faults Induced by Simultaneous Fluid Injection–Extraction. *Pure and Applied Geophysics*, *173*(8), 2621–2636. http://doi.org/10.1007/s00024-016-1319-7.

Darold, A.P. & Holland, A.A. (2015). Preliminary Oklahoma Optimal Fault Orientations: Oklahoma Geological Survey, scale 1:750,000.

Davis, S.D. & Frohlich, C. (1993). Did (or will) fluid injections cause earthquakes?—criteria for a rational assessment. *Seismological Research Letters*, *64*(3–4), 207–224.

Denison, R.E. (1981). Basement Rocks in Northeastern Oklahoma. Circular 84: Oklahoma Geological Survey.

Ellsworth, W.L. (2013). Injection-Induced Earthquakes. *Science*, *341*(1225942), 1–7. http://doi.org/10.1126/science.1225942.

Frohlich, C., Hayward, C., Stump, B., & Potter, E. (2011). The Dallas-Fort Worth earthquake sequence: October 2008 through May 2009. *Bulletin of the Seismological Society of America*, *101*(1), 327–340. http://doi.org/10.1785/0120100131.

Frohlich, C. (2012). Two-year survey comparing earthquake activity and injection-well locations in the Barnett Shale, Texas. *Proceedings of the National Academy of Sciences*, *109*(35), 13934–13938. http://doi.org/10.1073/pnas.1207728109.

Healy, J.H., Rubey, W.W., Griggs, D.T., & Raleigh, C.B. (1968). The Denver Earthquakes. *Science*, *161*(3841), 1301–1310.

Herrmann, R. B., Park, S.-K., & Wang, C.-Y. (1981). The Denver earthquakes of 1967-1968. *Bulletin of the Seismological Society of America*, *71*(3), 731–745.

Holland, A.A. (2013). Optimal Fault Orientations within Oklahoma. *Seismological Research Letters*, *84*(5), 876–890. http://doi.org/10.1785/0220120153.

Horton, S. (2012). Disposal of Hydrofracking Waste Fluid by Injection into Subsurface Aquifers Triggers Earthquake Swarm in Central Arkansas with Potential for Damaging Earthquake. *Seismological Research Letters*, *83*(2), 250–260. http://doi.org/10.1785/gssrl.83.2.250.

Hough, S.E., & Page, M. (2015). A century of induced earthquakes in Oklahoma? *Bulletin of the Seismological Society of America*, *105*(6), 2863–2870. http://doi.org/10.1785/0120150109.

Hseih, P.A. & Bredehoeft, J.D. (1981). A reservoir analysis of the Denver earthquakes: A case of induced seismicity. *Journal of Geophysical Research: Solid Earth*, *86*(B2), 903–920. http://doi.org/10.1029/JB086iB02p00903.

Hubbert, M.K. & Rubey, W.W. (1959). Role of Fluid Pressure in Mechanics of Overthrust Faulting. *Geological Society of America Bulletin*, *70*(2), 115–166. http://doi.org/10.1130/0016-7606(1959)70[167:ROFPIM]2.0.CO;2.

Johnson, K. (2008). Geologic History of Oklahoma. *Educational Publication*, *9*, 3–8.

Kafka, A.L. (2000). Public Misconceptions About Faults and Earthquakes in the Eastern United States: Is it Our Own Fault?, *Seismological Research Letters*, 71(3), 311-312.

Kafka, A.L. (2002). Statistical analysis of the hypothesis that seismicity delineates areas where future large earthquakes are likely to occur in the central and eastern United States. *Seismological Research Letters*, *73*(6), 990-1001.

Kafka, A.L. (2007). Does seismicity delineate zones where future large earthquakes are likely to occur in intraplate environments? *The Geological Society of America*, (Continental Intraplate Earthquakes: Science, Hazard, and Policy Issues: Geological Society of America Special Paper 425), 35-48.

Keranen, K.M., Savage, H.M., Abers, G.A., & Cochran, E.S. (2013). Potentially induced earthquakes in Oklahoma, USA: Links between wastewater injection and the 2011 Mw 5.7 earthquake sequence. *Geology*, *41*(6), 699–702. http://doi.org/10.1130/G34045.1

Keranen, K.M., Weingarten, M., Abers, G.A., Bekins, B.A., & Ge, S. (2014). Sharp increase in central Oklahoma seismicity since 2008 induced by massive wastewater injection. *Science*, *345*(6195), 448–451.

Kim, W.Y. (2013). Induced seismicity associated with fluid injection into a deep well in Youngstown, Ohio. *Journal of Geophysical Research: Solid Earth*, *118*(7), 3506–3518. http://doi.org/10.1002/jgrb.50247.

Koronovskii, N.V. & Naimark, A.A. (2012). The unpredictability of earthquakes as the fundamental result of the nonlinearity of geodynamic systems. *Moscow University Geology Bulletin*, *67*(6), 323–331. http://doi.org/10.3103/S0145875212060026.

Main, I. (1999). Is the Reliable Prediction of Individual Earthquakes a Realistic Scientific Goal? *Nature Debates*. http://www.nature.com/nature/debates/earthquake/index.html?foxtrotcallback=true.

Marsh, S. & Holland, A.A. (2016). Comprehensive Fault Database and Interpretive Fault Map of Oklahoma: Oklahoma Geological Survey Open-File Report, OF2-2016, 15 p.

McCurdy, R. (2011). Underground Injection Wells for Produced Water Disposal. https://www.epa.gov/sites/production/files/documents/21_McCurdy_-_UIC_Disposal_508.pdf. (accessed July 2017).

McGarr, A., Simpson, D., & Seeber, L. (2002). Case Histories of Induced and Triggered Seismicity. *International Handbook of Earthquake and Engineering Seismology Part A*, 647–661. http://doi.org/10.1016/S0074-6142(13)62898-3.

McGarr, A. (2014). Maximum magnitude earthquakes induced by fluid injection. *Journal of Geophysical Research: Solid Earth, 119*, 1008–1019. http://doi.org/10.1002/2013JB010597.

Murray, K.E. (2013). State-scale perspective on water use and production associated with oil and gas operations, Oklahoma, U.S. *Environ. Sci. Technol.*, *47* (9), 4918–4925. http://doi.org/10.1021/es4000593.

Murray, K.E. (2014). *Class II Underground Injection Control Well Data for 2010 – 2013 by Geologic Zones of Completion*. *Oklahoma Geological Survey Open File Report*. Open-File Report (OF1-2014).

Murray, K.E. & Holland, A.A. (2014). Subsurface Fluid Injection in Oil and Gas Reservoirs and Wastewater Disposal Zones of the Midcontinent. *Search and Discovery*, *80377*, 1–8. http://www.searchanddiscovery.com/documents/2014/80377murray/ndx_murray.pdf

Murray, K.E. (2015). *Class II Saltwater Disposal for 2009 – 2014 at the Annual, State, and County Scales by Geologic Zones of Completion, Oklahoma*. Open-File Report (OF5-2015).

Murray, K.E. (2016). Relationships between Geologic Zones, Produced Water, Saltwater Management, and Seismicity in Oklahoma, *Search and Discovery*, 23.

Nicholson, C., Roeloffs, E., & Wesson, R. (1988). The northeastern Ohio earthquake of 31 January 1986: Was it induced? *Bulletin of the Seismological Society of America*, *78*(1), 188–217. Retrieved from http://www.bssaonline.org/content/78/1/188.short.

Petersen, M.D., *et al.* (2016). *2016 One-Year Seismic Hazard Forecast for the Central and Eastern United States from Induced and Natural Earthquakes*. Open-File Report.

Petersen, M.D., *et al.* (2017). 2017 One-Year Seismic Hazard Forecast for the Central and Eastern United States from Induced and Natural Earthquakes. *Seismological Research Letters*, *88*(No. 3), 1–12. http://doi.org/10.3133/OFR20161035.

Rayleigh, C.B., Healy, J.H., & Bredehoeft, J.D. (1976). An experiment in earthquake control at Rangely, Colorado. *Science (New York, N.Y.)*, *191*(4233), 1230–7. http://doi.org/10.1126/science.191.4233.1230.

Rottmann, K., Beaumont, E.A., Northcutt, R.A., Al-Shaieb, Z., Puckette, J., & Blubaugh, P. (2000). History of Hunton Oil and Gas Exploration and Development in Oklahoma. In *Hunton Play in Oklahoma (including Northeast Texas Panhandle)* (p. 115). Oklahoma Geological Survey.

Rubinstein, J.L. & Mahani, A.B. (2015). Myths and Facts on Wastewater Injection, Hydraulic Fracturing, Enhanced Oil Recovery, and Induced Seismicity. *Seismological Research Letters*, *86*(4), 1060–1067. http://doi.org/10.1785/0220150067.

Scanlon, B.R., Reedy, R.C., & Nicot, J.P. (2014). Comparison of water use for hydraulic fracturing for unconventional oil and gas versus conventional oil. *Environmental Science and Technology*, *48*(20). http://doi.org/10.1021/es502506v.

Schlumberger Oilfield Glossary. “packer”: http://www.glossary.oilfield.slb.com/Terms/p/packer.aspx

Segall, P. & Lu, S. (2015). Injection-induced seismicity: Poroelastic and earthquake nucleation effects. *Journal of Geophysical Research: Solid Earth*, *120*, 1–22. http://doi.org/10.1002/2015JB012060.Received.

Snead, M.C. (2002). The Economic Impact of Oil and Gas Production and Drilling on the Oklahoma Economy. *Oklahoma Commission on Marginally Producing Oil and Gas Wells*.

Tello, M. (2016). Analysis of Induced Seismicity and Basement Rock Fluid Flow.

Townend, J., & Zoback, M. D. (2000). How faulting keeps the crust strong. *Geology*, *28*(5), 399–402. http://doi.org/10.1130/0091-7613(2000)28<399:HFKTCS>2.0.CO.

United States Energy Information Administration (U.S. EIA). (2011). Review of Emerging Resources: U.S. Shale Gas and Shale Oil Plays: https://www.eia.gov/analysis/studies/usshalegas/. (accessed July 2017).

U.S. EIA. (2013). Technically Recoverable Shale Oil and Shale Gas Resources: An Assessment of 137 Shale Formations in 41 Countries Outside the United States:

https://www.eia.gov/analysis/studies/worldshalegas/pdf/fullreport.pdf. (accessed August 2017).

U.S. EIA. (2016). Hydraulically fractured wells provide two-thirds of U.S. natural gas production: https://www.eia.gov/todayinenergy/detail.php?id=26112. (accessed July 2017).

U.S. EIA. (2016). Hydraulic fracturing accounts for about half of U.S. crude oil production: https://www.eia.gov/todayinenergy/detail.php?id=25372. (accessed July 2017).

United States Environmental Protection Agency (U.S. EPA). (2016). Class II Oil and Gas Related Injection Wells: https://www.epa.gov/uic/class-ii-oil-and-gas-related-injection-wells (accessed June 2016).

U.S. EPA. (2016). Compliance Reporting Requirements for Injection Well Owners and Operators, and State Regulatory Programs: https://www.epa.gov/uic/compliance-reporting-requirements-injection-well-owners-and-operators-and-state-regulatory (accessed June 2016).

U.S. EPA. (2016). Underground Injection Control in EPA Region 6 (AR, LA, NM, OK, and TX): https://www.epa.gov/uic/underground-injection-control-epa-region-6-ar-la-nm-ok-and-tx (accessed June 2016).

U.S. EPA. (2016). Primary Enforcement Authority for the Underground Injection Control Program: https://www.epa.gov/uic/primary-enforcement-authority-underground-injection-control-program (accessed June 2016).

Walsh, F.R., & Zoback, M.D. (2015). Oklahoma's recent earthquakes and saltwater disposal. *Science Advances*, *1*(5), e1500195–e1500195. http://doi.org/10.1126/sciadv.1500195.

Weingarten, M., Ge, S., Godt, J.W., Bekins, B.A, & Rubinstein, J.L. (2015). High-rate injection is associated with the increase in U.S. mid-continent seismicity. *Science*, *348* (6241), 1336–1340. http://doi.org/10.1126/science.aab1345.

Zoback, M.D., & Healy, J.H. (1992). In situ stress measurements to 3.5 km depth in the Cajon Pass Scientific Research Borehole: Implications for the mechanics of crustal faulting. *Journal of Geophysical Research*, *97*(B4), 5039. http://doi.org/10.1029/91JB02175.

APPENDIX A. OCC CLASS II WELL DATA

Description

Weingarten *et al.* (2015) compiled a national well database for all Class II UIC wells from 2015 back to 1974, and the EPA requires states with primacy over their UIC program to report semi-annually (U.S. EPA, 2016). However, no publicly available, comprehensive (i.e. including *all* operational parameters of a well over its entire lifetime) federal database of those wells currently exists. With the exception of nine states that have not been granted regulatory primacy from the EPA over their injection wells, the central sources of well data for each state are state regulatory agencies. However, each agency varies in the format, amount, and type of data it compiles for these wells, depending on the state's regulatory requirements for oil and gas companies operating there.

The source of all Class II well data for the state of Oklahoma is the Oklahoma Corporation Commission (OCC) Oil and Gas Division, which currently assembles data into publicly available files through their website (U.S. EPA, 2016; OCC, 2017). The OCC regulates all wells in the state, with the exception of those in Osage County (home to the Osage Nation), which are regulated directly by the EPA (U.S. EPA, 2016). This agency collects data through the required Annual Fluid Injection Reports (Form 1012a) from all oil and gas companies operating in the state, each of which operates one or multiple extraction and disposal wells over a period of one or more years (Murray, 2015). It should be noted that 2011 was a regulatory transition year, as new rules required Form 1012a data to be submitted electronically as opposed to via paper copies as they were submitted prior to this year (Murray, 2014). Therefore, 2011 may have missing well data.

A permanent API number uniquely identifies each well, which is assigned to all oil and gas wells in the U.S. by the American Petroleum Institute ("API Numbering Guidelines", 2014). Databases of the Oklahoma Class II UIC wells compiled by the OCC are some of the most comprehensive, as they provide several injection parameters per well, many of which other state regulatory agencies do not report. The OCC organizes data from 2010 to 2016 into separate databases by year, each including only wells that were active during that year. These databases also include all of the following data in addition to the API number: well name, operator or well number, geographic location, type of well (e.g., SWD, 2D, 2DNC, 2DCm, 2R, 2RIn, 2RSI, or INJ, whose abbreviations are defined in Table 1), total monthly injected or disposed volume of fluids in bbls/month, an average monthly wellhead pressure in psi, and depths to the packer, which is a sealing device that protects well formations above or below the injection zone (Benz *et al.*, 2015; Murray, 2015; Schlumberger Oilfield Glossary). UIC well data from 2006-2009 include annual, instead of monthly, injection volumes, fluid type (e.g., Brackish Water, Fresh Water, or Salt Water) instead of well type data, and do not include wellhead pressures. Complete well records prior to 2006 are not as easily accessible through comprehensive OCC files, as much of those data are held either in scanned copies of well logs, through a well-browse database in which each well is recorded in an individual file (OCC, 2017), or in the database created by Weingarten *et al.* (2015) that has undergone data quality revisions to account for typing errors and gaps.

Tables

Table A1. List of all well types and their definitions by the OCC

SWD	Salt Water Disposal
2D	Disposal
2DNC	Non-Commercial Disposal
2DCm	Commercial Disposal
2R	Enhanced Recovery Production
2RIn	Injection Recovery
2RSI	Enhanced Recovery Production well with simultaneous injection and disposal
INJ	Injection

APPENDIX B. MCS MAPS

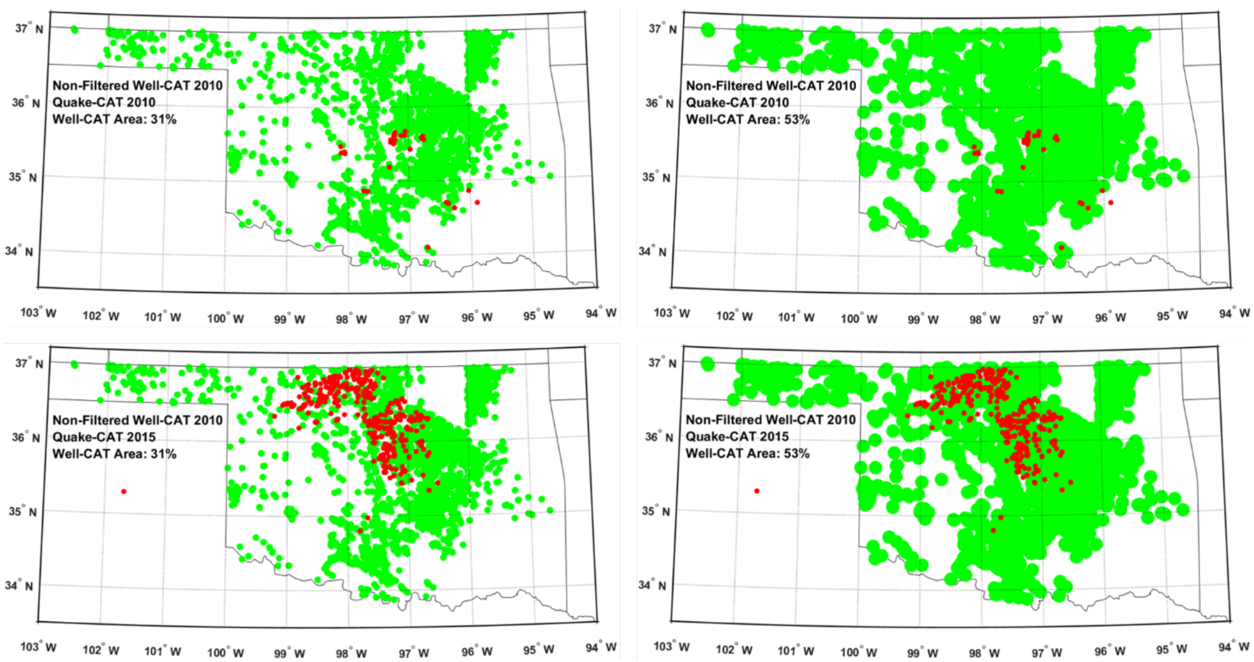

Figure B1. Non-filtered catalog of all active SWD wells in Oklahoma as green circles and all M≥3.0 earthquakes in Oklahoma as red dots. For all maps in this appendix, green circles in the left column have a 5 km radius, and those in the right column have a 10 km radius. All maps in this appendix show wells from 2010, but the two maps on the top show earthquakes from 2010, and the two on the bottom show earthquakes from 2015. The percent coverage of wells from the total area of Oklahoma is the “Well-CAT Area”.

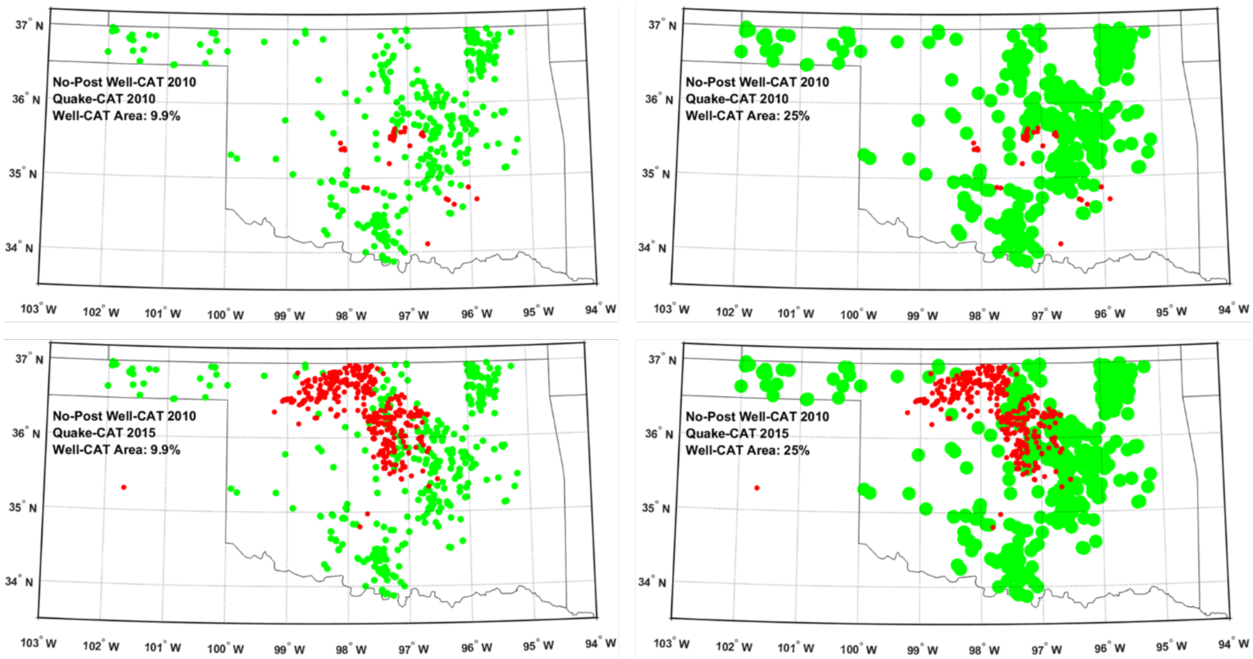

Figure B2. The "no post" catalog of SWD wells in Oklahoma in which wells active (or within 1 km of wells active) in years after 2010 are filtered out.

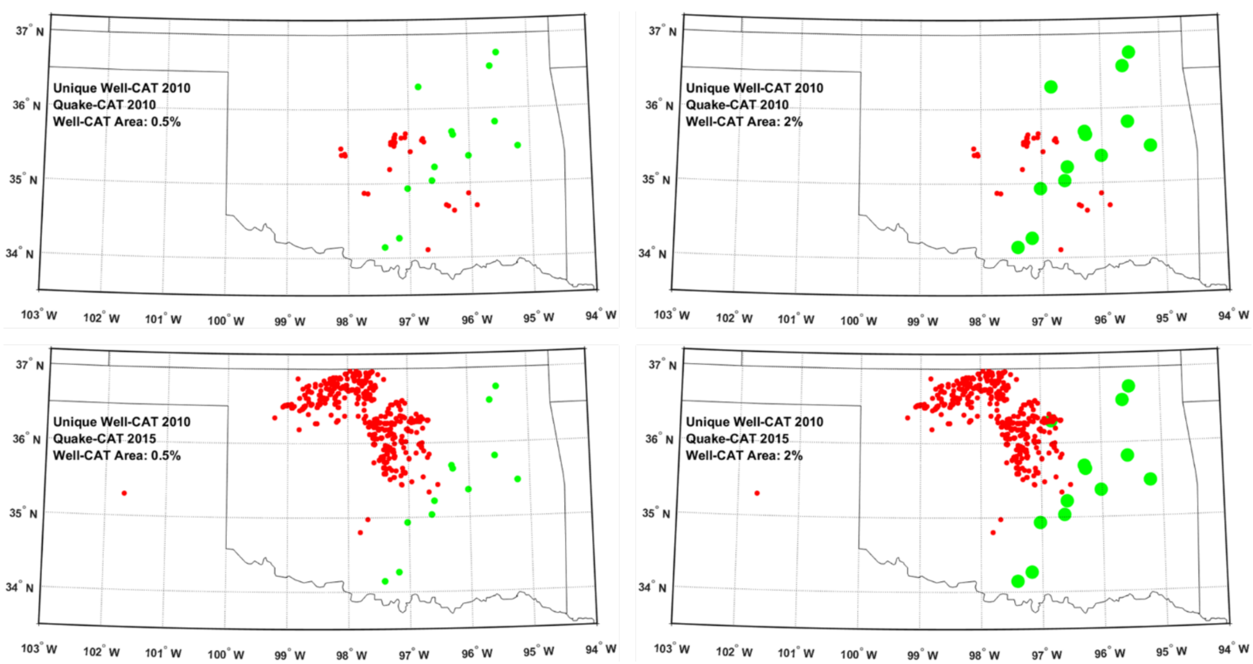

Figure B3. The "unique year" catalog of SWD wells in Oklahoma in which wells active (or within 1 km of wells active) in years both before and after 2010 are filtered out.

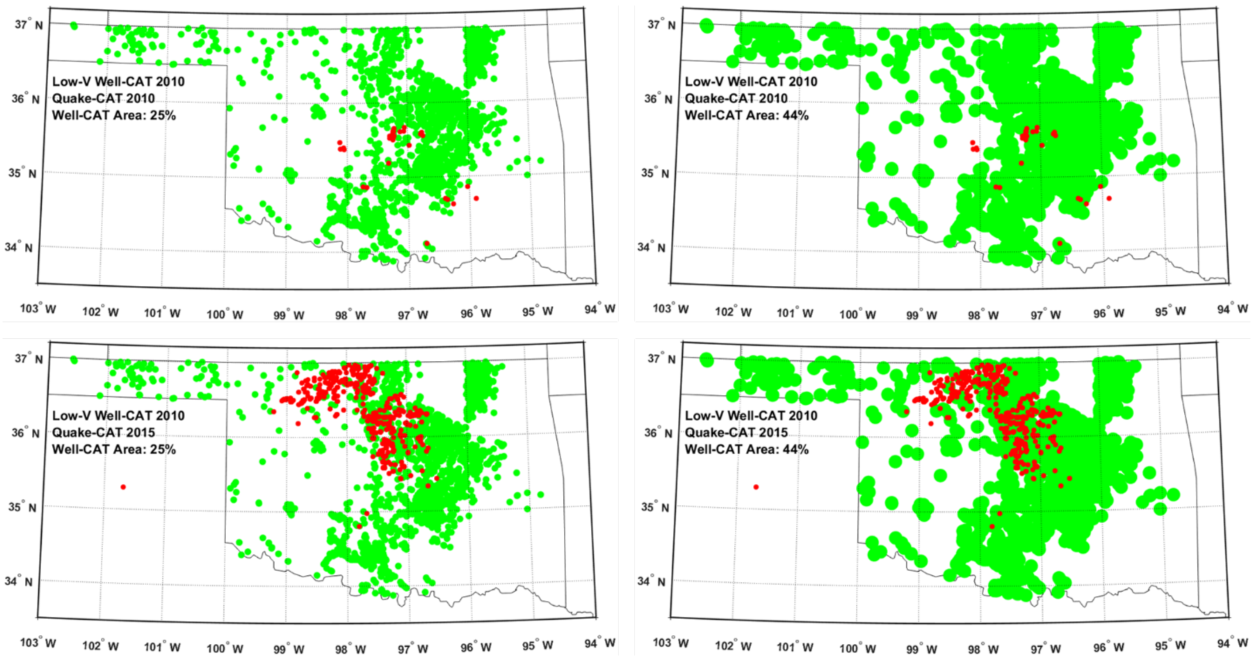

Figure B4. The catalog of all active low-volume (i.e. injecting ≤ 100,000 bbls/year) wells in Oklahoma in 2010.

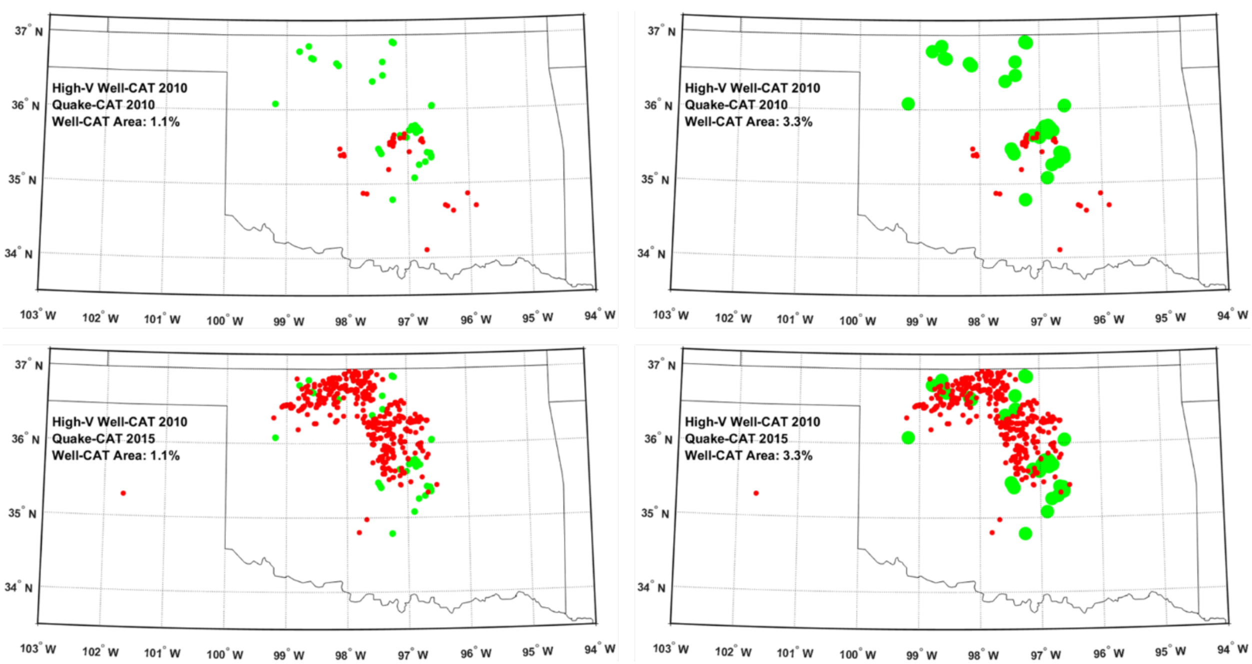

Figure B5. The catalog of all active high-volume (i.e. injecting ≥ 3.6 Mmbbls/year) wells in Oklahoma in 2010.

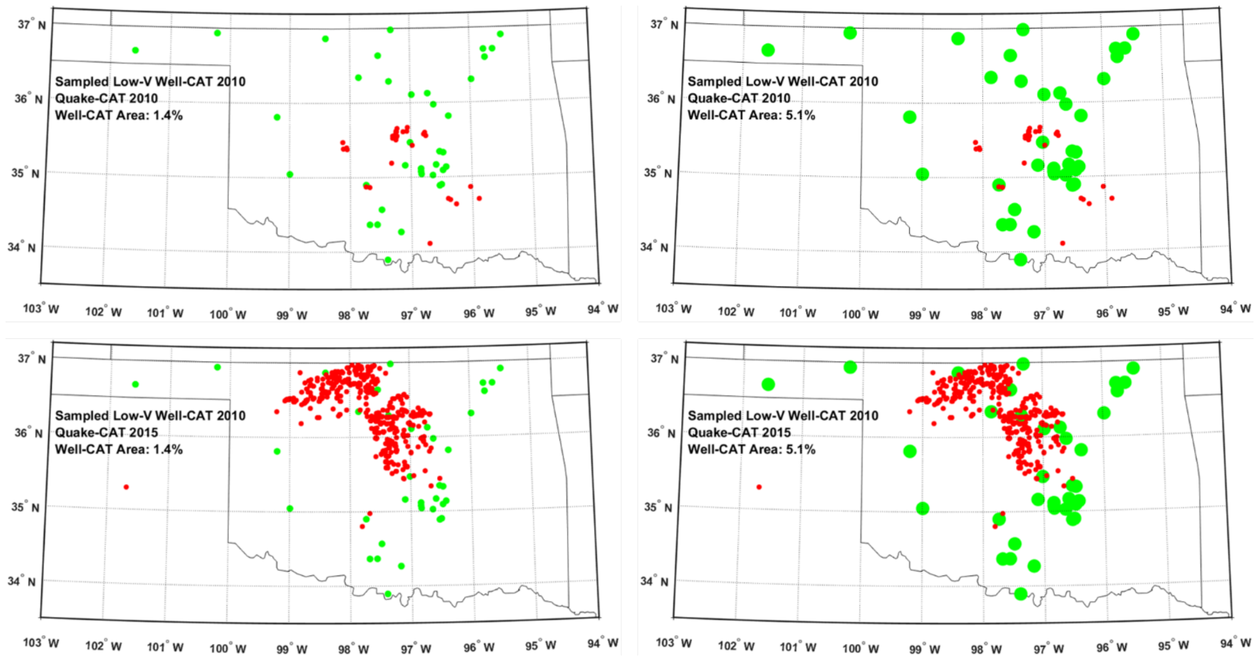

Figure B6. The catalog of a sample of 37 active low-volume wells in Oklahoma in 2010.

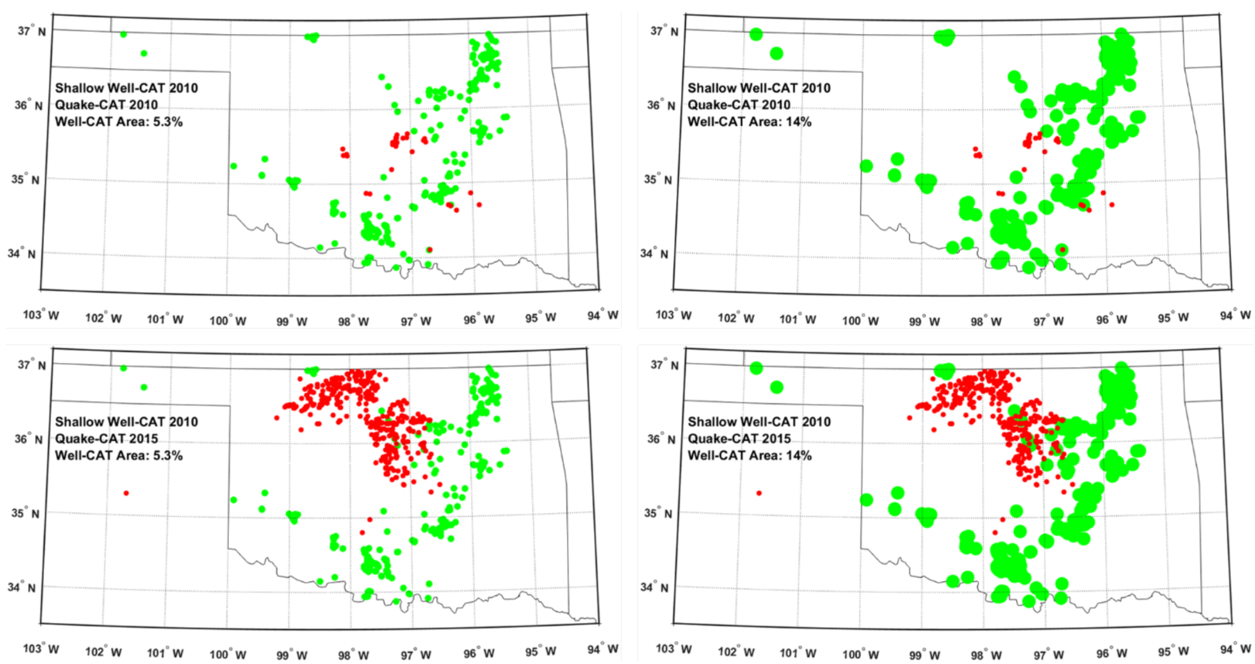

Figure B7. The catalog of all active, shallow (i.e. injecting at < 1,000 ft.) wells in Oklahoma.

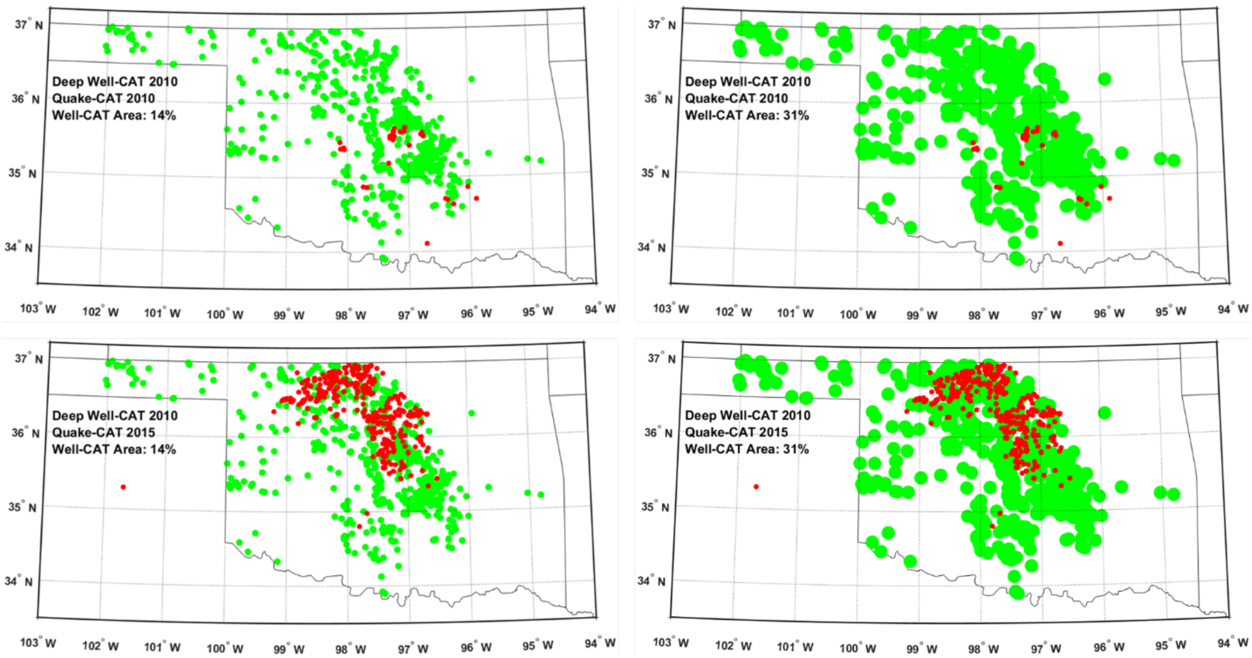

Figure B8. The catalog of all active, deep (i.e. injecting at > 4,000 ft.) wells in Oklahoma.

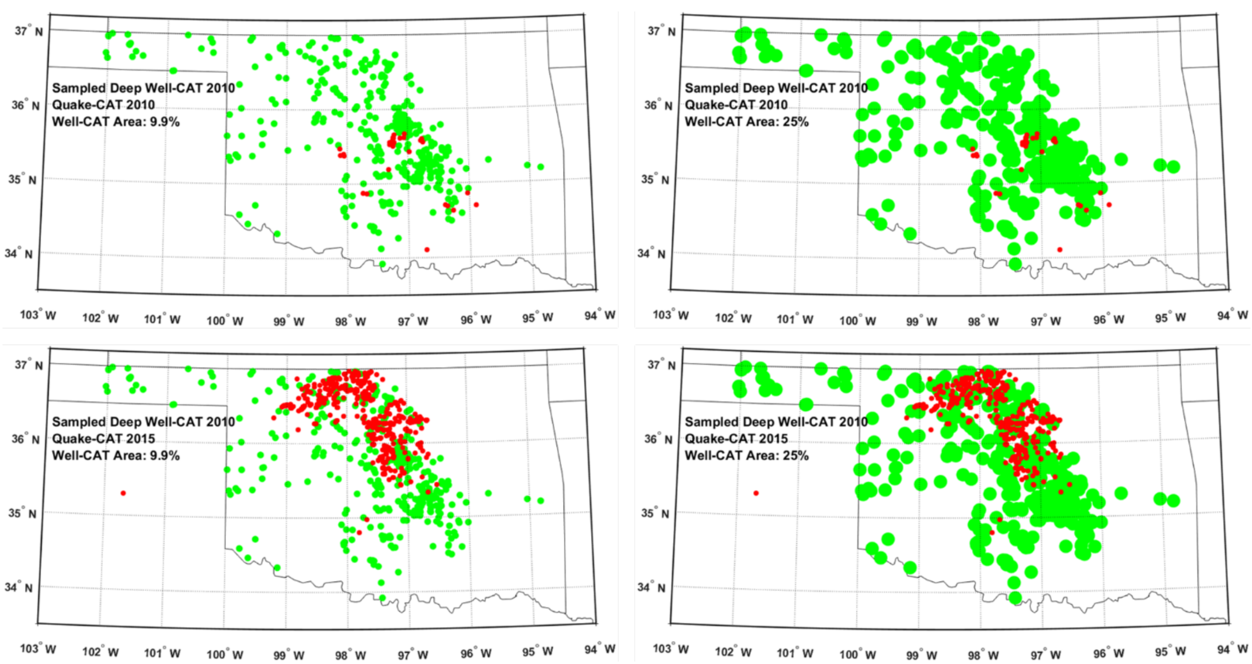

Figure B9. The catalog a sample of 402 deep wells in Oklahoma.

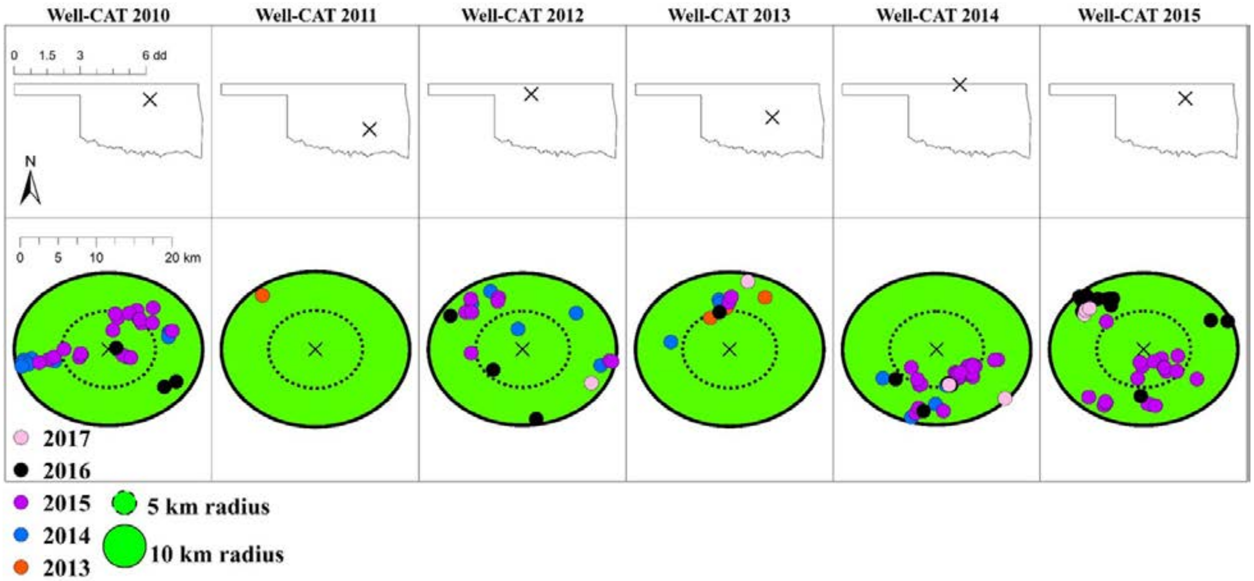

Figure B10. Individual wells from the "unique year" Well-CATS 2010-2015 as points marked by "x" in the green circles. Their locations in the state of Oklahoma are shown by the top panels, and the distances from the wells within which earthquakes are considered to be associated (i.e., are counted as "hits") are delineated by the green circles or 5 and 10 km radii. These hits are displayed as points of various colors depending on the year in which they occurred.

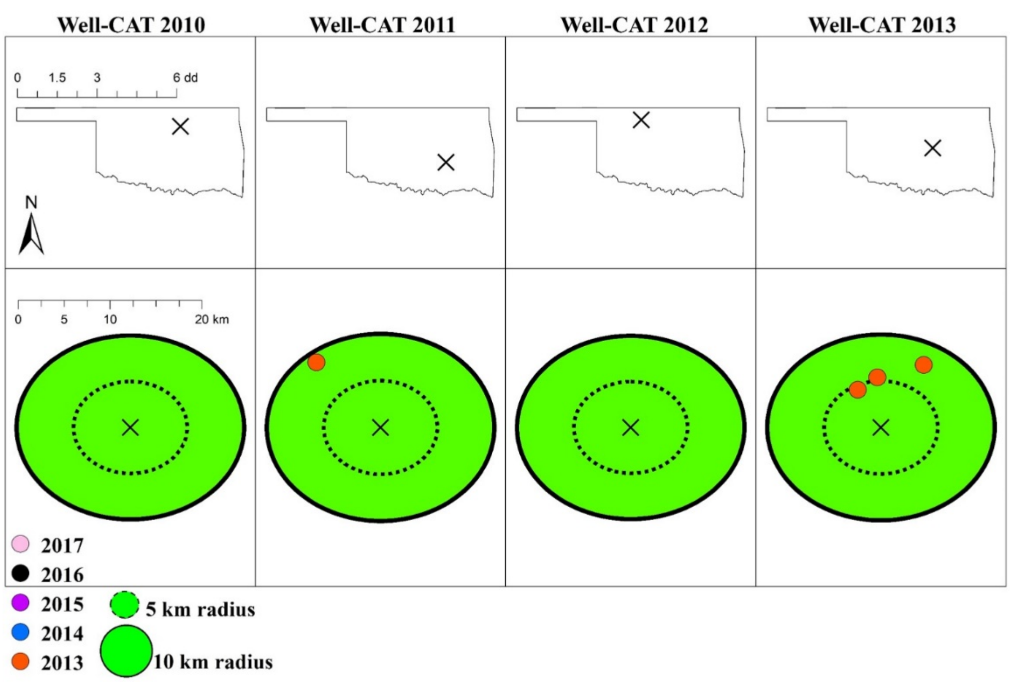

Figure B11. The same wells from 2010-2013, but only hits from 2013 are displayed.

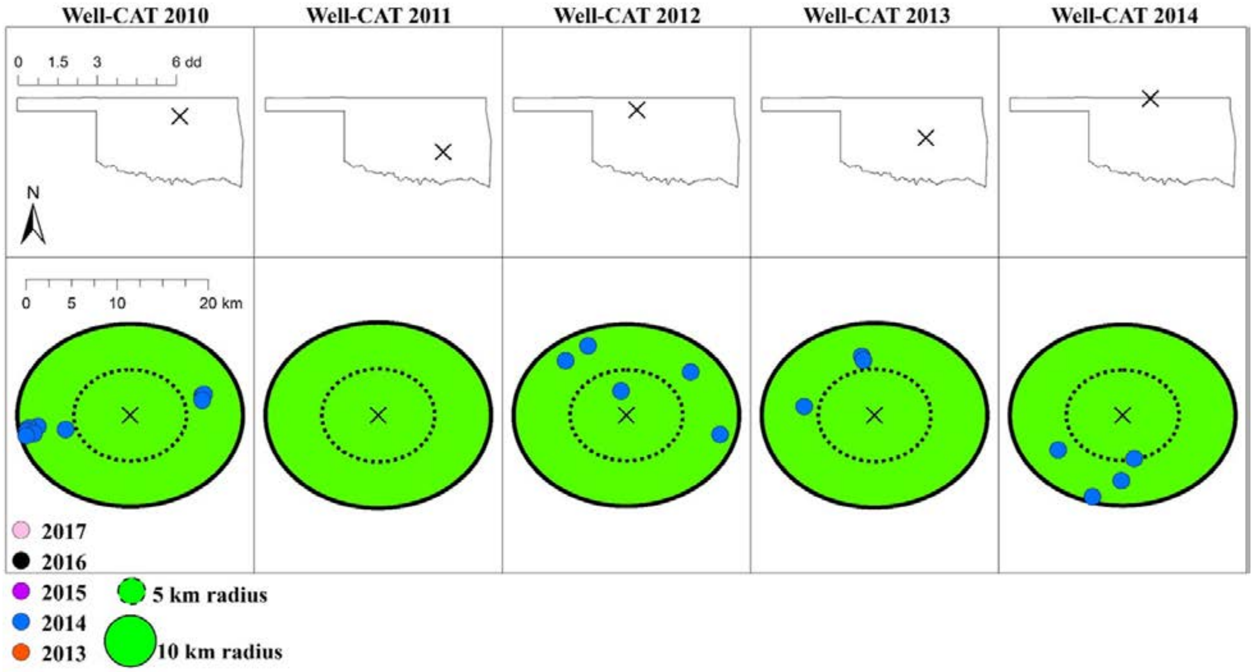

Figure B12. The same wells from 2010-2014, but only hits from 2014 are displayed.

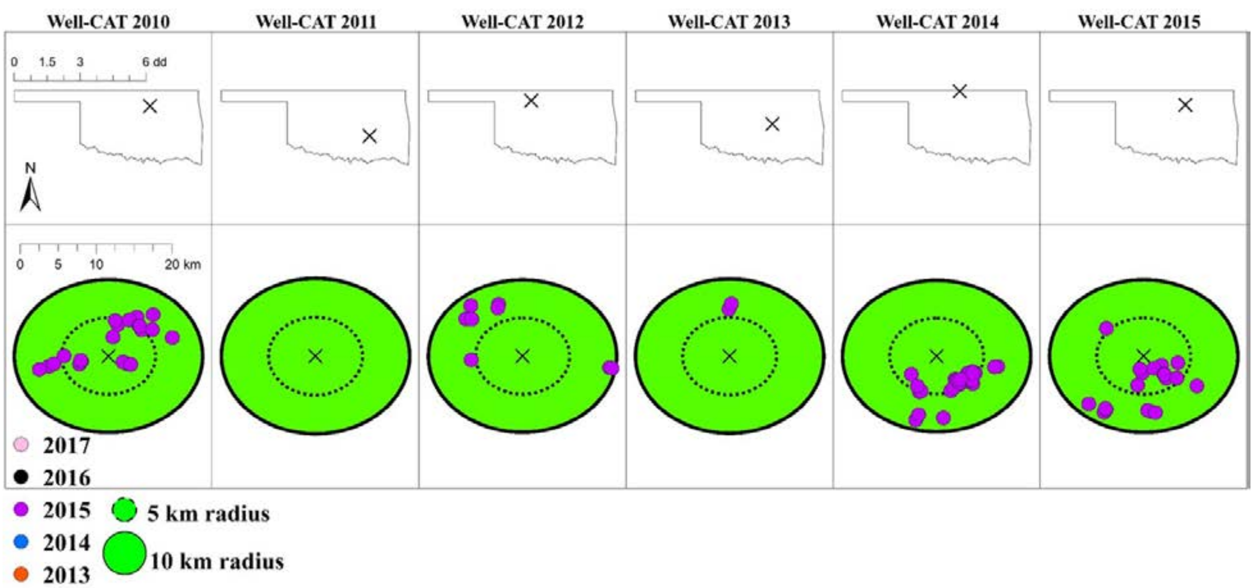

Figure B13. The same wells from 2010-2015, but only hits from 2015 are displayed.

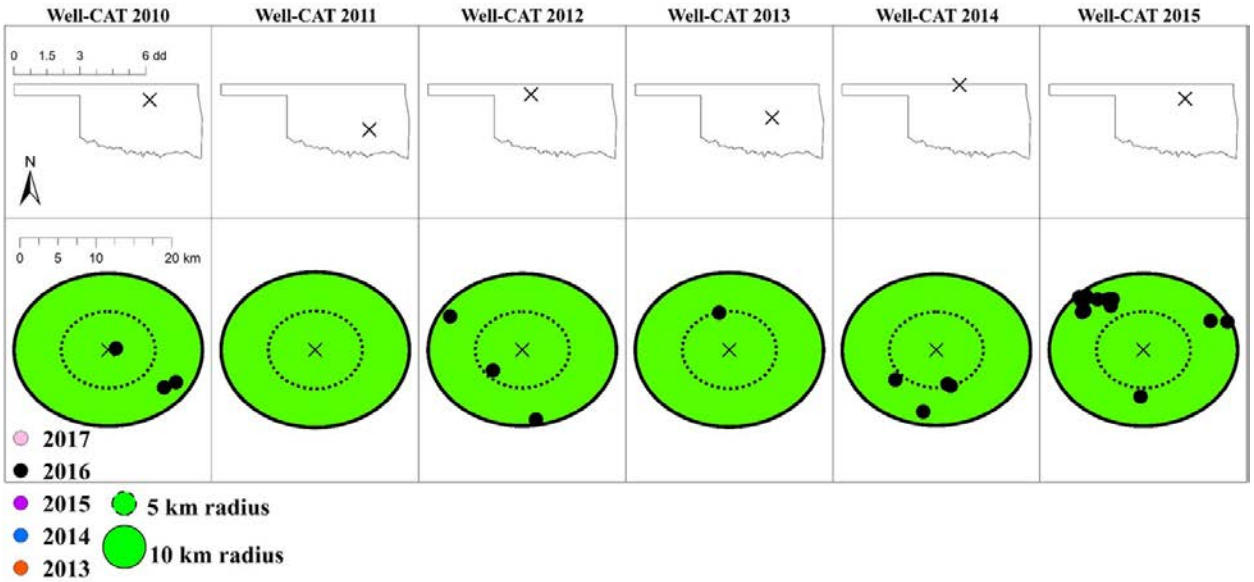

Figure B14. The same wells from 2010-2015, but only hits from 2016 are displayed.

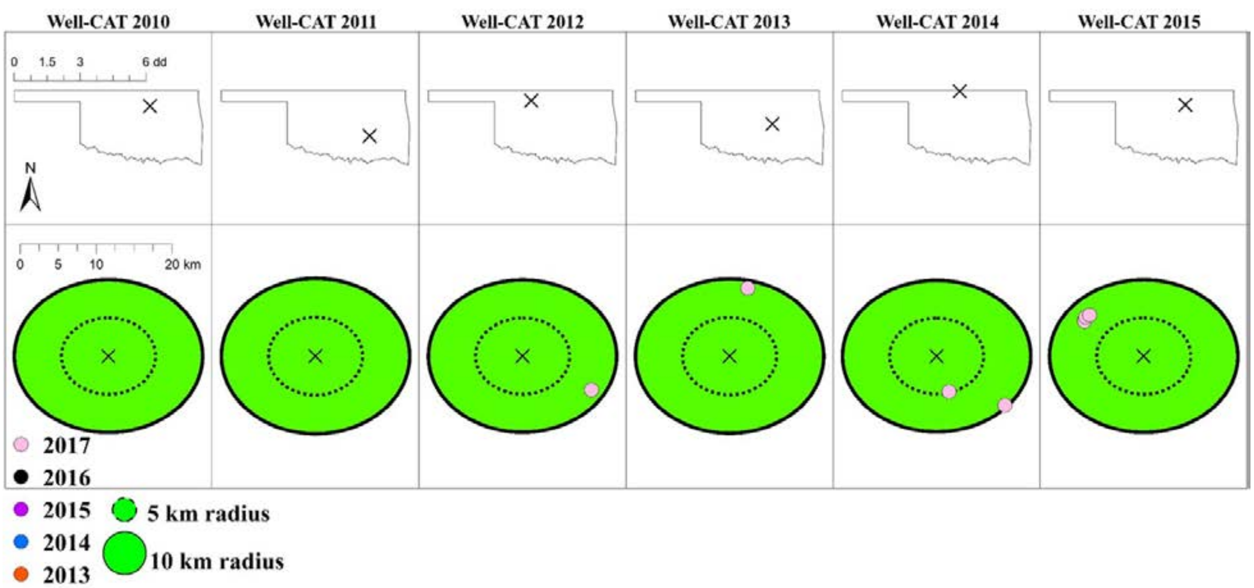

Figure B15. The same wells from 2010-2015, but only hits from 2017 are displayed.

APPENDIX C.

Figures

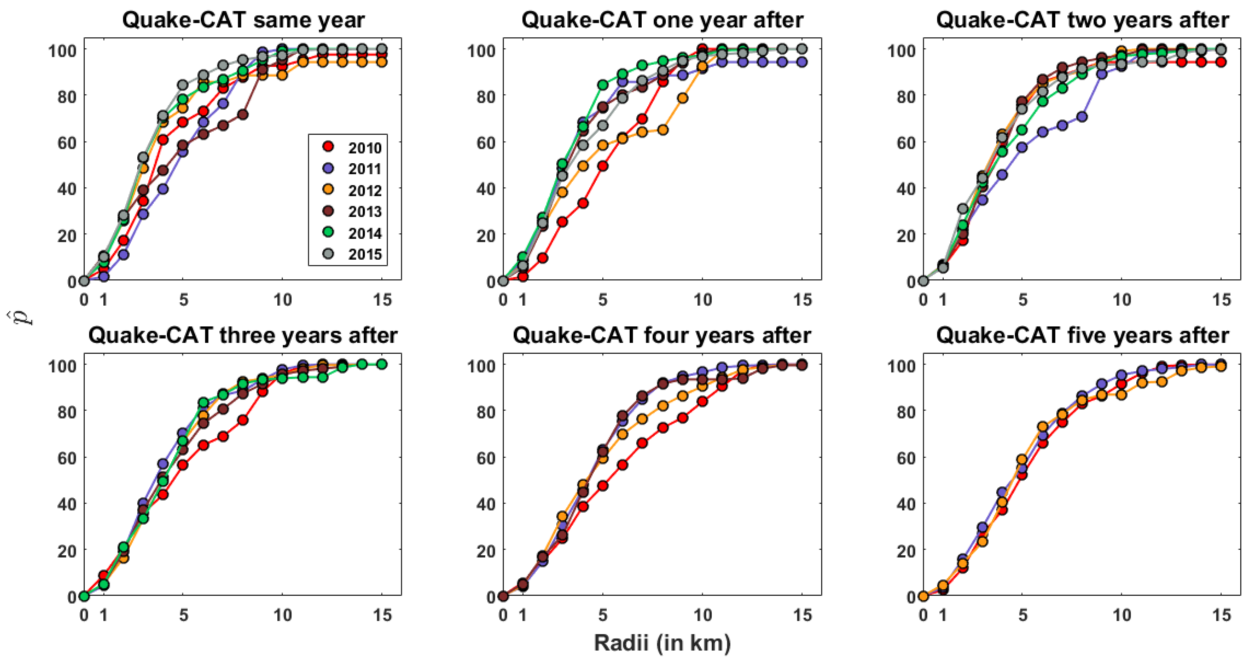

Figure C1. Cumulative hit percentage ($\hat{p}$) against MCS radii for all active SWD wells in Oklahoma in Well-CATs 2010-2015. Each line is a different Well-CAT year, and each $\hat{p}$ value within each year is calculated for all whole number radii from 1 to 15 km. Subplots show $\hat{p}$ values calculated from Well-CATs and Quake-CATs from the same year to Well-CATs and Quake-CATs that are five years apart.

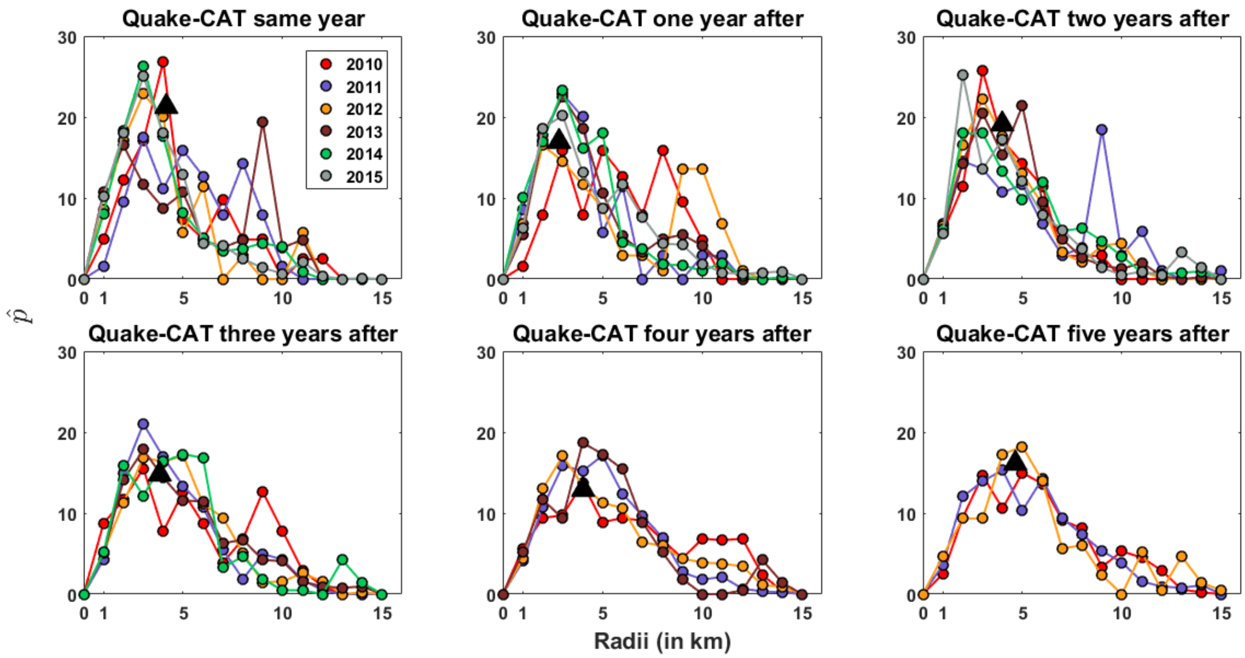

Figure C2. Non-cumulative hit percentage ($\hat{p}$) against MCS radii for all active SWD wells in Oklahoma in Well-CATs 2010-2015. Each line is a different Well-CAT year, and each $\hat{p}$ value within each year is calculated for all whole number radii from 1 to 15 km. Subplots show $\hat{p}$ values calculated from Well-CATs and Quake-CATs from the same year to Well-CATs and Quake-CATs that are five years apart. The primary peaks in $\hat{p}$ are shown by the black triangles.

Tables

Table C1. Linear regression statistics for all time progression analyses of Well-CAT years 2010-2012 for both 5 and 10 km Well-CAT radii. Slope values that increased with distance (i.e. the 10 km slope value was higher than the 5 km one) are highlighted in yellow. Those that decreased with distance are highlighted in green. Slope values that changed from negative to positive are highlighted in teal, and those that changed from positive to negative are highlighted in purple.

Well-CAT Year	Slope	R value	P-value	Well-CAT %Area	Total change in $\hat{p}$ (Slope*time)
Non-Filtered Well and Quake-CAT					
5 KM RADIUS					
2010	-0.904	0.231	0.582	31.0	-6.328
2011	-1.50	0.388	0.390	30.1	-9
2012	-2.38	0.555	0.254	31.8	-11.9
Averages	**-1.60**	**0.391**			**-9.08**
10 KM RADIUS					
2010	-0.842	0.432	0.285	53.2	-5.894
2011	-0.711	0.401	0.372	53.4	-4.266
2012	-0.488	0.204	0.699	54.9	-2.44
Averages	**-0.680**	**0.346**			**-4.20**
Non-Filtered Well-CAT, Multi-Year Quake-CAT					
5 KM RADIUS					
2010	1.18	0.748	0.032	31.0	8.26
2011	-1.60	0.882	0.009	30.1	-9.6
2012	-1.70	0.915	0.01	31.8	-8.5
Averages	**-0.707**	**0.848**			**-3.28**
10 KM RADIUS					
2010	0.113	0.249	0.552	53.2	0.791
2011	-0.841	0.755	0.05	53.4	-5.046
2012	-1.45	0.812	0.014	54.9	-7.25
Averages	**-0.726**	**0.605**			**-3.84**

"No Post" Well-CAT, Non-Filtered Quake-CAT					
5 KM RADIUS					
2010	-2.64	0.546	0.162	9.89	-18.48
2011	0.200	0.221	0.634	1.72	1.2
2012	0.139	0.166	0.753	2.18	0.695
Averages	**-0.767**	**0.311**			**-5.53**
10 KM RADIUS					
2010	-2.33	0.392	0.336	25.0	-16.31
2011	0.978	0.267	0.563	6.26	5.868
2012	1.58	0.563	0.245	7.83	7.9
Averages	**0.076**	**0.407**			**-0.847**
Unique Year Well-CAT, Non-Filtered Quake-CAT					
5 KM RADIUS					
2010	0.054	0.305	0.471	0.51	0.378
2011	0	N/A	N/A	0.07	0
2012	0.009	0.189	0.721	0.12	0.045
Averages	**0.021**	**0.247**			**0.141**
10 KM RADIUS					
2010	0.133	0.347	0.400	1.97	0.931
2011	-0.031	0.183	0.695	0.27	-0.186
2012	0.108	0.516	0.295	0.48	0.54
Averages	**0.070**	**0.347**			**0.428**
Low Volume Well-CAT, Non-Filtered Quake-CAT					
5 KM RADIUS					
2010	-2.08	0.554	0.154	25.2	-14.56
2011	-2.99	0.894	0.007	22.9	-17.94
2012	-1.57	0.629	0.181	24.5	-7.85
Averages	**-2.21**	**0.692**			**-13.5**
10 KM RADIUS					
2010	-3.98	0.810	0.015	44.2	-27.86
2011	-4.72	0.899	0.006	42.5	-28.32
2012	-4.54	0.732	0.098	44.4	-22.7
Averages	**-4.41**	**0.814**			**-26.3**

High Volume Well-CAT, Non-Filtered Quake-CAT					
5 KM RADIUS					
2010	-0.813	0.277	0.506	1.07	-5.691
2011	-2.28	0.529	0.211	0.87	-13.68
2012	-4.02	0.772	0.072	1.09	-20.1
Averages	**-2.37**	**0.526**			**-13.2**
10 KM RADIUS					
2010	-1.73	0.316	0.446	3.34	-12.11
2011	-3.21	0.495	0.259	2.91	-19.26
2012	-6.52	0.855	0.030	3.66	-32.6
Averages	**-3.82**	**0.555**			**-21.3**
Sampled Low Volume Well-CAT, Non-Filtered Quake-CAT					
5 KM RADIUS					
2010	-0.557	0.521	0.185	1.38	-3.899
2011	0.206	0.483	0.273	1.03	1.236
2012	0.137	0.339	0.511	1.29	0.685
Averages	**-0.071**	**0.448**			**-0.659**
10 KM RADIUS					
2010	-0.972	0.536	0.171	5.08	-6.804
2011	0.960	0.858	0.013	3.88	5.76
2012	1.05	0.520	0.291	4.37	5.25
Averages	**0.346**	**0.638**			**1.40**
Shallow Well-CAT, Non-Filtered Quake-CAT					
5 KM RADIUS					
2010	-0.199	0.214	0.611	5.28	-1.393
2011	0.302	0.502	0.251	4.48	1.812
2012	0.194	0.296	0.570	4.76	0.97
Averages	**0.099**	**0.337**			**0.463**
10 KM RADIUS					
2010	1.28	0.714	0.047	13.5	8.96
2011	1.36	0.813	0.026	11.7	8.16
2012	1.09	0.784	0.065	12.7	5.45
Averages	**1.24**	**0.770**			**7.52**

Deep Well-CAT, Non-Filtered Quake-CAT					
5 KM RADIUS					
2010	0.424	0.076	0.859	13.6	2.968
2011	-3.34	0.577	0.175	13.2	-20.04
2012	-5.52	0.845	0.034	15.0	-27.6
Averages	**-2.81**	**0.499**			**-14.9**
10 KM RADIUS					
2010	0.406	0.064	0.881	30.9	2.842
2011	-2.68	0.878	0.009	29.4	-16.08
2012	-2.52	0.600	0.208	31.5	-0.192307692
Averages	**-1.60**	**0.514**			**-4.48**
Sampled Deep Well-CAT, Non-Filtered Quake-CAT					
5 KM RADIUS					
2010	2.39	0.547	0.161	9.86	16.73
2011	1.52	0.489	0.265	8.08	9.12
2012	-0.374	0.108	0.838	8.31	-1.87
Averages	**1.18**	**0.381**			**7.99**
10 KM RADIUS					
2010	-3.00	0.450	0.263	25.3	-21
2011	0.844	0.311	0.497	21.2	5.064
2012	2.50	0.310	0.549	20.4	12.5
Averages	**0.115**	**0.357**			**-1.15**